THE USE OF ICHNOFOSSILS IN GEOLOGICAL AND PETROPHYSICAL CHARACTERIZATIONS OF AQUIFERS AND RESERVOIRS: EXAMPLES FROM SOUTH-CENTRAL TEXAS AND SOUTHEAST UTAH

By

James Aaron Golab

B.S., Mercyhurst University, 2007
M.S., Colorado School of Mines, 2010

Submitted to the graduate degree program in Geology and the Graduate Faculty of the University of Kansas in partial fulfillment of the requirements for the degree of Doctor of Philosophy.

_____

Co-chair, Dr. Jon J. Smith

_____

Co-chair, Dr. Luis A. González

_____

Dr. Paul A. Selden

_____

Dr. Charles D. Blome

_____

Dr. William C. Johnson

Date Defended: 12/08/2016

The Dissertation Committee for James Aaron Golab
certifies that this is the approved version of the following dissertation:

THE USE OF ICHNOFOSSILS IN GEOLOGICAL AND PETROPHYSICAL CHARACTERIZATIONS OF AQUIFERS AND RESERVOIRS: EXAMPLES FROM SOUTH-CENTRAL TEXAS AND SOUTHEAST UTAH

_____

Chairperson, Dr. Jon J. Smith

_____

Co-chair, Dr. Luis A. González

Date approved: 12/08/2016

ABSTRACT

James A. Golab
Department of Geology, December 2016
The University of Kansas

This dissertation presents three studies that show ichnological assessment is a vital part of both hydrogeology and petroleum geology. Ichnological assessments lead to a better understanding of the effects of bioturbation on aquifer or reservoir quality and consequently on subsurface fluid pathways. Ichnofossils may be studied in both outcrop and core, making them easily accessible to most studies. Ichnological assessment has become increasing common in petroleum geology but is still overlooked in hydrogeology.

The Trinity aquifer is a primary source of water for the San Antonio and Austin metropolitan areas. The Lower Cretaceous (Aptian–Albian) Lower Glen Rose Limestone (GRL) contains the middle Trinity aquifer and has previously been subdivided into six hydrostratigraphic units (HSUs). The GRL is a dual-permeability system and fluid flow is directed through both solution-enhanced fractures and pervasive *Thalassinoides* networks. Faults and fractures in the region are generally vertical and allow meteoric water to enter the subsurface. *Thalassinoides*-networks are commonly filled with coarser sediment than the surrounding matrix and act as lateral fluid pathways between fractures. Strata with well-developed burrow networks (ii3–4) are the most transmissive. Heavily bioturbated beds (ii5–6) are homogenized and restrict fluid flow. Beds with little to no bioturbation (ii1–2) can transmit water only through intergranular permeability, which is generally low.

The GRL HSUs were first identified in the subsurface via core examination at the Camp Stanley Storage Activity (CSSA) and were then correlated to associated gamma-ray and resistivity logs. Resistivity logs show that resistance values greater than 300 Ω-m correlate with well-developed biogenic porosity (ii3–4) and values greater than 650 Ω-m are associated with solution enhancement of the *Thalassinoides* networks. These high resistivity zones are cyclical and are identified in confining units, in the absence of karstic development. Natural gamma-ray logs are inversely correlated to resistivity logs and can be used to correlate lithology. Combining resistivity and natural gamma-ray datasets allows for the subsurface correlation of GRL fluid pathways.

Ichnologic assessment is not limited to physical properties and can be used for refined paleoenvironmental and paleogeographic histories. The Pennsylvanian–Permian (Virgilian–Wolfcampian) Halgaito Formation (HF) is a succession of carbonate and siliciclastic strata in southeastern Utah. The HF has been the subject of differing paleoenvironmental interpretations by various authors. This study refines the depositional history of the HF using a combined ichnological, paleopedological, and sedimentological approach. This study indicates that the retreat of the Elephant Canyon seaway out of the Paradox basin was punctuated by at least four transgressions. Above these transgressive units paleosol development generally increases upsection and ichnofossils suggest better-drained conditions. The uppermost beds of the HF contain little paleosol development and few ichnofossils, indicating a transition to more arid conditions prior to the deposition of the overlying Cedar Mesa Formation.

ACKNOWLEDGEMENTS

This project was made possible with the help and support of many people and I am grateful to each and every one of them for everything they have done. I would like to thank my advisor Dr. Jon Smith, for his support and help in making this dissertation a reality. Jon taught me not only how to improve my skills as a researcher, but to have confidence in myself and my abilities. I am indebted to him for taking me on as a student, helping me with my research, and making me strive for excellence.

I would like to thank my committee members Drs. Luis Gonzalez, Paul Selden, Chuck Blome, and William Johnson for their comments and assistance with editing and finalizing this dissertation. I would like to especially thank Chuck for agreeing to be part of my committee remotely from Denver. Chuck was my supervisor at USGS for three years prior to me starting my dissertation and it was during that time that I was introduced to the Edwards and Trinity aquifer project and began to take an interest in the work. It almost goes without saying that this entire project would not have been possible without him.

I want to send special thanks to Allan Clark and Bob Morris from the USGS in San Antonio. Allan, Bob, and I spent many days mapping and exploring central Texas together before and during my Ph.D. Allan's in depth knowledge of the geology of the Texas Hill Country and his connections to the many land owners and organization in Texas made it possible to accomplish this project. Additionally, Bob has been the best field partner I could ever hope for and I was

able to work through many questions with him. I hope I will be able to work with both of them in the future.

My advisors and instructors prior to my time at the University of Kansas also had an undeniable effect on me and this research. I thank Piret Plink-Björklund of the Colorado School of Mines for her time and assistance throughout and after my Master's degree. I thank James Adovasio and Judy Thomas of Mercyhurst University (both now retired) for their advising and teaching during my undergraduate degree. I would also like to extent particular thanks to Scott McKenzie of Mercyhurst University for first introducing me to the field of paleontology and encouraging me to add geology as a major next to my anthropology degree. Scott's breadth of knowledge and seemingly endless enthusiasm and energy inspires me to this day. I would also like to thank my former scoutmaster, Skip Keegan, who taught me to never accept less than the absolute best I could do and to never give up.

This research was supported by: The U.S. Geological Survey's Geology and Environmental Change Science Center (Contract G14PX00925 for services by James A. Golab); The Geological Society of America's Student Research Grant; The Paleontological Society Richard Osgood Award; The University of Kansas Summer Support Grant; and the Kansas Interdisciplinary Carbonates Consortium Graduate Research Assistantship. Additional support and equipment was provided by the U.S. Geological Survey's Crustal and Geophysics Science Center and the University of Texas, San Antonio.

The students of the Department of Geology have been an important part of my time here. I send particular thanks out to Adam Jackson, Christa Jackson, Sean Fischer, Bob Rader, Andy Connolly, and Sean Hammersburg for their support and friendship throughout these years. I hope our paths cross again in the future.

I would like to thank my mother, Louise and late father Jim for their help and support throughout my life. I also thank all of my friends and family in Pennsylvania for their support over the years. I promise I will visit more often in the future.

Finally, during my years as a doctoral student, my friends in the Denver area gave me support and provided me a home when I was in between field areas or needed to take a breather from what I was working on. Katie and David Karr, Marie and Dustin Rittenhouse, Sandy and Chris Gaul, and Nick Gaul, I truly am indebted to you for all you have done for me.

Your effort to remain what you are is what limits you

~Masamune Shirow, *Ghost in the Shell*, 1989

TABLE OF CONTENTS

CHAPTER 1. INTRODUCTION

This dissertation consists of three individual studies that use ichnofossils for the characterization of freshwater aquifers and hydrocarbon reservoirs. Ichnological assessment has previously been shown to be useful in aquifer and reservoir characterization (e.g., Keswani and Pemberton, 2007; Gingras et al., 2007; Tonkin et al., 2010), but is commonly overlooked in many studies. Bioturbation commonly decreases porosity and permeability in siliciclastic and carbonate aquifers that contain significant intergranular flow (e.g., Gingras et al., 2007; Tonkin et al., 2010); however, many karstic systems cannot transmit fluids through interparticle porosity and rely on bioturbation to create porosity and permeability (Mathews, 1967; Achauer, 1977; Cunningham and Sukop, 2011, 2012). It is therefore useful to assess these systems using an integrated approach that takes into account sedimentology, structural features, and ichnofossils.

Ichnofossils may also aid in the analysis of the depositional history of a deposit and improve the prediction of vertical and lateral facies changes, even when seismic data is limited (Ekdale et al., 1984; Bromley, 1996; Hasiotis, 2006; Smith et al., 2008; Hasiotis and Platt, 2012). Assessing the complex depositional history of reservoirs is important for understanding large-scale regional architectures and identifying targets for oil and gas production. In particular, reservoirs within continental deposits commonly contain thin beds with rapidly changing facies as well as subaerial exposure resulting in soil formation. Such paleosol horizons contain ichnofossils created by soil-dwelling organisms reacting to physicochemical factors such as soil moisture, temperature, seasonality, and precipitation (e.g., Hasiotis and Mitchell, 1993; Hasiotis et al., 1993; Hasiotis and Dubiel, 1994; Hasiotis and Platt, 2012). Due to the lateral variability of continental ichnofossil suites, the associated paleosols are used to put these traces into stratigraphic context. (Hasiotis, 2006; Smith et al., 2008; Hasiotis and Platt, 2012).

Chapters 2 and 3 illustrate how ichnofossils can be used in the characterization of fluid pathways within a telogenetic karstic aquifer system. These two chapters include both outcrop and subsurface studies from the Trinity aquifer and illustrate how wide-spread *Thalassinoides* networks influence water flow within this system.

Chapter 2 uses changes in ichnofabric index as a proxy for bioturbation within the Glen Rose Limestone (GRL) of south-central Texas and relates these changes to fluid flow within the Trinity aquifer system. Fluid pathways within the Trinity aquifer are controlled by the complex interaction of faults and fractures, karst development, and large-scale bioturbation-influenced porosity and permeability. Extensive studies have previously been conducted on the effects of fracturing and karst development on Trinity aquifer flow paths; however, few studies focused on the bioturbation-influenced porosity of this system (i.e., Cunningham and Sukop, 2012). This study illustrates that large-scale *Thalassinoides* networks within the GRL act as the primary fluid conduits to move water laterally between faults and fractures.

Chapter 3 uses two GRL cores and logs from monitoring wells recovered from the U.S. Army's Camp Stanley Storage Activity to characterize the effect of bioturbation on the petrophysical properties of the Trinity aquifer. This study focuses on resistivity and natural gamma-ray responses to the presence of large-scale *Thalassinoides* networks within the Lower GRL and shows that the bioturbation-influenced fluid pathways identified in Chapter 2 may be correlated into the subsurface via traditional geophysical logs. Additionally, this study shows that the identification of laterally continuous zones of bioturbation-influenced porosity will be valuable for developing a three-dimensional geologic framework for the Trinity aquifer as a whole.

Chapter 4 focuses on the larger-scale use of ichnofossils for the interpretation of depositional environments and refines the depositional history of the mixed carbonate and siliciclastic Halgaito Formation (HF) in southeast Utah in order to rectify competing interpretations of this system and verify its position within the stratigraphic nomenclature. Due to the lateral variability of continental ichnofossil suites, paleosols are used to put these traces into context (Hasiotis, 2006; Smith et al., 2008; Hasiotis and Platt, 2012). This study characterizes HF at a higher resolution than previously possible with sedimentological techniques alone and will aid in further developing the depositional history of the northern Paradox basin, a well-known oil and gas producing region.

The results of this dissertation show that ichnofossils are an important characteristic of many aquifers and reservoirs that is commonly overlooked in many studies. The characterization of fluid pathways in systems with wide-spread bioturbation often requires the integration of lithology, structural and karstic features, and ichnology. Such ichnological analyses can improve the prediction and correlation of subsurface fluid pathways and overall stratigraphic architecture of aquifers and reservoirs.

References

Achauer, C.A., 1977, Contrasts in Cementation, Dissolution, and Porosity Development Between Two Lower Cretaceous Reefs of Texas, in Bebout, D.G., and Loucks, R.G., eds., Cretaceous carbonates of Texas and Mexico—Applications to subsurface exploration: Austin, University of Texas, Bureau of Economic Geology Report of Investigation 89, p. 127–137.

Bromley, R.G., 1996, Trace Fossils: Biology, Taphonomy and Applications: Chapman & Hall, London, 361 p.

Cunningham, K.J. and Sukop, M.C., 2011, Multiple Technologies Applied to Characterization of the Porosity and Permeability of the Biscayne Aquifer, Florida: U.S. Geological Survey Open-File Report 2011-1037, 8 p.

Cunningham, K.J. and Sukop, M.C., 2012, Megaporosity and Permeability of Thalassinoides-Dominated Ichnofabrics in the Creataceous Karst-Carbonate Edwards-Trinity Aquifer System, Texas: U.S. Geological Survey Open-File Report 2012-1021, 4 p.

Ekdale, A.A. and Bromley, R.G., 1984, Comparative Ichnology of Shelf-Sea and Deep-Sea Chalk: Journal of Paleontology, vol. 58, p. 322–332.

Gingras, M.K., Baniak, G., Gordon, J., Hovikoski, J., Konhauser, K.O., La Croix, A.D., Lemiski, R., Mendoza, C., Pemberton, S.G., Polo, C., and Zonneveld, J., 2007, Porosity and Permeability in Bioturbated Sediments: Developments in Sedimentology, vol. 64, p. 837–868.

Hasiotis, S.T., 2006, Continental Trace Fossils. SEPM Short Course Notes no. 51, Tulsa, OK, 134 p.

Hasiotis, S.T. and Platt, B.R., 2012, Exploring the Sedimentary, Pedogenic, and Hydrologic Factors That Control the Occurrence and Role of Bioturbation in Soil Formation and

Horizonation in Continental Deposits: An Integrative Approach: The Sedimentary Record, vol. 10, p. 4–9.

Hasiotis, S.T. and Dubiel, R.F., 1994, Ichnofossil Tiering in Triassic Alluvial Paleosols: Implications for Pangean Continental Rocks and Paleoclimate: Memoirs of the Canadian Society of Petroleum Geologists. v.17, p.311-317.

Hasiotis, S.T., and Mitchell, C.E., 1993, A Comparison of Crayfish Burrow Morphologies: Triassic and Holocene Fossil, Paleo- and Neo-Ichnological Evidence, and the Identification of Their Burrowing Signatures: Ichnos, vol. 2, p. 291–314.

Hasiotis S.T., Mitchell, C.E., and Dubiel, R.F., 1993, Application of Morphologic Burrow Interpretations to Discern Continental Burrow Architects: Lungfish or Crayfish?: Ichnos, vol. 2., no. 4, p. 315–333.

Keswani, A. D. and Pemberton, S. G., 2007, Applications of Ichnology in Exploration and Exploitation of Mississippian Carbonate Reservoirs, Midale Beds, Weyburn Oilfield, Saskatchewan. In Alberta, Canada, Canadian Society of Petroleum Geologists and Canadian Society of Exploration Geophysicists Conference, p. 14–17.

Matthews, R.K., 1967, Diagenetic Fabrics in Biosparites from the Pleistocene of Barbados, West Indies: Journal of Sedimentary Petrology, vol. 36, no. 4, p. 1147–1153.

Tonkin, N.S., McIlroy, D., Meyer, R., and Moore-Turpin, A., 2010, Bioturbation Influence on Reservoir Quality: A Case Study from The Cretaceous Ben Nevis Formation, Jeanne d'Arc Basin, Offshore Newfoundland, Canada: AAPG Bulletin, v. 94, p. 1059–1078.

Smith, J.J., Hasiotis, S.T., Kraus, M.J., and Woody, D.T., 2008, Relationship of Floodplain Ichnocoenoses to Paleopedology, Paleohydrology, and Paleoclimate in the Willwood

Formation, Wyoming, During the Paleocene–Eocene Thermal Maximum: PALAIOS, vol. 23, p. 683–699.

CHAPTER 2. BIOTURBATION-INFLUENCED FLUID PATHWAYS WITHIN A CARBONATE PLATFORM SYSTEM: THE LOWER CRETACEOUS (APTIAN–ALBIAN) GLEN ROSE LIMESTONE

Currently in press as:

Golab, J.A., Smith, J.J., Clark, A.K., and Morris, R.R., 2016, Bioturbation-Influenced Fluid Pathways Within a Carbonate Platform System: The Lower Cretaceous (Aptian–Albian) Glen Rose Limestone: Palaeogeography, Palaeoclimatology, Palaeoecology, doi: 10.1016/j.palaeo.2016.10.025.

Abstract

The Aptian–Albian Glen Rose Limestone (GRL) is an argillaceous shallow-marine carbonate deposit on the Central Texas Platform and contains the upper Trinity aquifer and the upper part of the middle Trinity aquifer. The GRL is divided into Upper and Lower GRL members, which have been further subdivided into hydrostratigraphic units (HSUs). This study uses an integrated ichnological and sedimentological approach to record changes in ichnofabric index (ii) as a proxy for bioturbation within the GRL and relates these changes to fluid flow. Fluid pathways within HSUs are controlled by the complex interaction of faults and fractures, karst development, and large-scale bioturbation-influenced porosity and permeability. The effect of bioturbation-influenced porosity as an aquifer characteristic is the least studied of these factors. Postdepositional solution enhancement of ichnofossils is also common and has increased lateral and vertical fluid connectivity in some HSUs. Most GRL strata are dominated by *Thalassinoides* networks, but also contain *Palaeophycus*, *Planolites, Ophiomorpha*, Serpulid worm tubes, rhizoliths, and *Cruziana*. *Thalassinoides* are commonly filled with coarser sediment

than the surrounding matrix and act as fluid conduits within an otherwise low permeability matrix. Beds with ii3–4 and burrows with permeable fill transmit water readily. Beds with ii5–6 are commonly muddy and heavily homogenized, restricting fluid flow. Grainstone beds commonly have ii1–2 and are well cemented, restricting fluid flow to low intergranular flow. Pore systems dominated by *Thalassinoides* ichnofabrics, such as the GRL, are difficult to characterize on a large scale using many laboratory methods because they create heterogeneous flow paths depending on difference in permeability between the matrix and burrow fill. Understanding the effects of bioturbation-influenced porosity and permeability on subsurface fluid pathways is vital for creating a geologic and hydrostratigraphic framework for the Trinity aquifer.

1.0 Introduction

The Lower Cretaceous (Aptian–Albian) Glen Rose Limestone (GRL) forms the upper Trinity aquifer and the upper part of the middle Trinity aquifer in south-central Texas (TX). The combined Edwards and Trinity aquifer system provides the sole source of freshwater for San Antonio, TX, the seventh largest city in the United States, and the surrounding area (Clark, 2003). It is, therefore, vital to create a robust geologic framework in order to understand the subsurface fluid pathways of the GRL for developmental planning and regulating water usage in south-central TX.

Fluid pathways within the GRL are controlled by the complex interaction of faults and fractures, karst development, and large-scale bioturbation-influenced porosity and permeability (Horvoka et al., 1994). Extensive studies have been conducted on the effects of fracturing (e.g., George, 1952; Maclay and Small, 1976, 1986; Grimshaw and Woodruff, 1986; Maclay 1989; Pantea et al., 2008) and karst (e.g., Horvorka et al, 1994; Maclay, 1995; Scanlon et al., 2003;

Faith, 2004; Gary et al., 2013) on Edwards and Trinity aquifer quality; however, few studies have focused on bioturbation-influenced porosity and ichnofabrics within these systems (i.e., Cunningham and Sukop, 2012).

Ichnofossils are common throughout the carbonate strata of south-central TX and are significant controls on fluid flow. Cunningham and Sukop (2012) showed permeability associated with *Thalassinoides*-dominated ichnofabrics controlled horizontal fluid flow within the overlying Edwards aquifer, where unfilled ichnofossils form interconnected fluid conduits. The mudstone and marl within the GRL; however, complicates such ichnofabric analysis as many GRL *Thalassinoides* are filled with carbonate mudstone to grainstone acting either as barriers or conduits respectively. Dissolution of existing ichnofossils is also common in the GRL and may have increased the vertical and lateral fluid connectivity of some beds. Dissolution of material via meteoric water along fluid pathways is a prominent feature in similar carbonate settings (Mylroie and Carew, 1990; Cunningham et al., 2009; Wright et al., 2014) and dissolution of ichnofossils has been shown to increase porosity and permeability in such systems (Cunningham et al., 2009; Tonkin et al., 2010).

This study uses an integrated ichnological and sedimentological approach to record changes in ichnofabric index (ii) as a proxy for bioturbation within the GRL and interprets how these changes relate to subsurface fluid pathways. The GRL is a carbonate platform composed of rudist reefs and subtidal to supratidal facies assigned to the Thalassinoides ichnofacies. The majority of GRL strata are dominated by coarsening-upward successions of wackestone to packstone with some carbonate mudstone and grainstone. These successions have been interpreted to have been deposited by a tide-dominated system and are commonly muddy with low intergranular permeability. Associated rudist-dominated facies are also muddy, but contain

abundant fractures and have high permeability, but limited lateral extent (Petta, 1977). The GRL, therefore, cannot transmit fluid through interparticle porosity easily, but may rely, in part, on bioturbation-influenced porosity (Mathews, 1967; Achauer, 1977; Cunningham and Sukop, 2012; Golab et al., 2015). This biogenic aspect of karstic aquifers has generally been overlooked in the literature (Cunningham et al., 2009; Cunningham and Sukop, 2011, 2012; Golab et al., 2015).

2.0 Geological background

2.1 Depositional and tectonic history

The GRL is the uppermost formation of the Lower Cretaceous Trinity Group, which is present across most of south-central TX (Fig. 1; von Roemer, 1852; Imlay, 1945). The Trinity Group is a succession of three distinct, second-order, transgressive–regressive sequences composed of a lower siliciclastic lowstand unit and an upper carbonate highstand unit deposited on the shallow-marine Central Texas Platform, which spans from the Llano Uplift southeast to the Stuart City Reef (Fig.1; George, 1952; Winter, 1961; Barnes, 1965; Stricklin et al., 1971; Inden, 1974; Bebout et al., 1977; Barnes, 1981). The three sequences of the Trinity Group in the study area are: 1) the Hosston and Sligo formations; 2) the Hammett Shale and Cow Creek Limestone; and 3) the Hensel Sand and the Glen Rose Limestone (Fig. 2; Stricklin et al., 1971). The Trinity Group is overlain by the Albian Edwards Group, a 120–180 m succession of platform carbonates that accumulated north of the Stuart City Reef across most of central and southern Texas (Fig.1; Rose, 1972). The GRL forms the upper Trinity aquifer and the upper part of the middle Trinity aquifer, which act as a catchment for the Edwards aquifer where it is exposed at the surface (Small and Lambert, 1998; Blome et al., 2007; Clark et al., 2009).

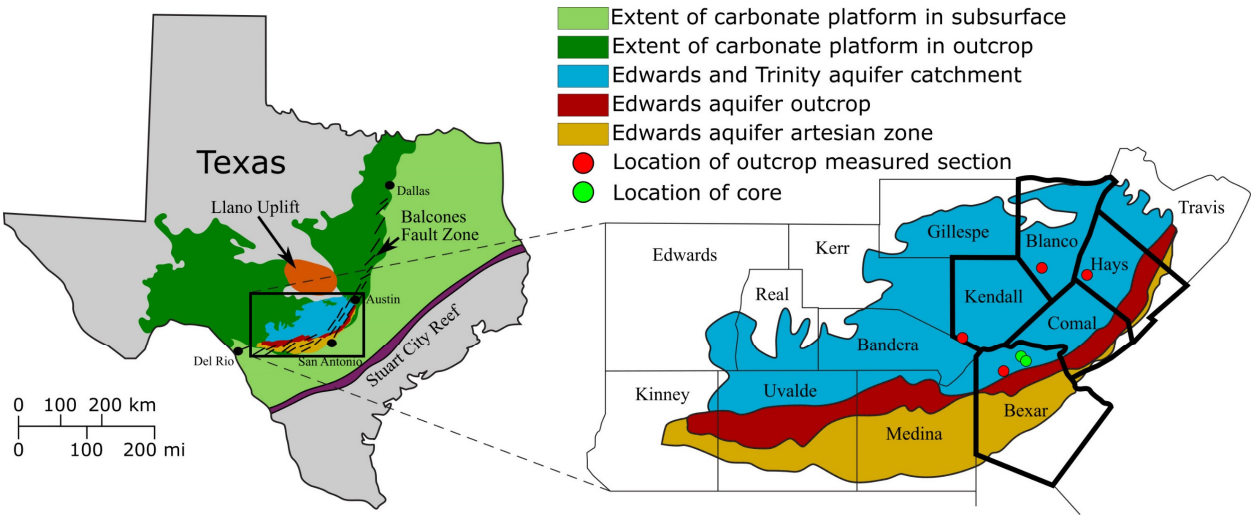

Figure 1. Location map showing the regional extent of the Edwards and Trinity aquifer outcrop and subsurface catchment area as well as the extent of carbonate platform deposition in Texas. Locations of the Llano Uplift and Stuart City Reef, which affected GRL deposition, are also shown. Approximate locations of the four measured sections and two cores used in this study are indicated. Regional aquifer extent modified from Blome et al. (2007); extent of carbonate deposition and location of regional features modified from Pittman (1989).

The GRL is an ~120-m-thick succession of argillaceous carbonates with few beds of siliciclastics and is divided into two members: the Upper and Lower GRL (Lazo and Stricklin, 1956; Carew, 1967; Stricklin et al., 1971; Scott et al., 2007). The Lower GRL is ~70-74 m thick within the study area and is characterized by m-scale beds of mudstone and marls alternating with beds of wackestone to grainstone (Clark, 2003, 2005; Clark and Morris, 2015). These beds are fossiliferous and commonly contain the whole or fragmentary shells of gastropods (e.g., *Nerinea* sp.; *Tylostoma* sp.), bivalves (e.g., *Texigryphea* sp.; *Cucullaea terminalis*), echinoids (e.g., *Selenia* sp.; *Hemiaster* sp.) and foraminiferans (e.g., *Orbitolina* sp.; *Milioid* sp.; Adkins, 1928; Behrens, 1965; Clark and Morris, 2015). In some localities, Lower GRL beds grade laterally into discontinuous rudist facies dominated by *Caprinid* sp. The presence or absence of rudist reef facies within vertical intervals of the Lower GRL was caused by changes in regional seawater chemistry, as well as localized changes in depth and water currents (Petta, 1977). The

Lower GRL is topped by a regional "*Corbula* bed" (*Corbula* packstone–grainstone facies, this study), an ~15 cm marker unit dominated by the tiny bivalve *Eoursivivas harveyi* and commonly containing ripples (Scott et al., 2007; Ward and Ward, 2007). The Upper GRL is ~92–119 m thick in the study area and is dominated by m-scale marly–argillaceous wackstone to packstone beds and rare gypsum beds. The presence of evaporites is attributed to restricted circulation conditions shoreward of the Stuart City Reef (Fisher and Rodda, 1969). Rudist-dominated facies are present, but not common in the Upper GRL.

Individual beds within the GRL are heterogeneous and vary significantly laterally and vertically. Stratigraphic control has traditionally been maintained using the distinct fossil beds such as the *Corbula* and *Selenia* marker beds (e.g., George, 1952; Whitney, 1952; Ward and Ward, 2007; Clark and Morris, 2015). Central Texas Platform GRL strata are characterized by cyclic successions of facies grading from fine-grained mudstones and wackestones to fine- to medium-grained packstones and grainstones (Behrens, 1965; Clark 2003, 2005). Regional subsurface architecture forms clinoforms that span from the Llano Uplift to the Stuart City Reef (Cleaves, 1977; Braun, 2011).

All of the Trinity Group siliciclastic and carbonate units, including the GRL, were extensively faulted during the Miocene, creating the Balcones Fault Zone; a northeast–southwest trending zone of normal faults that extend from central to north Texas (Fig. 1; George, 1952; Horvorka et al., 1994). Miocene faulting occurred along preexisting zones of weakness in Paleozoic rocks along the Ouachita front (Collins, 1995). Most faults within the Balcones Fault Zone are high angle and form a series of *en echelon* fault blocks in which relay ramps are common (Collins, 1995; Pantea et al., 2008).

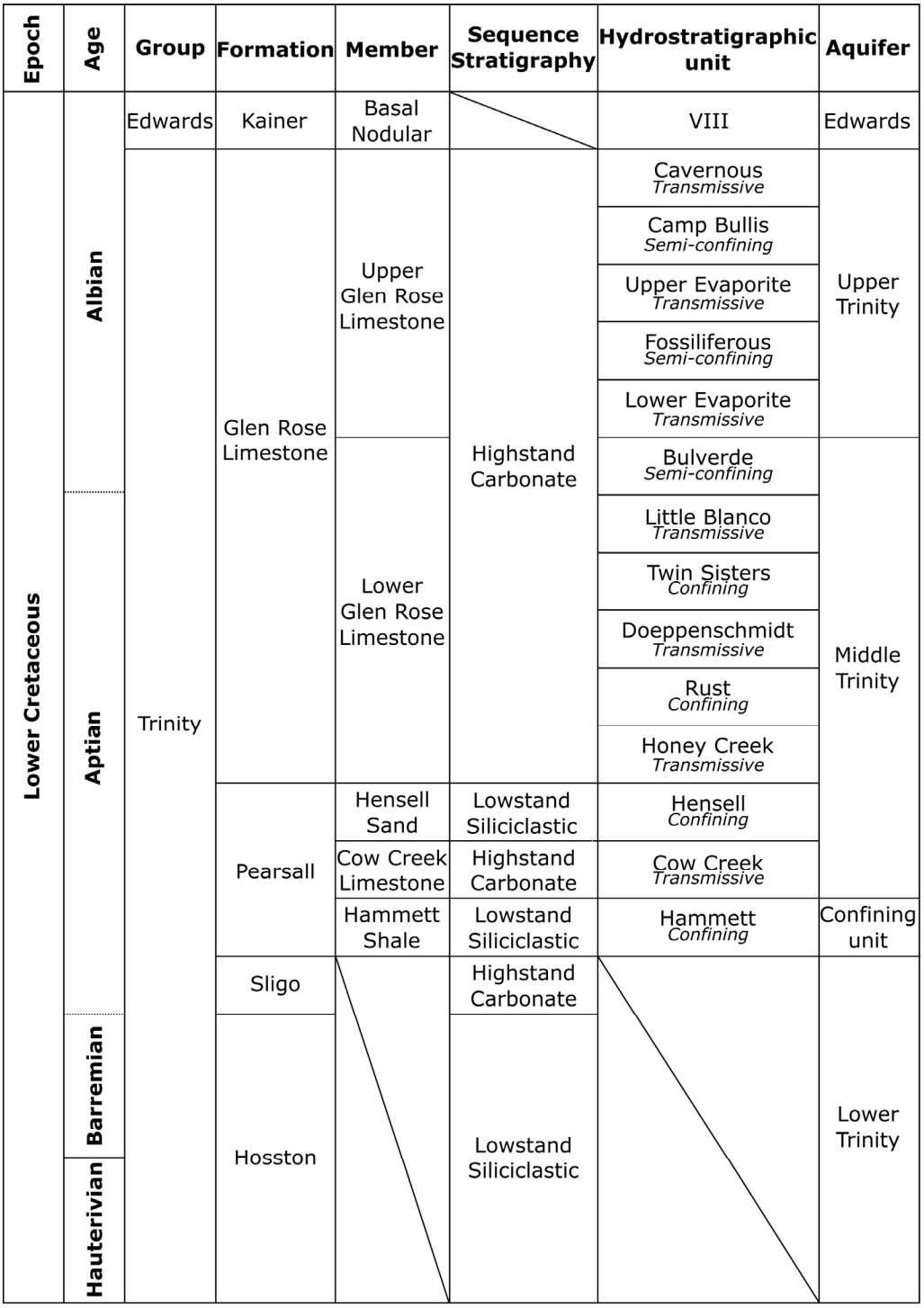

Figure 2. Chart summarizing the lithostratigraphy, sequence stratigraphy, and hydrostratigraphy of the Trinity Group on the Central Texas Platform. Hosston and Sligo formations are found only in the subsurface within the study area. The Pearsall Formation and Glen Rose Limestone were examined in outcrop and core. The overlying Edwards Group is found in some outcrops within the study area. Ages of formations and members from Stricklin et al. (1971) and Clark and Morris (2015).

2.2 Hydrostratigraphy

The Upper and Lower GRL have been subdivided into eleven hydrostratigraphic units (HSUs; Fig. 2) using the porosity-based classification system defined by Choquette and Pray (1970). Hydrostratigraphic units are stratigraphic divisions with distinct hydrologic characteristics (Maxey, 1964; Choquette and Pray, 1970). This definition was developed because there are various factors that affect aquifer fluid flow such as lithology, sedimentary structures, bioturbation, and structural features (Maxey, 1964; Choquette and Pray, 1970; Clark and Morris, 2015). The concept of HSUs was combined with the characterization of fabric and not-fabric selective porosity defined by Choquette and Pray (1970) for studies on the Edwards aquifer, which divided the Edwards aquifer into eight HSUs (I–VIII; Maclay and Small, 1976; Maclay, 1995; Barker and Ardis, 1996; Bumgarner et al., 2012). These studies on the Edwards aquifer severed as the basis for the subdivision of the GRL by Clark (2003, 2004) and Clark et al., (2009, 2014). The types of fabric-selective porosity within the GRL are in descending order of abundance: burrowed, bedding plane, moldic, shelter, and interparticle (Clark et al., 2009, 2014; Clark and Morris, 2015). The GRL also contains, in descending order of abundance, not-fabric selective fracture, vug, channel, cave, and breccia porosity (Clark and Morris, 2015). All of the tidal-dominated strata of the GRL may contain one or more of these porosity types. Porosity created by biologic activity (i.e., burrowed) is the least studied feature within the GRL.

The Lower GRL was subdivided into six informal units by Blome and Clark (2014). The Lower GRL HSUs were named by Clark et al. (2014) as, in ascending order: the Honey Creek, Rust, Doeppenschmidt, Twin Sisters, Little Blanco, and Bulverde HSUs (Fig. 2). The Upper GRL was informally subdivided into five HSUs by Clark (2003) and named by Clark et al. (2009). These five units are, in ascending order: the Lower Evaporate, Fossiliferous, Upper

Evaporate, Camp Bullis, and Cavernous HSUs. Water well cores and petrophysical logs including gamma-ray, spontaneous potential, and resistivity logs were also used to identify the 11 HSUs in the subsurface (Blome and Clark, 2014; Pantea et al., 2014; Clark and Morris, 2015). Changes in well log response are relative to changes in mud content and permeability; both of which are affected by the amount of bioturbation, as well as epikarst and fracture development (Zhou et al., 2002).

The Trinity aquifer is subdivided into the lower, middle, and upper Trinity aquifers. The upper Trinity aquifer is contained within the five Upper GRL HSUs (Ashworth, 1983; Clark et al., 2009). The middle Trinity aquifer is contained within the six Lower GRL HSUs, the Hensell Sand, and the Cow Creek Limestone (Ashworth, 1983; Blome and Clark, 2014; Pantea et al., 2014). The Hammett Shale is an impermeable aquitard between the middle and lower Trinity aquifers. The lower Trinity aquifer is contained within the Hosston and Sligo formations (Ashworth, 1983).

Due to the mud and siliciclastic material present in the GRL, wells within the Trinity aquifer commonly have a lower flow rate than wells within the Edwards aquifer (Maclay, 1995; Mace et al., 2000). However, the Trinity aquifer covers a much larger regional extent and rapid development within the Texas “Hill Country” between Austin and San Antonio has brought the aquifer to the attention of local groundwater users, water purveyors, and resource managers (Clark and Morris, 2015).

3.0 Methods

3.1 Field methods

Four outcrop measured sections were made across the study area, covering all HSUs except the Little Blanco and Bulverde HSUs, which were examined in core (Appendices I–V). Outcrop sections were measured with a hand level and a Jacob's staff that was demarcated in decimal ft and extended up to 25 ft in length. Beds were described lithologically, sedimentologically, and ichnologically. Lithologies were described using the classification system of Dunham (1962) for carbonates, the Embry and Klovin (1971) classification for rudist reef material, and the Wentworth (1922) classification scale for siliciclastics. Sedimentological features and ichnofossils were examined and described *in situ*; some representative ichnofossil samples were collected for photographs. Ichnofossils were described using morphology, surface textures, and burrow fill (e.g., Pemberton and Frey, 1982; Hasiotis and Mitchell, 1993). Additionally, two near-complete GRL cores from Camp Stanley, San Antonio, TX (MW9-CC, MW5-LGR), stored at the U.S. Geological Survey's Core Research Center in Denver, Colorado, were also described similarly to outcrop sections.

Ichnofabric indices were recorded in the field and used to interpret the percent amount of bioturbation as defined by Droser and Bottjer (1986). Ichnofabric index (ii) is a semiqualitative field interpretation of the amount of bioturbation within strata. This scale rates the amount of bioturbation from 1–6, where ii1 is a lack of bioturbation and ii6 is sediment that has been completely homogenized due to biologic activity. Ichnofabric indices of individual lithologic beds within HSUs were compared over the entire vertical extent of the GRL.

Additionally, field data collection was assisted by the use of an Apple iPad 2 loaded with geospatially registered 7.5-minute USGS topographic maps. Locations of visible and interpreted contacts, faults and fractures, marker units, and other areas of interest were recorded using the integrated 3G assisted global positioning system (GPS) on the iPad, which is accurate to <1.5m if cellular data service is present, as over most of the study area. Major lithologic contacts were first identified and subadjacent strata were then described.

3.2 Laboratory methods

One hundred petrographic thin section samples were taken from core MW9-CC in Bexar County, TX, the approximate location of which is indicated on Figure 1. Wagner Petrographic in Lindon, Utah produced the thin sections which were 24x46 mm in size and impregnated with clear epoxy. These thin sections were used to analyze mineralogy, cementation, micropaleontology, and microporosity. Analysis was conducted using an AmScope T490B-MT digital compound trinocular microscope with an integrated digital camera for pictomicrographs. Additionally, each thin section from MW9-CC was point counted using an Olympus BX53 microscope with an automated stepper stage controlled by PetrogLite 3.0 softwareto determine the matrix porosity of the sample and amount of cement (Conwy Valley Systems Ltd., 2011). Three hundred points were counted on each section and the results are summarized in Appendix VI.

Plug samples from both outcrop and core were drilled and sent to Weatherford International in Golden, Colorado for porosity and permeability testing via helium expansion. Core plugs were taken from GRL core MW5-LGR in Bexar County using a drill press with a diamond-tipped, 2.54 cm-diameter core bit (Appendix VI). Outcrop plugs were taken in Kendall

County using a cordless hand drill fitted with a 1.91 cm-diameter diamond core bit and water coolant tank (Appendix VI). Helium expansion testing used Boyle's law to determine the porosity, permeability, and grain volume of a sample under 400 psi confining pressure (Winters et al., 1999). Results for porosity testing included ambient and neutron capture gamma-ray spectroscopy porosity, air and Klinkenberg permeability, and grain density.

4.0 Results

4.1 Lithofacies

In the study area, the GRL is subdivided into nine end-member lithofacies listed in deceasing order of relative abundance: (1) nodular and massive marly wackestone–packstone (Nwp); (2) cross-bedded argillaceous wackestone–packstone (Cwp); (3) fossiliferous grainstone (Fgs); (4) evaporitic mudstone (Ems); (5) *Corbula* packstone–grainstone (Cpg); (6) rudist-dominated floatstone (Rdf); (7) rudist-dominated bafflestone (Rdb); (8) laminated calcareous mudstone (Lcm); and (9) carbonate-cemented sandstone (Ccs). Lithofacies characteristics are summarized in Table 1 and illustrated in Figures 3 and 4. The described lithofacies are specific to the study area and do not include the full extent of previously published depositional environments for the GRL (e.g., Lozo and Stricklin, 1956; Behrens, 1965; Perkins, 1974; Pittman, 1989; Mancini and Scott, 2006).

4.2 Ichnology

Ichnofossils are common in the GRL and are pervasive within most beds on the Central Texas Platform. Marine organisms react to a variety of physicochemical factors such as substrate composition, nutrient availability, salinity, turbidity, temperature, and oxygen (e.g., Ekdale and

Bromley, 1984a,b; Bromley and Ekdale, 1986; Uchman, 1995). Ichnofossils are listed in decreasing relative order of abundance and include: (1) *Thalassinoides*; (2) *Palaeophycus*; (3) *Planolites*, (4) *Ophiomorpha*, (5) rhizoliths, (6) *Serpulid* traces, and (7) *Cruziana*. The relationships between ichnofossils and lithofacies are summarized in Table 1.

4.2.1 Thalassinoides isp. (Fig. 5A–C)

Thalassinoides are unlined, three-dimensional boxworks of cylindrical burrows. These traces range from ~0.5–2.5 cm in diameter within the GRL. Some burrows are >4 cm in diameter due to solution enhancement in locations proximal to karstic features. Infill of burrows is similar to surrounding matrix or overlying beds and may consist of mudstone or wackestone–grainstone. *Thalassinoides* in the GRL are commonly multigenerationally tiered, with burrow density decreasing upsection in individual beds (Bromley and Ekdale, 1986). These networks comprise the majority of ichnofossils in all GRL lithofacies, but are most prevalent in wackestone–packstone facies. Cunningham and Sukop (2012) showed that abundant *Thalassinoides* ichnofabrics in the Edwards Group affected lateral fluid flow within beds, but the mudstone and siliciclastic sediment within the GRL complicates such direct interpretations. Computer modeling has also shown that *Thalassinoides* networks begin to continuously interconnect when burrows comprise as little as ~10% of the strata (La Croix et al., 2012). These *Thalassinoides* networks provide the majority of bioturbation-influenced fluid pathways within the GRL.

4.2.2 Palaeophycus isp. (Fig. 5D)

Palaeophycus are mud-lined, cylindrical burrows with infill similar to the matrix or overlying unit. These traces range from 0.5–2.0 cm in diameter within the GRL. The mud lining

Table 1. Lithofacies within the Glen Rose Limestone

Code	Lithofacies Name	Lithology and Sedimentary Structures	Thickness	Porosity	Ichnofossils	Bioturbation
Nwp	Nodular and massive marly wackestone–packstone (Figs. 3A–B)	Gray–tan, wackestone–packstone containing mostly shell fragment clasts. Clasts include foraminiferans, gastropods, bivalves, mollusks, and echinoid shells. Few sedimentary structures present. Appears nodular in outcrop.	0.1–1.8 m	Fracture, moldic, and shelter. 8–35% matrix porosity.	*Thalassinoides*, *Ophiomorpha*, *Palaeophycus*, *Planolites*, rhizoliths, Serpulid tubes	ii3–6
Cwp	Cross-bedded argillaceous wackestone–packstone (Figs. 3C–D)	Gray, argillaceous wackestone–packstone containing whole and very fine- to medium-grained fragmentary shell clasts. Shells include gastropod, bivalve, mollusk, and echinoid shells. Contains low-angle trough cross-beds and some laminations. Iron staining and dendrites are common.	0.2–0.4 m	Biotutbation-infl uenced, fracture, moldic, shelter, fenestral, and interparticle. 8–23% matrix porosity.	*Thalassinoides*, *Ophiomorpha*, *Palaeophycus*, *Planolites*, rhizoliths, Serpulid tubes, *Cruziana*	ii1–3
Fgs	Fossiliferous grainstone (Fig. 3E)	Gray–tan, grainstone consisting of shell fragments and submarine calcite cement. Clasts include gastropod, and echinoid shell fragments. Commonly massive, but some beds contain low-angle to trough crossbedding. Dendrites and pervasive iron staining are common.	0.5–1.3 m	Intergranular and fracture. 3–35% matrix porosity.	None	ii1
Ems	Evaporitic mudstone (Fig. 4A)	Gray–tan, carbonate mudstone with boxwork crystalline gypsum and anhydrite.Clasts rare, but contains some bivalve, gastropod, and echinoid shell fragments and whole *Orbitolina minuta*. Little to no primary sedimentary structures. Commonly massive and convoluted.	< 1 m	Fracture and moldic. 14–22% matrix porosity.	*Planolites*	ii1–2
Cpg	Corbula packstone–grainstone (Figs. 4B–C)	Dark gray to brown, packstone–grainstone composed of mostly Eoursivivas harveyi. Rare fragmented ostracods and bivalve shells, fecal pellets, and some whole *Orbitolina texana*. Commonly has a red tint due to iron staining. May contain ripples and climbing ripples. Composed of 1–3 individual beds of this faciesfound regionally over the entire Central Texas Platform.	<0.25 m	Intergranular. 20–24% matrix porosity.	None	ii1

Table 1. Lithofacies within the Glen Rose Limestone

Code	Lithofacies Name	Lithology and Sedimentary Structures	Thickness	Porosity	Ichnofossils	Bioturbation
Rdf	Rudist-dominated floatstone	Gray–tan, floatstone with clasts consisting primarily of whole and fragmentary rudist shells. Rudists are mostly *Caprinid* sp., but also contains *Toucasia* sp. and *Monoplurid* sp. Little to no sedimentary structures and clasts are in random orientations. Beds may dip up to 12°.	0.2–1.8 m	Fracture, moldic, and bedding plane. ~20% matrix porosity.	*Palaeophycus*, *Planolites*	ii1–2
Rdb	Rudist-dominated bafflestone (Fig. 4D)	Gray–tan, calcareous mudstone with vertically oriented rudist shells. Rudists are mostly *Caprinid* sp., but also contains *Toucasia* sp. and *Monoplurid* sp.Vertically-oriented Caprinids may be anchored to recumbent Caprinids within floatstones as well as gastropods and bivalves within wackestones–packstones.	0.3–1.5 m	Fracture and moldic. ~28% matix porosity.	*Palaeophycus*, *Planolites*	ii1–2
Lcm	Laminated calcareous mudstone (Fig. 4E)	Gray–dark gray, calcareous mudstone with <10% very fine- to fine-grained biogenic clasts. Clasts include bivalve and ostracod shell fragments, charophytes, and some foraminiferans. contains serpulid worm tubes and algal borings on some shell fragments.	~0.75 m	Fracture. ~28% matrix porosity	*Planolites*, Serpulid tubes	ii1–2
Ccs	Carbonate-cemented sandstone (Fig. 4F)	Brown–tan, very fine- to fine-grained sandstone with carbonate cement. Iron staining and dendrites are common. Contains whole and fragmented bivalves and gastropod shells.	< 0.5 m	Moldic and intergranular. ~28% matrix porosity.	*Thalassinoides*, *Palaeophycus*, *Planolites*, rhizoliths	ii1–6

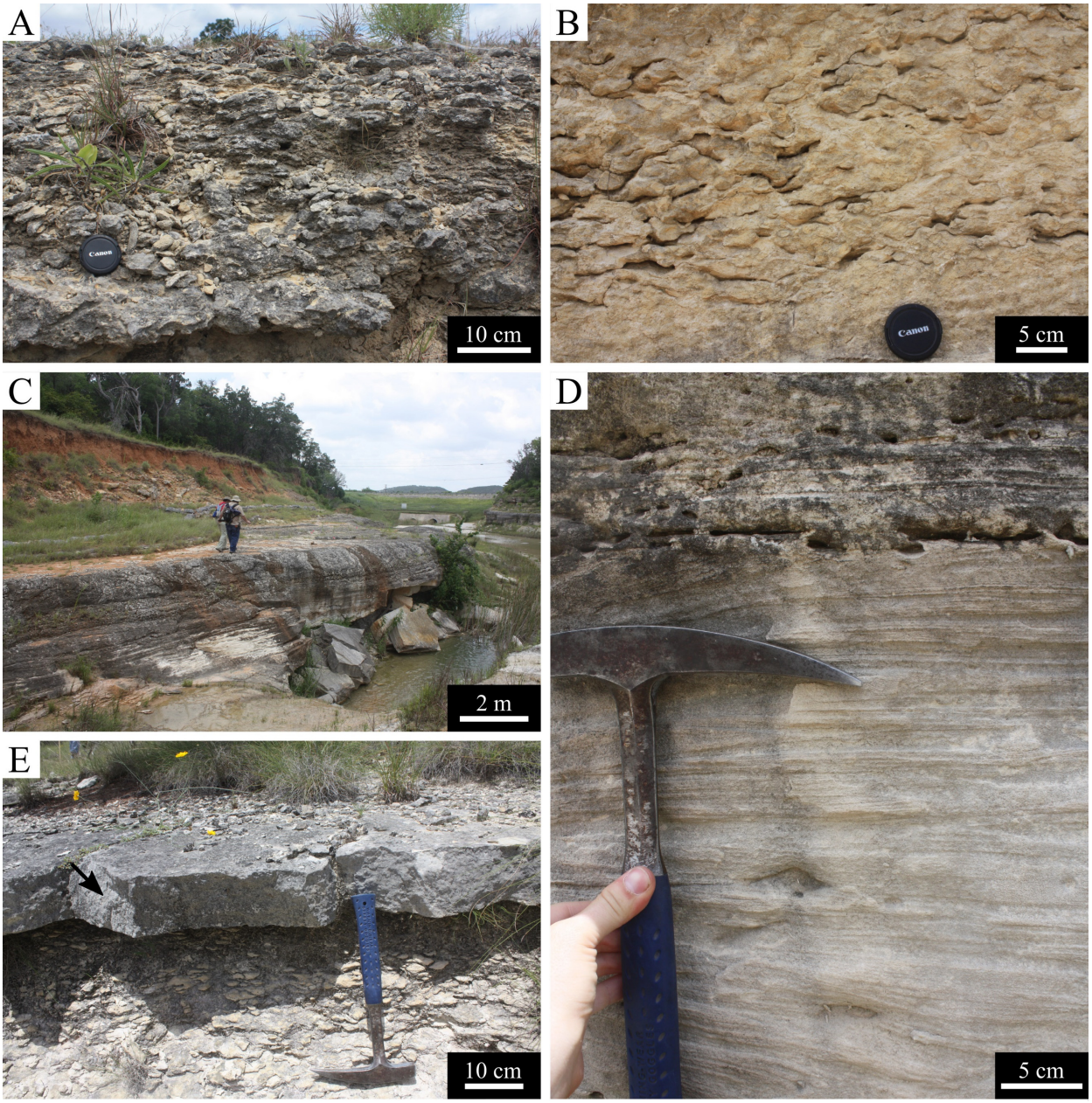

Figure 3. Lithofacies of the Glen Rose Limestone within the study area. A) Weathered outcrop section of nodular and massive marly fossiliferous wackestone–packstone. B) Roadcut section showing a detailed, unweathered face of nodular and massive marly fossiliferous wackestone–packstone. C) Outcrop of bedded and crossbedded argillaceous fossiliferous wackestone–packstone with low-angle crossbedding. D) Close-up photograph of bedded and crossbedded argillaceous fossiliferous wackestone–packstone showing low angle crossbedding. E) Outcrop of well indurated, ledge-forming fossiliferous grainstone (arrow) with a sharp basal contact above a nodular, marly fossiliferous wackestone–packstone.

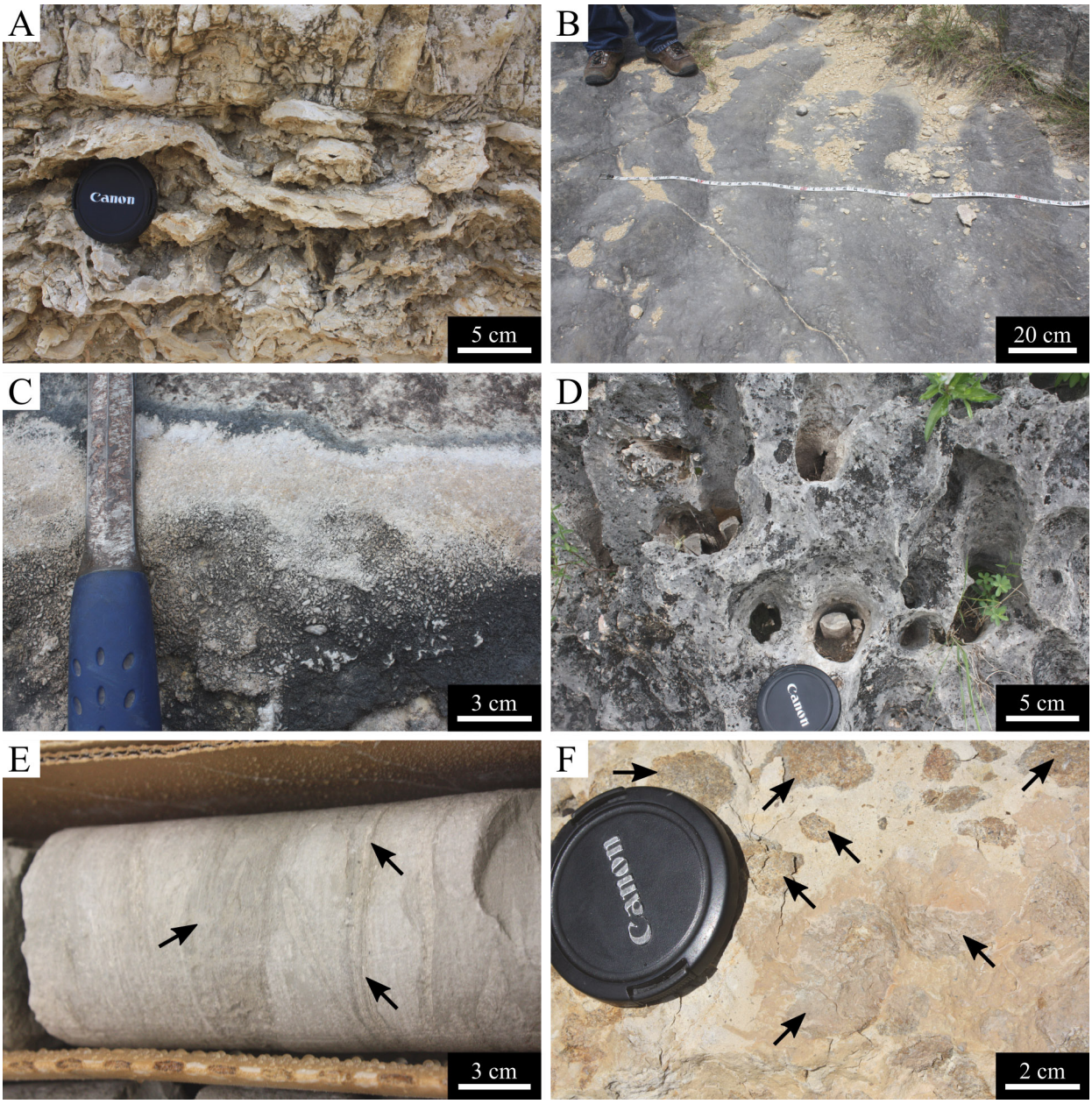

Figure 4. Lithofacies of the Glen Rose Limestone within the study area (continued). A) Weathered outcrop of boxwork gypsum and mudstone within evaporitic mudstone facies. B) Symmetrical ripples in *Corbula* packstone–grainstone facies. Top of bed shown in photograph is the contact between the Upper and Lower Glen Rose Limestone. C) Close-up photograph of *Corbula* packstone–grainstone facies showing detailed *Eoursivivas harveyi* shells. D) *Caprinid* sp. in life position within rudist-dominated bafflestone facies. E) Laminated calcareous mudstone in core MW6-LGR with convoluted laminae (arrows). F) Carbonate-cemented sandstone with brecciated limestone clasts (arrows).

is thin (~1 mm), micritic, and commonly dark yellow (Fig. 5D). *Palaeophycus* are commonly found associated with, and have similar sediment infill to, *Thalassinoides* networks. The infill within the traces shows no evidence of active backfilling such as meniscae and was likely deposited with overlying sediment. *Palaeophycus* is most often found overlaying significant *Thalassinoides* networks in beds with less bioturbation. Because of their similar morphology to and proximal association with *Thalassinoides*, these *Palaeophycus* were likely made by the same tracemakers. *Palaeophycus* are commonly found above *Thalassinoides* networks in marly wacketone-packstone facies. *Palaeophycus* commonly have coarse-grained, permeable infill and likely act as fluid pathways.

4.2.3 Planolites isp. (Fig. 5E–F)

Planolities are unlined, mud-filled, cylindrical burrows oriented parallel to bedding planes (Fig. 5E). These burrows vary in diameter slightly along their length and range from 0.2–1.5 cm in diameter. *Planolites* are commonly found isolated from *Thalassinoides* networks within beds with relatively low bioturbation. The matrix of these beds varies from mudstone to packstone and is commonly argillaceous, though *Planolites* is found associated with detrital conglomeratic material in one bed (Fig. 5F). *Planolites* have smooth walls and rarely branch or overlap. The infill of *Planolites* is muddy and distinct in color and fabric from the surrounding matrix and overlying units. The muddy infill of *Planolites* within the GRL means that they will act as fluid barriers. They are common in beds near the top of the Lower GRL and likely do not play a significant role in overall fluid flow.

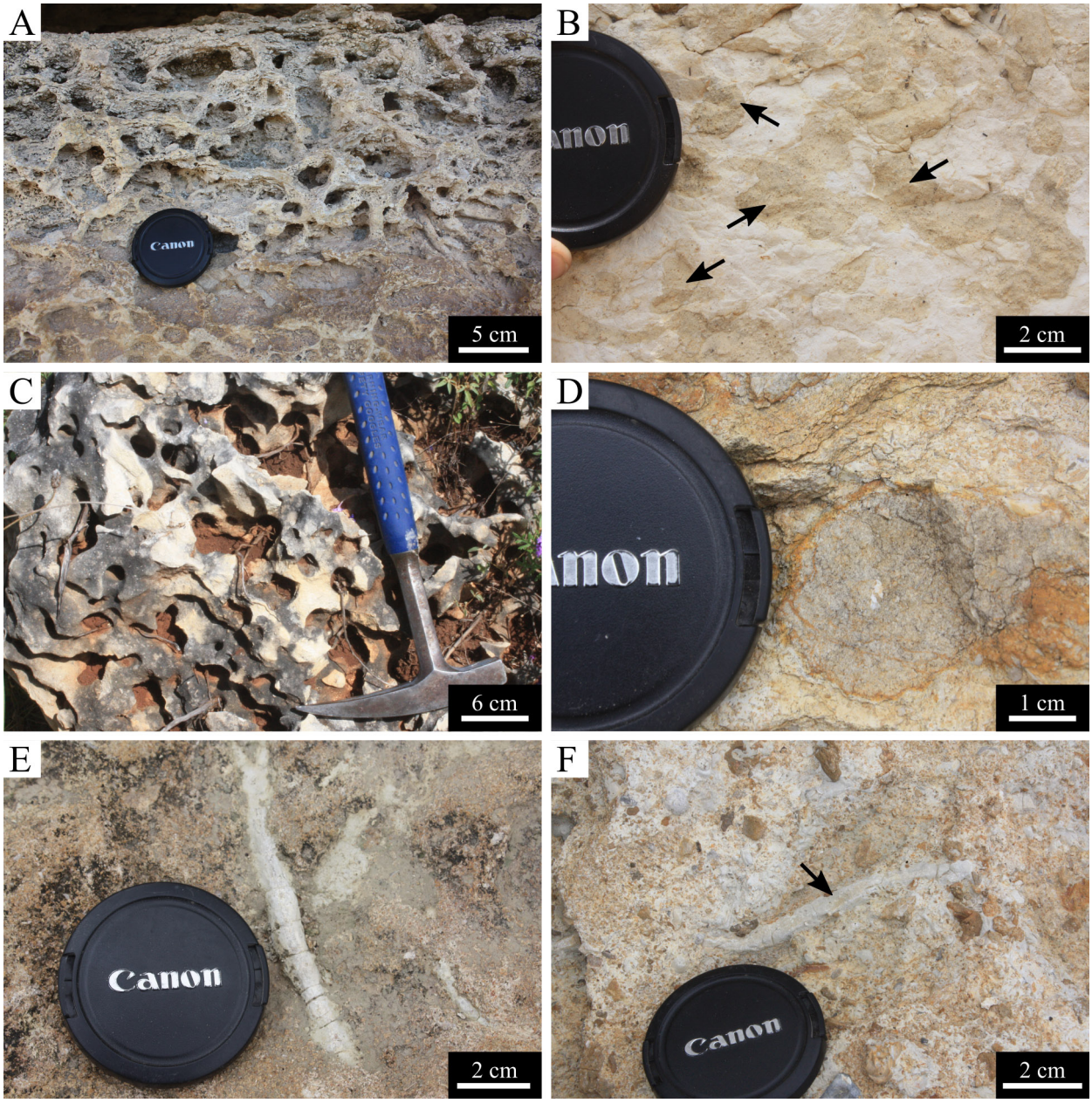

Figure 5. Ichnofossils of the Glen Rose Limestone within the study area. A) *Thalassinoides* network with packstone infill dominated by skeletal grains of the foraminfera *Orbitolina texana.* Matrix around the burrows has been weathered out following exposure, but was originally mudstone. B) Solution-enhanced *Thalassinoides* network with packstone infill within a wackestone matrix (arrows). Packstone infill is fossiliferous and similar to overlying wackestone–packstone strata. C) *Thalassinoides* network with solution-enhanced open burrows throughout the strata. D) *Palaeophycus* with packstone infill and a distinct, brown-tan oxidized mud lining. Found in association with *Thalassinoides* networks. E) *Planolites* with distinct, light-colored mudstone infill oriented parallel to bedding surface within a wackstone matrix. F) *Planolites* with distinct, light-colored mudstone infill (arrow) within a conglomeratic matrix containing detrital clasts.

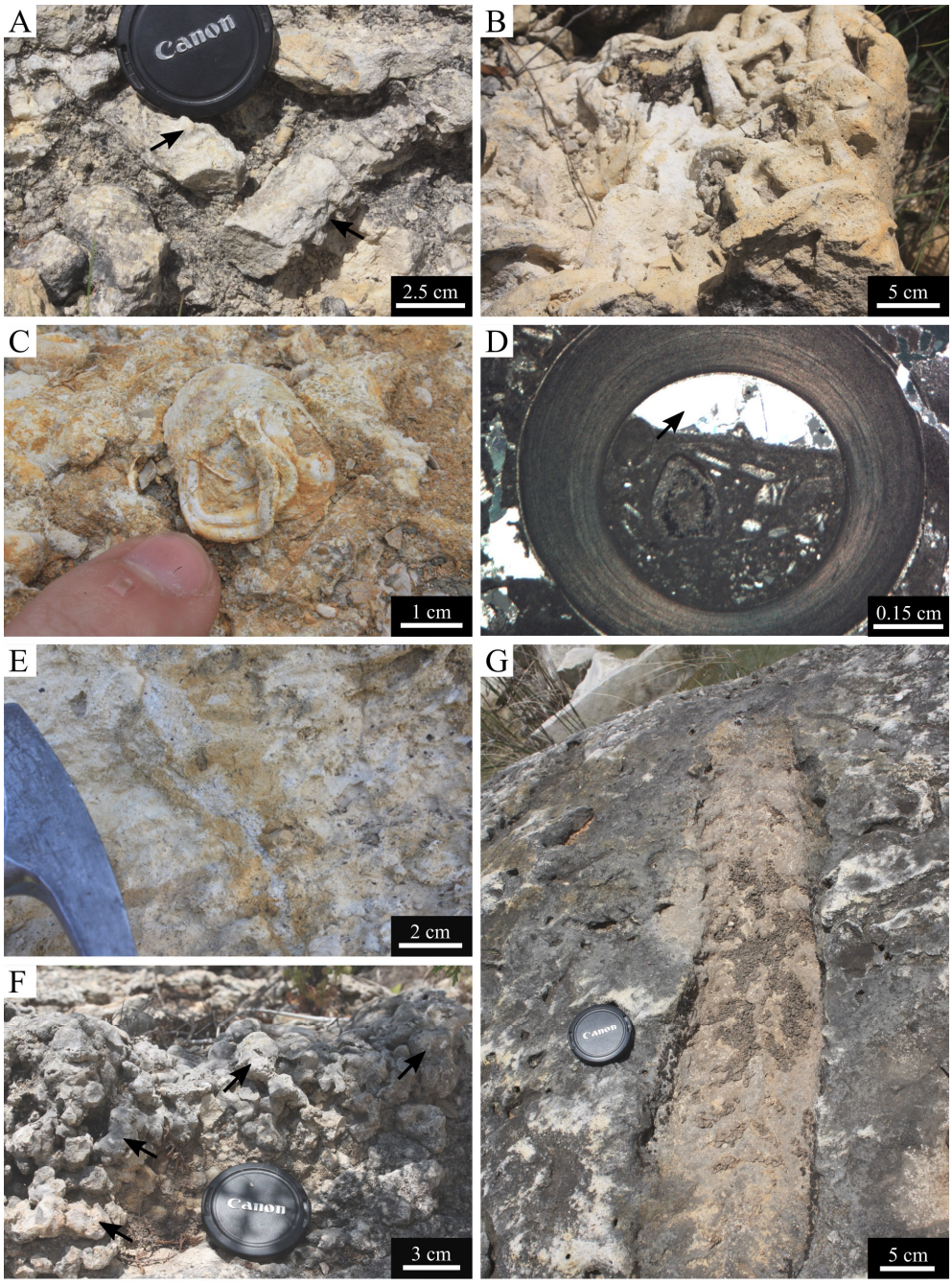

Figure 6. Ichnofossils of the Glen Rose Limestone within the study area. A) *Ophiomorpha* within a packstone matrix with similar packstone infill. Pellets are visible around the burrow (arrow) B) *Ophiomorpha* with branching networks and weathered-out matrix due to subaerial exposure. C) Serpulid tube on a bivalve shell showing typical coiled morphology. D) Thin-section pictomicrograph of a serpulid tube from core MW9-CC showing cement coating and laminated mud infill. Growth of sparry cement acts as a geopetal (arrow). E) Rhizolith and rhizohalo within a highly bioturbated (ii5) marly wacketone. F) Spherical rhizocretions formed around roots and root hairs indicating abundant plant growth during subaerial exposure (arrows). G) *Cruziana* oriented along a bedding surface and indicating firmground–hardground conditions. This *Cruziana* is ~13.0 cm wide and ~59.3 cm long; lens cap is 5.7 cm in diameter.

4.2.4 Ophiomorpha isp. (Fig. 6A–B)

Ophiomorpha are pellet-lined, cylindrical burrows that may branch and range from 2.5–3.0 cm in diameter (Fig. 6A). Burrow infill is similar to surrounding matrix and pellets are composed of mud, but may contain various small clasts. *Ophiomorpha* are commonly horizontally-oriented, found associated with *Thalassinoides* networks, and may grade into unlined burrows within units. Similar to *Thalassinoides*, *Ophiomorpha* may branch and be multigenerationally tiered (Fig. 6B; Bromley and Ekdale, 1986). These ichnofossils are found within higher-energy crossbedded wackestone-packstone facies in the Upper GRL and within units with larger clast sizes on average. These traces were likely made by the same tracemaker as *Thalassinoides* and *Palaeophycus*. The mud pellets are simple peloids and are created by the tracemaker to increase the structural integrity of the burrow (Uchman, 1995; Vaziri and Fürsich, 2000). Many *Thalassinoides* burrows within the GRL may have originally been *Ophiomorpha*, but have been altered by subsurface and meteoric water flow, removing evidence of the pelleted lining (Bromley and Frey, 1974; Myrow, 1995). Also similar to *Thalassinoides,* these traces likely act as significant fluid pathways in both the Upper and Lower GRL, particularly within crossbedded strata. Additionally, *Ophiomorpha*-dominated ichnofabrics have been shown to be the primary hydrologic driver of the similar karstic Biscayne aquifer of southern Florida (Cunningham et al., 2009)

4.2.6 Serpulid tubes (Fig. 6C–D)

Serpulid tubes are carbonate cement-lined, cylindrical, coiled tubes filled with mudstone that are oriented parallel to bedding planes. Single tubes may be tens of cm long and may coil on themselves several times (Fig. 6C). The tubes have a distinct brown-tan color with transverse

striations and mud infill that is concentrically laminated (Fig. 6D). Serpulid tubes are commonly found attached to bivalve and gastropod shells. The tubes may have been filled with sediment after burial and the presence of sparry infill acts as a geopetal in thin section (Fig. 6D). Similar modern tubes are created by annelid worms of the genus *Serpula* (Vinn et al., 2008). These tubes are found within muddy, fossiliferous units that consist primarily of nodular marly wackestone and packstone and play a very minor role in fluid flow.

4.2.5 Rhizoliths (Fig. 6E–F)

Root traces have several different forms within the GRL, and include rhizoliths, rhizohaloes, and rhizocretions. Generally, these are tapered traces that extend downward from subaerial exposure surfaces into underlying strata and may crosscut underlying bedding surfaces. True rhizoliths are found in muddy units and have distinct downward tapering morphologies and wood-like textures in cross-section (Fig. 6E). Some rhizoliths have a light-colored rim around the entire structure called rhizohaloes (Fig. 6E). Some beds show light colored discoloration interpreted to be rhizohaloes with no remaining fossilized woody material. Rhizocretions have a nodular texture that appears as interlocking and overlapping spheres that contain root hair traces in cross section (Fig. 6F). Nodular beds showing rhizocretions are typically <0.5m thick. Rhizoliths are associated with only insipient soil development in the study area, but enough development to concentrate clay minerals via illuviation in subaerially exposed horizons (Kraus and Hasiotis, 2006; Smith et al., 2008; Hasiotis and Platt, 2012). Beds and surfaces suggesting subaerial exposure and showing rhizoliths are rare in the study area, but previous studies have shown that such beds increase in abundance northward on the Central Texas Platform (Lozo and

Stricklin, 1956; Perkins, 1974; Ward and Ward, 2007). Rhizoliths are therefore potential hydrologic indicators as the increased amount of clay may act as a barrier to fluid flow.

4.2.7 Cruziana isp. (Fig. 6G)

Cruziana are bilobate furrows with a medial ridge and transverse, ridged striations that gently curve back away from the direction of travel. *Cruziana* traces in the GRL average ~13 cm wide and range from 47.4–59.3 cm long (Fig. 6G). These furrows are ~2–3 cm deep with preserved mounding and drag marks along the sides of trace. All observed *Cruziana* are associated with crossbedded wackestone–packstone at a single location in Comal County and several of the traces overlap on a single bedding surface. Other ichnofossils, such as *Thalassinoides,* are relatively rare in the associated strata. The tracemaker for these *Cruziana* in the GRL has previously been interpreted as horseshoe crabs (Ward and Ward, 2007). This study; however, interprets the tracemaker as a different large arthropod or possible isopod because horseshoe crab trackways generally lack distinct scratch marks such as the curved striations seen in these trackways, but commonly have individual limb traces (Babcock et al., 2000). Although these traces are associated with otherwise transmissive facies, the location of these trackways along bedding planes and their limited preserved extent indicates that these ichnofossils have no effect on fluid flow.

4.3 Ichnofabric index analysis

The GRL is muddy and has low intergranular porosity; therefore, fluid pathways are often larger-scale features such as faults and fractures, ichnofossils, and molds. Ichnofabric indices (ii), as a measure of ichnofossil density and overall bioturbation, can be used as

hydrologic indicators within the GRL and similar karstic aquifers (Fig. 7). An ii1 unit will have no bioturbation (Droser and Bottjer, 1986) and fluid flow will be restricted to intergranular porosity if faults and karstic development are not present. Beds with ii2 have less than 10% of their total volume bioturbated; such beds within the GRL commonly contain *Palaeophycus, Planolites,* and visible sedimentary structures (Fig. 7A). Beds with ii3 have 10–40% percent of their total volume bioturbated; most GRL ii3 beds are dominated by *Thalassinoides* networks and have few to no visible sedimentary structures (Fig. 7A). Beds in the GRL that are ii4 have 40–60% of their total volume bioturbated, are dominated by *Thalassinoides* networks, and generally have no sedimentary structures visible (Fig. 7B). Beds with ii5 have over 60% of their volume bioturbated; some individual *Thalassinoides* are visible within these beds (Fig. 7C). Beds that are completely homogenized and nodular in appearance are assigned to ii6 and dominated by cryptobioturbation (Fig. 7D).

Thalassinoides-dominated ichnofabrics become interconnected throughout beds at ii3 and above (La Croix et al., 2012). Beds within the wackstone-packstone facies in the GRL that have ii3–4 contain *Thalassinoides* networks that may act as fluid pathways. In fine-grained facies; however, *Thalassinoides* are often infilled with mud and do not increase overall porosity. Beds that are ii5–6 are generally homogenized and do not transmit fluids easily. Ichnofabric index must therefore be examined in conjunction with lithology, porosity, and permeability characteristics of strata to infer whether beds are transmissive or confining. The ii trends, porosity characteristics, and interpreted transmissivity within the individual HSUs of the Lower and Upper GRL are described below (Fig. 8) and summarized in Table 1.

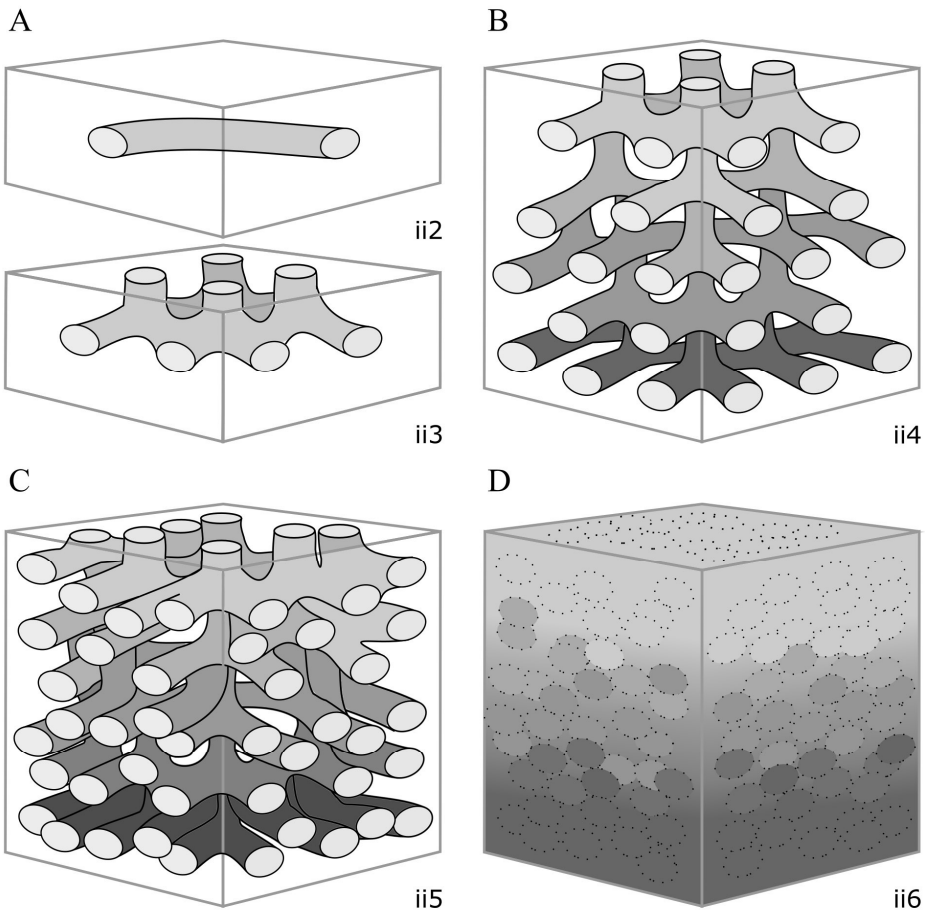

Figure 7. Model of ichnofabric index (ii) progression in *Thalassinoides*-dominated Glen Rose Limestone strata based on the scheme of Droser and Bottjer (1986). A) Top shows a single bed with ii2 and *Palaeophycus* and bottom shows the development of an untiered *Thalassinoides* network with ii3. B) Bed with ii4 and interconnected *Thalassinoides* network. C) Further development of a tiered *Thalassinoides* network over time leading to ii5 and nodular bedding. D) Further development of *Thalassinoides* networks leading to completely homogenized sediment with ii6

4.3.1 Lower Glen Rose Limestone

The Lower GRL is primarily characterized by coarsening-upward successions of marly wackestone to packstone facies that grade laterally into discontinuous rudist-dominated bafflestone and floatstone facies (Fig. 8). The Lower GRL has been subdivided into six HSUs, which have been designated as either transmissive or confining based on porosity characteristics,

as well as lithology (Table 1; Clark et al., 2014; Clark and Morris, 2015). Generally, transmissive units have been defined based on the presence of wide-spread fracture porosity and karstic development; however, trends in bioturbation-influenced porosity can also be seen in these units (Clark et al., 2014) The Lower GRL includes, from stratigraphically lowest to highest, the Honey Creek, Rust, Doeppenschmidt, Twin Sisters, Little Blanco, and Bulverde HSUs.

Transmissive HSUs—Lower GRL transmissive units include the Honey Creek, Doeppenschmidt, and Little Blanco HSUs. These HSUs consist of tidal-dominated, m-scale successions of coarsening-upward nodular and massive marly wackestone–packstone beds with ii4–5 and some identifiable *Thalassinoides* networks (Table 2; Fig. 9). These successions grade upsection into marly wackestone–packstone with ii3–4 characterized by open and wackestone–packstone-filled *Thalassinoides* networks. Some beds of laminated calcareous mudstone with ii1 are located at the base of successions and grade upsection into the more typical nodular wackestone with ii4–5 (Table 2; Fig. 9). In some locations, transmissive HSUs grade laterally into discontinuous patch reefs consisting of rudist-dominated floatstone and bafflestone having ii1–ii2, with some *Planolites* observed in the mudstone matrix of floatstones. Although the tidal-dominated strata of transmissive HSUs have less permeability than the rudist facies, bioturbation-influenced porosity is likely connected throughout the units and is a major component of this unit's transmissivity.

While transmissive strata share the above characteristics, unique features are observed in each HSU. The bottom ~6.7 m of the Honey Creek HSU (Fig. 9) consists of the typical successions described; however, the top ~3 m of the unit has lower ii and consists of interbedded laminated calcareous mudstone and nodular wackestone with ii1–2 and containing *Palaeophycus* with some *Thalassinoides* networks. While defined as a transmissive unit, most of the

Table 2. Properties of Glen Rose Limestone hydrostratigraphic units

Hydrostratigraphic Unit	Lithofacies	Ichnofossils	Transimissivity	Bioturbation-influenced Permeability
Cavernous	Nwp	*Thalassinoides*	Transmissive	High
Camp Bullis	Nwp, Fgs, Lcm	*Thalassinoides, Ophiomorpha, Palaeophycus,* rhizoliths	Semi-confining	High
Upper Evaporite	Ems	*Planolities*	Transmissive	Very low
Fossiliferous	Nwp, Lcm, Rdf, Rdb	*Thalassinoides, Ophiomorpha, Palaeophycus,* rhizoliths, Serpulid tubes	Semi-confining	High
Lower Evaporite	Ems	*Planolities*	Transmissive	Very low
Bulverde	Nwp, Cwp, Cpg, Lcm, Rdf, Rdb	*Thalassinoides, Palaeophycus, Planolites, Cruziana,* rhizoliths	Semi-confining	Moderate
Little Blanco	Nwp, Cwp, Rdf, Rdb	*Thalassinoides, Palaeophycus, Planolites*	Transmissive	High
Twin Sisters	Nwp, Rdf, Rdb	*Thalassinoides*	Confining	Low
Doeppenschmidt	Nwp, Lcm, Rdf, Rdb	*Thalassinoides, Palaeophycus*	Transmissive	High
Rust	Nwp, Rdf, Rdb	*Thalassinoides, Palaeophycus, Planolites*	Confining	Low
Honey Creek	Nwp, Lcm, Rdf, Rdb, Ccs	*Thalassinoides, Palaeophycus, Planolites*	Transmissive	High

bioturbation-influenced porosity of the Honey Creek HSU appears to be restricted to the bottom 6.7 m of the unit in beds with ii3–4. Most fracture and karstic development also appears in the lower portions of the Honey Creek HSU (Clark and Morris, 2015). The Doeppenschmidt HSU

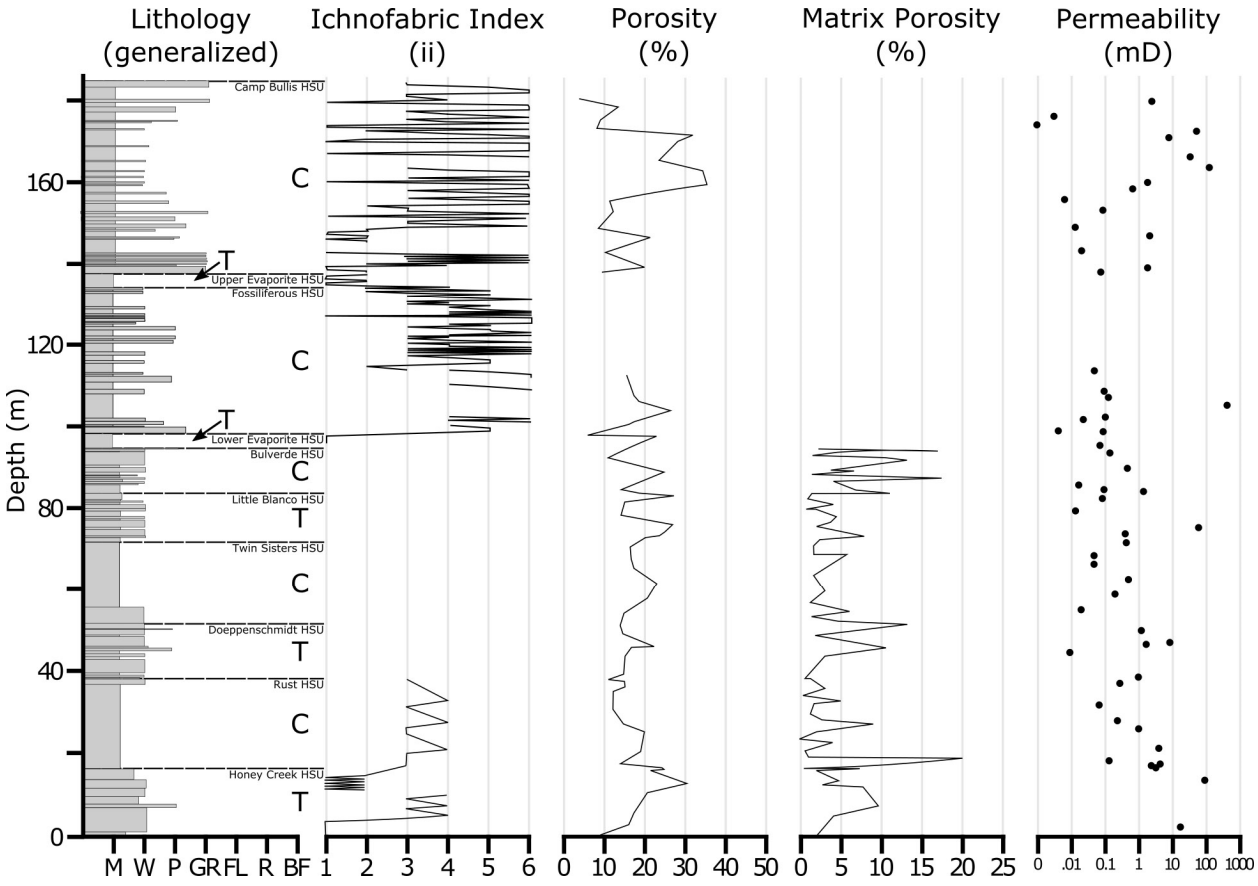

Figure 8. . Chart showing overall dataset for the Glen Rose Limestone within the study area including: composite stratigraphic section, porosity and permeability data from He-expansion testing, matrix porosity from point counted data. Hydrostratigraphic units are designated as either transmissive (T) or confining (C) according to Clark (2003) and Clark and Morris (2015). Porosity and permeability data from He-expansion testing in Lower Glen Rose Limestone core MW5-LGR modified from Blome and Clark (2014). Uppermost Cavernous hydrostratigraphic unit not shown on column as it is not present in outcrop within the study area.

also consists of wackestone–packstone facies typical of transmissive units, but contains less mud than the Honey Creek HSU and should have higher permeability as a result (Fig. 8). The Little Blanco HSU contains some successions that grade upward into crossbedded wackestone–packstone with ii1–2. Therefore, fluid flow is restricted to intergranular porosity and is low in these less-bioturbed units. Additionally, fluid flow is also likely restricted in the top ~1.8 m of

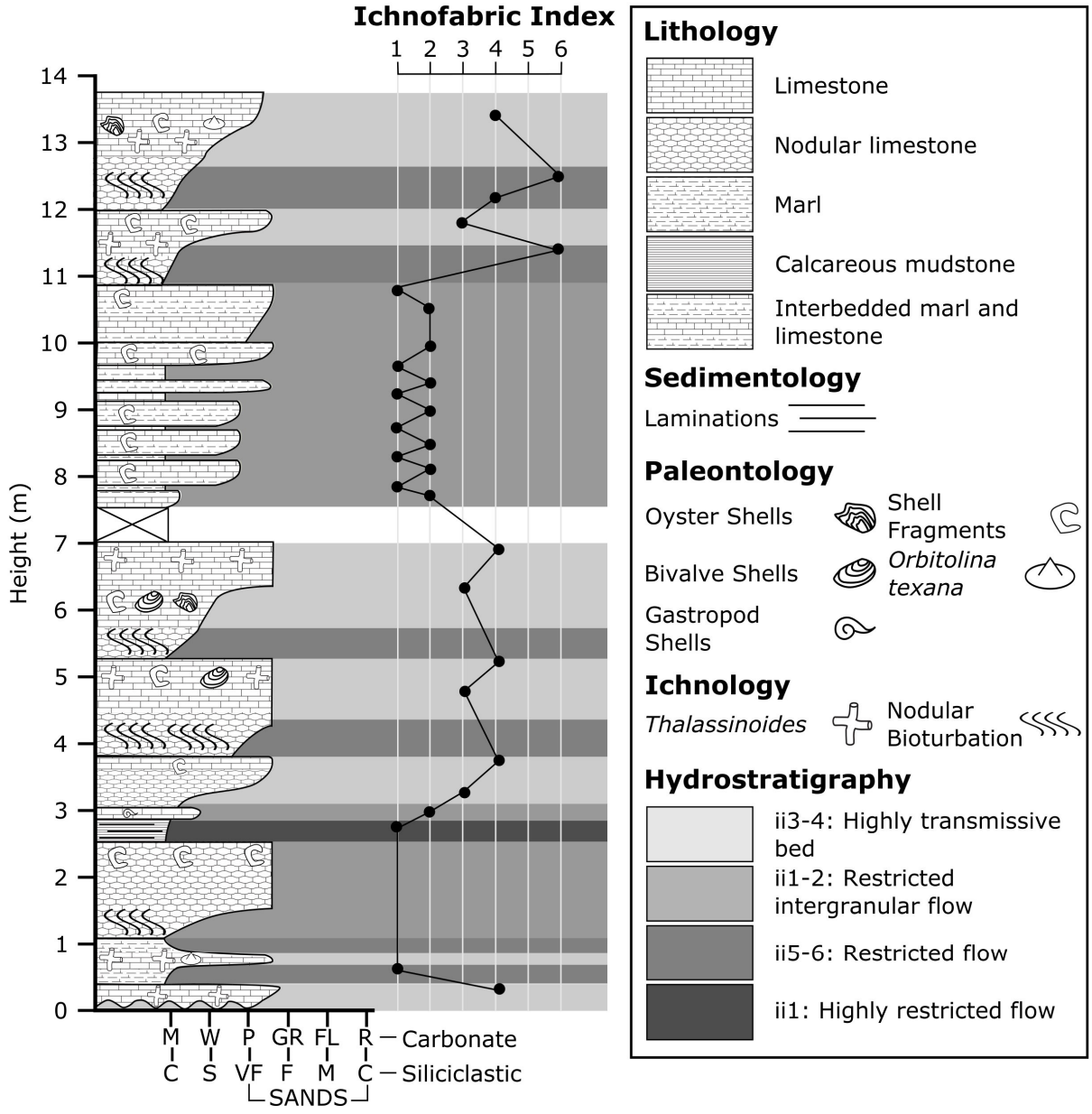

Figure 9. Stratigraphic column from the Lower Glen Rose Limestone (GRL) Honey Creek hydrostratigraphic unit in Hays County, Texas showing the typical coarsening-upward successions and ichnofabric index (ii) patterns seen in Lower GRL transmissive units. Interpretations of fluid-flow characteristics shown under Hydrostratigraphy.

the Little Blanco HSU where muddier wackestone units are interbedded with ii1–2 laminated calcareous mudstone.

Confining HSUs— Lower GRL confining units consist of the Rust, Twin Sisters, and Bulverde HSUs (Fig. 8). Confining HSUs usually consist of m-scale beds of nodular, marly wackestone with ii5–6 that are thoroughly homogenized by pervasive cryptobioturbation with some identifiable *Thalassinoides* (Table 2; Fig. 10). Unlike transmissive HSUs, confining units generally do not display coarsening upward trends, contain more mud, and show less fracture porosity. Similar to transmissive units, confining HSUs in some locations grade laterally into discontinuous patch reefs consisting of rudist-dominated floatstone and bafflestone having ii1–ii2 (Fig. 8). These patch-reefs have high moldic and fracture porosity, but because of their lateral isolation within otherwise confining strata they cannot transmit water within the HSU. These patch reefs may; however, transmit water vertically between transmissive units (Hunt and Smith, 2010).

While the Twin Sister HSU is typical of these confining units (Fig. 10), the Rust HSU displays some coarsening upward successions similar to transmissive units. Burrow infill in the Rust HSU ranges from wackestone–packstone, and the uppermost beds contain *Palaeophycus* and mud-filled *Planolites*. These mud-filled ichnofossils in the Rust HSU do not increase bioturbation-influenced porosity as much as seen in transmissive units. The Bulverde HSU is complex—it consists mainly of coarsening-upward successions of nodular and crossbedded wackestone–packstone with overall well-developed bioturbation-influenced porosity (ii4-5) similar to transmissive units. However, it contains interbedded laminated calcareous mudstone intervals (ii1) at the base and is capped by *Corbula* packstone–grainstone (ii1), both of which severely restrict fluid flow. Although the Bulverde HSU has been classified as a confining unit, the transmissive middle portion contains well-developed biogenic and moldic porosity and may

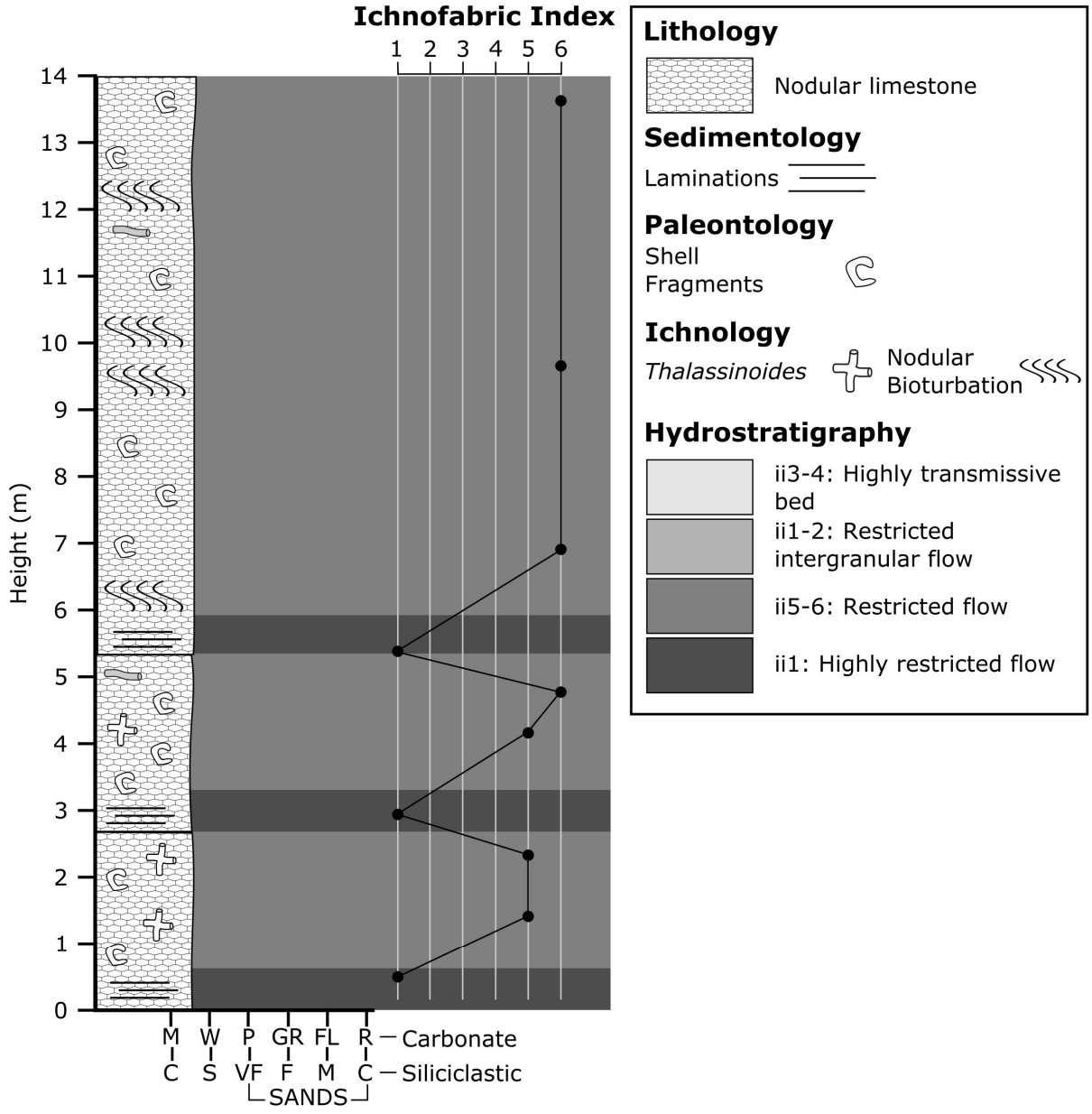

Figure 10. Stratigraphic column from the Lower Glen Rose Limestone (GRL) Twin Sisters hydrostratigraphic unit from core in northern Blanco County, Texas showing the typical marly sedimentation and ichnofabric index (ii) patterns seen in Lower GRL confining units. Interpretations of fluid-flow characteristics shown under Hydrostratigraphy.

transmit significant amounts of water. Thus, the Bulverde HSU may be better classified as a semi-confining unit.

4.3.2 Upper Glen Rose Limestone

The Upper GRL primarily consists of coarsening upward successions of marly wackestone to packstone facies similar to the Lower GRL, but contains abundant evaporites and few rudist dominated patch reefs (Table 2; Fig. 8). Conditions during the deposition of the Upper GRL appear to have never fully returned to the normal marine conditions seen in the Lower GRL after the deposition of the *Corbula* bed (Fisher and Rodda, 1969). The Upper GRL has been subdivided into five HSUs: the Lower Evaporite, Fossiliferous, Upper Evaporite, Camp Bullis, and Cavernous HSUs (Clark, 2004; Clark et al., 2009). Transmissive HSUs are associated with significant evaporitic beds and karstic development. Confining units in the Upper GRL are lithologically and ichnologically similar to transmissive units in the Lower and are interbedded with the karstic transmissive units.

Transmissive HSUs—Upper GRL transmissive units include the Lower Evaporite, Upper Evaporite, and Cavernous HSUs. These Lower Evaporite and Upper Evaporite HSUs are each ~3 m thick and characterized by evaporitic mudstone with ii1–2 and pervasive dissolution features in both evaporites and carbonates (Table 2). Both the Lower and Upper Evaporite HSUs also contain significant moldic porosity and karstic development from the dissolution of evaporitic minerals (Clark, 2004; Clark et al., 2009). These Evaporite HSUs were deposited in brackish conditions preventing wide-spread bioturbation in this unit (Fisher and Rodda, 1969).

The Cavernous HSU overlies the Camp Bullis HSU and is highly transmissive because of significant karstic and cave features present in the subsurface (Clark, 2004). Defined in core and through geophysical analysis (Clark, 2004) in northern Bexar County, TX (see Fig. 1), the Cavernous HSU is typically less than 10.5 m thick, has a limited lateral extend and is not present

at the surface through most of the study area. This HSU consists of marly wackestone–packstone successions similar to transmissive units in the Lower GRL, but has been significantly faulted and fractured. The high permeability of the overlying Edwards Group has introduced meteoric water into these faults and fractures creating karstic features (Smith et al., 2005; Clark, 2004). Pervasive solution enhancement has destroyed most evidence of bioturbation in this unit, particularly in close proximity to faults and fractures. Within the GRL, the Upper GRL HSUs display more solution enhancement due to the high infiltration rates of the overlying Edwards aquifer (Maclay, 1995; Smith et al., 2003; Clark, 2004). The steep, near vertical orientation of the Balcones Fault Zone faults has allowed for the introduction of meteoric water deep within the aquifer, which has infiltrated laterally from the faults following interconnected *Thalassinoides* networks and other ichnofossils and molds within the GRL.

Confining HSUs—The Upper GRL confining units are the Fossiliferous and Camp Bullis HSUs (Fig. 8). Similar to Lower GRL transmissive units, the Fossiliferous and Camp Bullis HSUs consist of coarsening-upward successions that grade from nodular, marly wackestone with ii5–6 dominated by pervasive cryptobioturbation to marly wackestone–packstone with ii3–4 and pervasive *Thalassinoides* networks (Table 2; Fig. 11). These *Thalassinoides* are commonly infilled with wackestone–packstone from overlying units. Additionally, sequence bases may contain thin beds of laminated calcareous mudstone with ii1. These HSUs share many similarities with the transmissive units of the Lower GRL and contain well-developed burrow and bedding-plane porosity with some fracture development (Fig. 11; Clark, 2004; Clark et al., 2009). These units, however, are significantly less permeable than the evaporitic and Cavernous HSUs because of their mud content and lack of dissolution features and fractures (Clark, 2004; Clark et al., 2009).

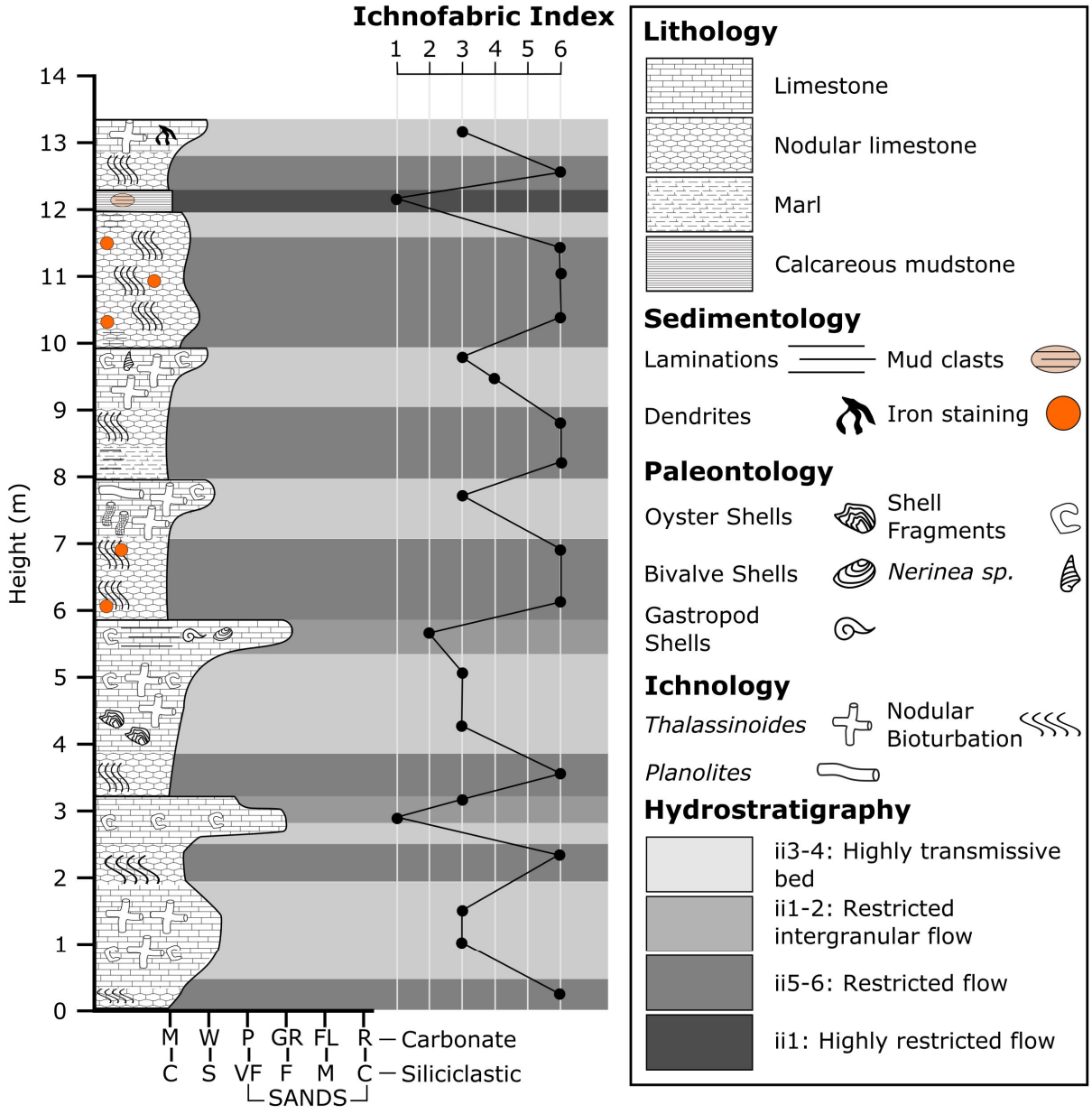

Figure 11. Stratigraphic column from the Upper Glen Rose Limestone (GRL) Camp Bullis hydrostratigraphic unit (HSU) in Kendall County, Texas showing the typical coarsening-upward successions and ichnofabric index (ii) patterns seen in Upper GRL confining units. These units have been described in this report as "semi-confining". Interpretations of fluid-flow characteristics shown under Hydrostratigraphy.

The Fossiliferous HSU is fairly muddy but coarsening-upward patterns of successions are observed, unlike most confining units in the Lower GRL. This HSU contains significant moldic

porosity due to the dissolution of shell material, as well as well-developed bioturbation-influenced porosity. This unit, however, does not transmit water as readily as the overlying and underlying evaporite units. Numerous seeps and springs are found at the top of this unit, indicating diverted flow of meteoric, similar to confining units in the Lower GRL. The Fossiliferous HSU does grade laterally into rudist patch reef strata with high fracture and moldic porosity in northern Bexar County.

The Camp Bullis HSU (Fig. 11) contains less mud than the other HSUs and successions within it grade from typical cryptobioturbated beds seen in the Fossiliferous HSU to marly wackstone–grainstone with ii3–4 with abundant *Thalassinoides* and *Ophiomorpha*. The grainstone at the top of many of these successions shows some crossbedding and has ii1 and is well-cemented leading to low intergranular porosity. Similar to transmissive units in the Lower GRL, the muddier ii5–6 beds at the base of successions in the Camp Bullis HSU likely prevent significant vertical fluid flow but water is transmitted laterally in overlying beds with ii3–4 to seeps and springs and to fractured areas.

The Fossiliferous and Camp Bullis HSUs have previously been defined as confining units because of diversion of ground and meteoric water seen at the surface of these units (Clark, 2004; Clark et al., 2009). This is likely because of the comparatively high permeability seen in the evoporitic and Cavernous HSUs, as well as the large amount of meteoric water that can quickly infiltrate the overlying Edwards Group. However, the similarity of these two units both ichnologically and lithologically to Lower GRL transmissive units and well developed porosity likely allows for the transmission of significant amounts of water. These two units may; therefore, be better described as “semi-confining HSUs”.

4.4 Solution enhancement of ichnofossils

Solution enhancement in the GRL has increased connectivity of fractures and burrows and caused autoclastic brecciation and cavern development in many cases. Multiple stages of solution enhanced features are preserved and forming in the GRL (Fig. 12). In the typical coarsening upward sequence, most ichnofossils are filled with sediment sourced from overlying strata that is coarser than the surrounding matrix. This initial condition is shown in figure 12 (T_1). This focuses water flow, particular from meteoric water, through the ichnofossil networks and will dissolve the matrix surrounding the burrow over time (Fig. 12; T_2). Meteoric water is not in equilibrium with the carbonate content of the surrounding matrix and will thus widen and further interconnect the burrow networks across the three-dimensional extent of the bed (Fig 12; T_3). These solution-enhanced burrow networks may subsequently either be filled with sediment (Fig 12; T_{4a}) or continue to have the matrix dissolved by infiltrating meteoric and ground water (Fig. 11; T_{4b}). If exposed, infilled solution enhanced burrows may weather differentially from the surrounding matrix and be preserved in positive relief (Fig. 12; T_{5a}). Alternatively, dissolution may continue until the matrix cannot support the overburden and the sediment compacts, evidenced by a bed of brecciated sediment (Fig. 11; T_{5b}).

Solution enhancement features are most significant in the GRL within close proximity to faults and fractures and in beds associated with karstic development. The Upper GRL HSUs are more solution enhanced than Lower GRL HSUs due to the high infiltration rates of the overlying Edwards aquifer (Hanson and Small, 1995; Maclay, 1995; Clark, 2004). The near vertical faults of the Balcones Fault Zone transmitted meteoric water into the subsurface where it infiltrated laterally into the strata along interconnected *Thalassinoides* networks and other ichnofossils and molds.

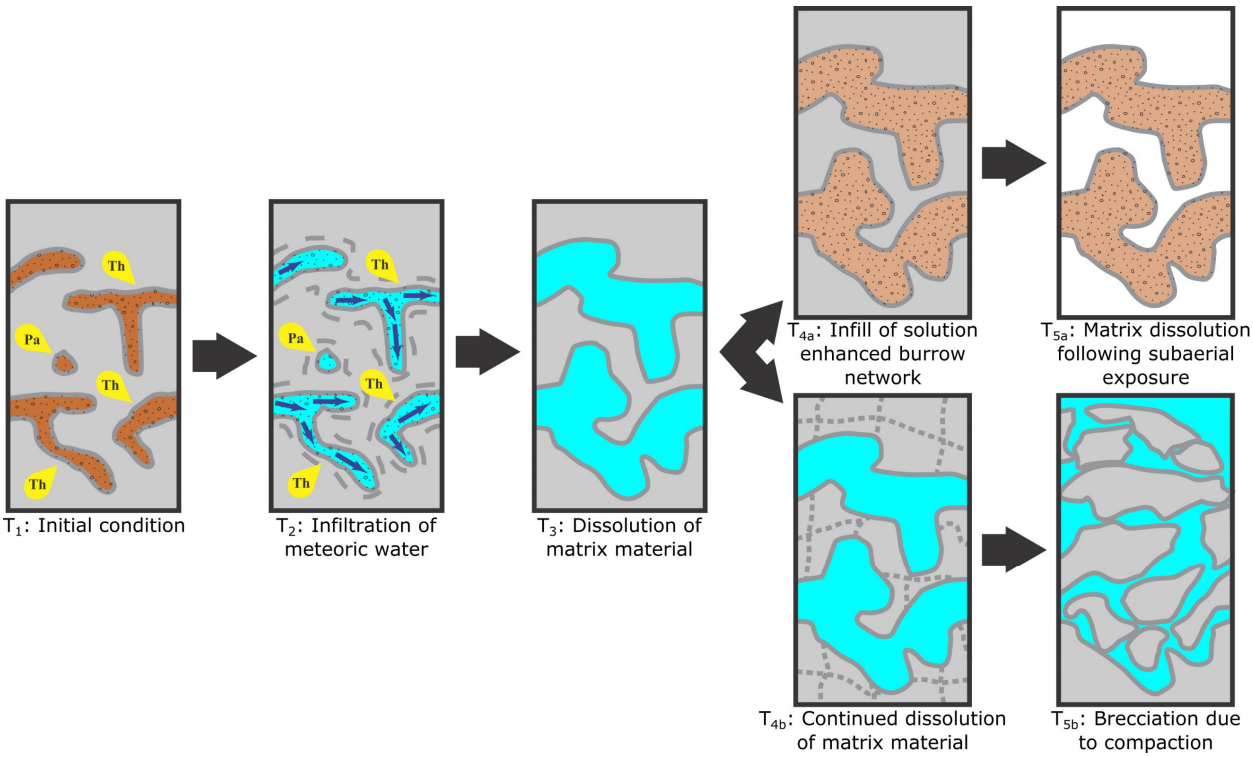

Figure 12. Diagram showing the progression of solution enhancement within the GRL. T_1) The initial condition of coarse-grained infilled Thalassinoides (Th) and Palaeophycus (Pa). T_2) Introduction of meteoric water begins to dissolve the matrix surrounding the burrows and dissolve infill. T_3) Dissolution of matrix material interconnects burrow networks across the three-dimensional extent of the bed. T_{4a}) Solution-enhanced burrow networks filled with sediment being moved by groundwater flow and cemented. T_{4b}) Cemented, solution-enhanced burrows weather differentially from the surrounding matrix and are preserved in positive relief. T_{5b}) Continued dissolution of matrix surrounding burrows from meteoric water thins rock between networks. T_{5b}) Weight of overburden collapses strata and creates a brecciated bed.

5.0 Discussion

Ichnologic assessment is important in aquifer and reservoir characterization, however, most studies have been conducted in siliciclastic units (e.g., Keswani and Pemberton, 2007; Tonkin et al., 2010; Gingras et al., 2012). Bioturbation commonly decreases porosity and permeability in both siliciclastic and carbonate aquifers that contain significant intergranular flow (e.g., Gingras et al., 2004; 2012). Karstic aquifers such as the Edwards and Trinity Groups;

however, cannot transmit significant quantities of fluid through interparticle porosity and rely on bioturbation to create porosity and lateral fluid pathways (e.g., Mathews, 1967; Gingras et al., 1999; Cunningham and Sukop, 2011; Baniak et al. 2013; Golab et al., 2015). Although previous authors have conducted ichnological assessment of some carbonate hydrocarbon reservoirs (e.g., Gingras et al., 1999, 2004; La Croix et al., 2012; Baniak et al., 2013), the biogenic aspect of karstic aquifers has been overlooked in the literature (Cunningham et al., 2009; Cunningham and Sukop, 2011, 2012; Golab et al., 2015; Clark et al., 2016). The GRL is a dual-permeability system and absent fracture and karstic porosity, ichnofossils with coarse-grained infill are the primary fluid pathways throughout most strata and are a significant factor in directing water between major faults and karstic features. All GRL beds have been shown to produce hydraulic head in water wells, even those that have been classified as confining and lack significant karstic features (Clark, 2003; Hunt and Smith, 2010).

5.1 Glen Rose Limestone depositional environment

The development of *Thalassinoides* networks is particularly common and abundant in tidal-dominated carbonate platform strata (e.g., Myrow, 1995). Common *Thalassinoides* tracemakers in modern carbonate settings include *Callianassa* sp., decapod crustaceans and other arthropods (Sheehan and Schiefelbein, 1984; Myrow, 1995). Similar to *Thalassinoides,* *Ophiomorpha* is common in high-energy, shallow marine systems (Uchman, 1995). *Ophiomorpha* are often found associated with rapid deposition in a high-energy, wave-dominated environment.

The Lower GRL was deposited in shallow subtidal–supratidal environments with some terrestrial input. Diversity of the fossil assemblage indicates normal ocean salinity (Behrens,

1965). The presence of dasycladaceae algae in thin section indicates < 30 m of water depth during deposition (Riding, 2007). Root traces and terrestrial plant material found in some beds indicate that sea-level fluctuated enough to subaerially expose the sediment at times during deposition. Siliciclastic material was sourced from the Llano Uplift by fluvial systems (Behrens, 1965), though freshwater input does not appear to have been significant enough to create widespread brackish conditions and decrease faunal diversity (Cleaves, 1977). The Lower GRL is capped by the regional *Corbula* bed in which the lack of fossil diversity has been previously interpreted to indicate highly restricted conditions behind the Stuart City Reef, leading to hypersaline conditions (Behrens, 1965). This restriction was likely caused by a significant drop in sea level, completely isolating the Central Texas Platform from oceanic water input leading to brackish conditions (Behrens, 1965).

The Upper GRL is characterized by higher depositional energy facies and evaporites. Restricted conditions on the landward side of the Stuart City Reef likely became widespread during the deposition of the *Corbula* packstone-grainstone facies (Fisher and Rodda, 1969). The laterally extensive evaporite units in the Upper GRL correlate to unconformities on reef deposits to the south and southeast (Bebout et al., 1977; Schlager, 1989). Regional evaporitic conditions created the Lower and Upper Evaporite HSUs of the Upper GRL.

Rudist-dominated facies were deposited as isolated patch reefs. These rudist-dominated patch reefs are common in the Lower GRL and rare in the Upper GRL. These reefs have a limited lateral extent of less than 300 m across (Petta, 1977). The talus slopes of rudist patch reefs commonly form on top of packstones and grainstones that are deposited laterally from the associated reef. Previous studies on rudist reefs in the GRL showed that *Caprinid* sp. likely formed in <5 m water depth (Perkins, 1974; Petta, 1977).

5.2 Hydrologic effects of Thalassinoides-dominated ichnofabric

Strata within the GRL contain significant amounts of mud and cement, leading to low intergranular porosity. Faults and karstic features have created most of the vertical fluid pathways within the Trinity aquifer and allow meteoric water to enter the subsurface (e.g., George, 1952; Maclay and Small, 1976; Horvorka et al, 1994; Faith, 2004; Pantea et al., 2008). Lateral fluid flow within beds; however, is more difficult to characterize and is primarily controlled by *Thalassinoides* networks. Baniak et al. (2013) showed that *Thalassinoides*-dominated ichnofabrics are more commonly interconnected horizontally and only become vertically connected throughout a stratum after pervasive bioturbation. Such *Thalassinoides*-dominated ichnofabrics act as conduits for fluids in the absence of faults or karstic development. These ichnofossils were also the precursor to most vug and channel porosity due to solution-enhancement of burrow networks, and facilitated the development of widespread moldic porosity.

La Croix et al. (2012) showed that *Thalassinoides* networks begin to become interconnected throughout the three-dimensional extent of a stratum at ii3 and above. This model matches well with the ichnofabric index trends seen in this study, where ii3–4 beds in the GRL are interpreted to be the most transmissive units. In *Thalassinoides*-dominated ichnofabrics lateral connectivity may exist at ii3, though vertical connectivity is generally only associated with ii5 and above (Baniak et al., 2013). Cunningham and Sukop (2012) showed that the *Thalassinoides*-dominated ichnofabrics of the overlying Edwards aquifer significantly increase permeability; however, the amount of mud and heterogeneity observed in the GRL makes this correlation less direct. Defining fluid pathways within the GRL requires the combined use of

ichnofabric indices, lithology, and structural features. Each of the eleven GRL HSUs is unique, but most transmissive units show similar trends within beds of upward coarsening in grainsize and decreasing ichnofabric indices (Fig. 9–10).

While each HSU displays some distinct hydrologic characteristics, most contain successions of decreasing-upward ii and show that biogenic fluid flow is restricted on a smaller scale within each GRL fifth-order sequence (Table 2; Figs. 9 and 11). The bases of successions are commonly muddy and consist of nodular strata with ii5–6. The ichnofossils at the bases of successions are dominated by multigenerationally tiered *Thalassinoides* networks. Much of the nodular appearance of these basal beds is attributed to cyrptobioturbation. The middle portions of successions are commonly characterized by strata with ii3–4 composed of *Thalassinoides* networks as well as *Ophiomorpha,* and occasional *Palaeophycus* and *Planolites.* These zones with ii3–4 are the most prominent area of biogenic fluid flow within the GRL as they are both interconnected throughout the strata and are commonly filled with infill coarser-grained than the surrounding matrix (La Croix et al., 2012; Baniak et al., 2013). The tops of successions may consist of massive to crossbedded packstone–grainstone with ii1–2 and contain *Palaeophycus* and *Planolites* as dominant traces. Fluid flow within these upper, low ii strata is restricted to intergranular pore space. While these upper beds contain less mud, they have significant amounts of sparry cement; therefore, permeability is still low.

5.3 Quantifying the hydrologic characteristics of dual-permeability systems

Quantifying changes in aquifer permeability and porosity is difficult as most available laboratory methods, such as point-counting and helium-expansion porosity testing, were developed to measure intergranular pore space of the matrix material and do not accurately

characterize the large-scale fluid pathways seen in the GRL (Fig. 8 and Table 1). No direct correlation could be observed between point-counted matrix porosity and the larger-scale hydrologic trends observed within the HSUs (Appendix VI). Average porosity from point counts averaged only 5.27%, and showed no significant difference between different facies. Helium-expansion porosity and permeability are also limited to small-scale matrix and fracture porosity, but some observable trends could be seen between lithofacies (Appendix VI). The results from the helium expansion testing averaged 17.6% porosity and 14.6 mD permeability. Crossbedded wackestone–packstone (0.69 mD) and evaporitic units (0.049) have the lowest measured permeability whereas fossiliferous grainstone (39.4 mD) has the highest.

The hydrologic flow observed in the GRL (Hunt and Smith, 2010) is at least 3 orders of magnitude greater than can be explained by permeability values measured from helium expansion and point counting of the matrix. The most extreme example of this is within the Lower and Upper Evaporite HSUs, which are interpreted to have the highest permeability in the GRL based on fluid flow, but contain the lowest measured helium expansion permeability values. This discrepancy in the Evaporite HSUs is likely due to abundant fractures. The other HSUs within the GRL; however, are dominated by ichnofossils instead of fractures. Unlike fracture-dominated dual-porosity systems, bioturbation-influenced pore systems are more heterogeneous and create variable flow depending on the difference in permeability between the matrix and burrow fill (Gingras et al., 1999; Baniak et al., 2013).

Studies by Cunningham et al. (2009) and Cunningham and Sukop (2011) on the karstic Biscayne aquifer of southern Florida used x-ray tomography scans of full-diameter core samples (~10 cm diameter) to measure the porosity of large-scale burrow networks. These studies then used lattice Boltzmann equations to estimate vertical and lateral permeability (Cunningham et

al., 2009). Although such datasets are, as of yet, unavailable for this study, the lithological and ichnological similarity of the GRL with the Biscayne aquifer means that values for the large-scale burrow permeability can be approximated for GRL strata. Cunningham et al. (2009) and Cunningham and Sukop (2011) estimated permeability values greater than five orders of magnitude higher than any previous study on the Biscayne aquifer system. Strata with ii3 were shown to have an average permeability of 8.2×10^7 mD, ii4 units averaged 2.7×10^9 mD, and ii5 strata averaged 8.6×10^9 mD (Cunningham et al., 2009). Although these numbers cannot be directly related to the GRL because the Biscayne aquifer's *Ophiomorpha*-dominated strata contain less mud and siliciclastic material, they illustrate the effect large-scale bioturbation-influenced porosity can have on karstic aquifer systems and may be used as a template for future studies on the Edwards (Cunningham and Sukop, 2012) and Trinity aquifers. Furthermore, the Biscayne may be more lithologically and ichnologically similar to the Edwards Group, as both contain less mud and siliciclastic content than the GRL.

5.4 Solution-enhancement and karstic development

The solution enhancement of ichnofossils has also played a role in the development of GRL fluid flow. Introduction of meteoric water likely began with the exhumation of strata along the normally faulted Balcones Fault zone during the Miocene (Horvorka et al. 1994; Clark et al. 2009). Solution enhancement by dissolution of material in contact with fluid pathways is a prominent feature in carbonate systems (e.g., Mylroie and Carew, 1990), and many GRL fluid pathways show evidence of having been enhanced by meteoric and groundwater flow. Dissolution in pre-existing three-dimensional geometric patterns of ichnofossils has significantly increased the lateral and vertical permeability of most transmissive HSUs by further

interconnecting *Thalassinoides* networks and widening fluid pathways. Within areas where such dissolution is extensive, complete dissolution of ichnofossils results in the formation of karstic features.

Karstic development, while primarily controlled by faulting and fracturing (Horvorka et al, 1994; Maclay, 1995; Faith, 2004), is influenced also by the presence or absence of ichnofossils (Keswani and Pemberton, 2007). Hydrostratigraphic units within the GRL that contain significant fault and fracture porosity have commonly been defined as the most transmissive (Clark, 2003, 2005; Clark et al., 2009; Clark and Morris, 2015). Additionally, karstic features associated with fractures are significant fluid pathways and catchments (Clark, 2003, 2005; Faith, 2004; Pantea et al, 2014). Beds with well-developed biogenic networks transmitted water laterally away from faults and fractures. This action aided in karstic development within transmissive bioturbated beds. These features can be observed easiest in the Lower GRL Honey Creek HSU and was a likely major component in the development of the Upper GRL Cavernous HSU.

6.0 Conclusions

Large-scale bioturbation-influenced porosity such as burrows, borings, and nodular preservation of bioturbation is one of several factors that affect fluid flow within the GRL of the Trinity aquifer; however, its significance in karstic aquifers and reservoirs has not been explored by many authors. While faulting and fracturing and karstic development are commonly the most prevalent fluid pathways within aquifers that lack significant intergranular porosity and permeability, biogenic fluid pathways (i.e., burrows) act as conduits to move fluids laterally between faulting and fracture features. Bioturbation-influenced porosity is of particular interest

to carbonate aquifers, many of which contain interconnected *Thalassinoides* or *Ophiomorpha* networks (e.g., Mazzullo and Chilingarian, 1996; Cunningham et al., 2009).

Previous studies have shown *Thalassinoides*-dominated ichnofabrics tend to increase the lateral connectivity of beds by creating interconnected 3-dimensional fluid pathways of either open burrows or burrows with permeable fill (e.g., Cunningham and Sukop, 2012; Baniak et al., 2013). The muddy and siliciclastic input present during GRL deposition; however, complicates such a straight-forward correlation. Transmissive beds in the GRL beds have ii3–4 and burrows are commonly open or have permeable fill. Beds with ii5–6 are commonly muddy and heavily homogenized, and restrict fluid flow. Additionally, grainstone beds commonly have ii1–2 and are cemented, restricting fluid flow to low intergranular flow.

Characterizing the lateral fluid pathways requires the integration of lithology, structural and karstic features, and ichnology. The overall transmissive or confining nature of hydrostratigraphic units in the GRL depends on the ichnofabric index, fracture density, and karstic features both within the beds and in the overall stratigraphy. For example, confining beds in the Upper GRL are lithologically and ichnologically similar to transmissive beds in the Lower GRL (see figs. 9 and 11). The Upper GRL contains evaporites and significantly more karstic development than the Lower GRL, meaning that transmissive units are more commonly characterized by evaporites with significant dissolution features. Although the confining units in the Upper GRL contain significant bioturbation-influenced porosity and less mud than Lower GRL transmissive units, they are significantly less permeable than the evaporitic and Cavernous HSUs and divert water to seeps and springs. All of these Upper GRL units; however, likely transmit water laterally and the two Upper GRL confining units may; therefore, be better described as “semi-confining HSUs”.

Analysis of fluid pathways is further complicated by the solution enhancement of ichnofossils by meteoric water. Solution enhancement features are most significant in close proximity to faults and fractures and within the GRL, the Upper GRL displays more solution enhancement due to the high infiltration rates of the overlying Edwards aquifer (Maclay, 1995; Smith et al., 2003; Clark, 2004). Solution enhancement greatly increases lateral and vertical connectivity and permeability of units and, in some beds, was the first step toward development of larger-scale karstic features.

Ichnofabric assessment of karstic aquifers may also be of benefit to hydrocarbon exploration. Large-scale vug porosity is a common feature in karstic reservoirs and aquifers and may have been mediated by biologic activity (Mazzullo and Chilingarian, 1996; Gingras et al., 1999; Cunningham et al., 2009; Baniak et al., 2013). Understanding the interaction of burrows and molds that may lead to such porosity may become increasingly important as part of reservoir characterization. The shelf carbonates of south TX have been explored for oil and gas plays with active fields targeting the Edwards Group and Austin Chalk Formation (Loucks, 1977). The shallow marine carbonates of the GRL from south of the study have documented hydrocarbon staining, but lacked significant structural or stratigraphic traps (Loucks, 1977). The hydrocarbon staining demonstrates the potential of karstic systems to act as reservoirs and ichnologic assessment may benefit such plays as the Edwards and Austin Chalk. This methodology may also be expanded into other potential reservoirs such as the Ellenburger Group of western TX (Loucks, 1999) or the Arbuckle Group of Central Oklahoma (Kerans, 1988; Puckette et al., 2009).

References

Achauer, C.A., 1977, Contrasts in Cementation, Dissolution, and Porosity Development Between Two Lower Cretaceous Reefs of Texas, in Bebout, D.G., and Loucks, R.G., eds., Cretaceous carbonates of Texas and Mexico—Applications to subsurface exploration: Austin, University of Texas, Bureau of Economic Geology Report of Investigation 89, p. 127–137.

Adkins, W.S., 1928, Handbook of Texas Cretaceous Fossils: University of Texas Bulletin, no. 2838, 385 p.

Ashworth, J.B., 1983, Ground-water Availability of the Lower Cretaceous Formations in the Hill Country of South-central Texas: Texas Department of Water Resources Report 273, 172 p.

Babcock, L.E., Merriam, D.F., West, R.R., 2000, *Paleolimulus*, an Early Limuline (*Xiphosurida*), from Pennsylvanian–Permian Lagerstätten of Kansas and Taphonomic Comparison with Modern *Limulus*: Lethaia, vol. 33, p. 129–141.

Baniak, G.M., Gingras, M.K., and Pemberton, S.G., 2013, Reservoir Characterization of Burrow-Associated Dolomites in the Upper Devonian Wabamun Group, Pine Creek Gas Field, Central Alberta, Canada: Marine and Petroleum Geology, vol. 48, p. 275–292.

Barker, R.A., and Ardis, A.F., 1996, Hydrogeological Framework of the Edwards-Trinity Aquifer System, West-central Texas: U.S. Geological Survey Professional Paper 1421–B, 61 p.

Barnes, V.E., 1981, Geologic Atlas of Texas, Llano Sheet: Austin, University of Texas: Austin, Bureau of Economic Geology, 1 sheet, scale 1:250,000.

Barnes, V.E., 1965, Geology of the Hays Quadrangle, Blanco, Gillespie and Kendall Counties, Texas: Austin, University of Texas-Austin, Bureau of Economic Geology, 1 sheet, scale 1:24,000.

Bebout, D.G., Schatzinger, R.A., and Loucks, R.G., 1977, Porosity distribution in the Stuart City Trend, Lower Cretaceous, South Texas: in Bebout, D. G. and Loucks, R. G., eds., Cretaceous Carbonates of Texas and Mexico: Bureau of Economic Geology, University of Texas at Austin, Report of Investigations No. 89, p. 234–256.

Behrens, E.W., 1965, Environment Reconstruction for a Part of the Glen Rose Limestone, Central Texas: Sedimentology, vol. 4, p. 65–111.

Blome, C.D., and Clark, A.K., 2014, Key Subsurface Data Help to Refine Trinity Aquifer Hydrostratigraphic Units, South-central Texas: U.S. Geological Survey Data Series 768, 1 sheet, http://dx.doi.org/10.3133/ds768.

Blome, C.D., Faith, J.R., and Ozuna, G.B., 2007, Geohydrologic Framework of the Edwards and Trinity Aquifers, South-Central Texas: U.S. Geological Survey Fact Sheet 2006-3145, 4 p.

Braun, A.S., 2011, East to West Stratigraphic Cross Section, Northern Hays County: Surface to Subsurface Trinity Lithostratigraphy: in Implications for Groundwater Availability in the Hill Country, Eastern Blanco and Northern Hays Counties, Texas: Austin Geological Society, Guidebook 33.

Bromley, R.G., and Ekdale, A.A., 1986, Composite ichnofabrics and tiering of burrows: Geological Magazine, vol. 123, p. 59–65.

Bromley R.G. and Frey R.W., 1974, Redescription of the Trace Fossil *Gyrolithes* and Taxonomic Evaluation of *Thalassinoides*, *Ophiomorpha*, and *Spongeliomorpha*: Bulletin of the Geological Society of Denmark, vol. 23, p. 312–335.

Bumgarner, J.R., Stanton, G.P., Teeple, A.P., Thomas, J,V., Houston, N,A., Payne, J.D., Musgrove, M., 2012, A Conceptual Model of the Hydrogeologic Framework, Geochemistry,

and Groundwater-flow System of the Edwards-Trinity and Related Aquifers in the Pecos County Region, Texas: SGS Scientific Investigations Report: 2012-5124, 74 p.

Carew, J.L., 1967, Study of a Portion of the Lower Glen Rose Formation, Steiner Ranch, Texas, in Scott, A.J. ed., Carbonate Depositional Environments, Central Texas, term reports: Department of Geology, Geology 383K, University of Texas, Austin, Texas, p. 54–63.

Choquette, P.W., and Pray, L.C., 1970, Geologic Nomenclature and Classification of Porosity in Sedimentary Carbonates: American Association of Petroleum Geologists Bulletin, vol. 54, no. 2, p. 207–250.

Clark, A.K., 2003, Geologic Framework and Hydrogeologic Features of the Glen Rose Limestone, Camp Bullis Training Site, Bexar County, Texas: U.S. Geological Survey Scientific Investigations Report 03–4081, 9 p., 1 pl., scale 1:24,000.

Clark, A.K., 2004, Geologic Framework and Hydrogeologic Characteristics of the Glen Rose Limestone, Camp Stanley Storage Activity, Bexar County, Texas: U.S. Geological Survey Scientific Investigations Map 2831, 1 pl., scale 1: 25,000.

Clark, A.K., Blome, C.D., and Morris, R.R., 2014, Geology and Hydrostratigraphy of Guadalupe River State Park and Honey Creek State Natural Area, Kendall and Comal Counties, Texas: U.S. Geological Survey Scientific Investigations Map 3303, 8 p., 1 sheet, scale 1:24,000.

Clark, A.K., Golab, J.A., and Morris, R.R., 2016, Geologic Framework, Hydrostratigraphy, and Ichnology of the Blanco, Payton, and Rough Hollow 7.5-minute Quadrangles, Blanco, Comal, Hays, and Kendall Counties, Texas: U.S. Geological Survey Scientific Investigations Map 3363, 21 p., 1 sheet, scale 1:24,000.

Clark, A.K., and Morris, R.R., 2015, Geologic and Hydrostratigraphic map of the Anhalt, Fischer, and Spring Branch 7.5-minute Quadrangles, Blanco, Comal, and Kendall Counties,

Texas: U.S. Geological Survey Scientific Investigations Map 3333, 13 p., 1 sheet, scale 1:50,000.

Clark, A.R., Blome, C.D., and Faith, J.R., 2009, Map Showing Geology and Hydrostratigraphy of the Edwards Aquifer Catchment Area, Northern Bexar County, South-Central Texas: U.S. Geological Survey Open-File Report 2009-1008.

Cleaves, A.W., 1977, Middle Glen Rose (Cretaceous) Facies Mosaic, Blanco and Hays Counties, Texas, in Bebout, D.G., and Loucks, R.G., eds., Cretaceous carbonates of Texas and Mexico—Applications to subsurface exploration: Austin, University of Texas, Bureau of Economic Geology Report of Investigation 89, 168 p.

Collins, E.W., 1992a, Geologic Map of the Anhalt 7.5-minute Quadrangle, Comal, Blanco, and Kendall Counties, Texas: The University of Texas at Austin, Bureau of Economic Geology Open-File Map OFM0095, 1 sheet, scale 1:24,000.

Collins, E.W., 1992b, Geologic Map of the Fischer 7.5-minute Quadrangle, Comal, Blanco, and Kendall Counties, Texas: The University of Texas at Austin, Bureau of Economic Geology Open-File Map OFM0030, 1 sheet, scale 1:24,000.

Collins, E.W., 1992c, Geologic Map of the Spring Branch 7.5-minute Quadrangle, Comal, Blanco, and Kendall Counties, Texas: The University of Texas at Austin, Bureau of Economic Geology Open-File Map OFM0011, 1 sheet, scale 1:24,000.

Collins, E.W., 1995, Structural Framework of the Edwards Aquifer, Balcones Fault Zone, Central Texas: Gulf Coast Association of Geological Societies, Transactions, vol. 38, p. 135–141.

Conwy Valley Systems Ltd., 2011, PetrogLite Version 3.0 for MS Windows OS. Conway, United Kingdom.

Cunningham, K.J. and Sukop, M.C., 2011, Multiple Technologies Applied to Characterization of the Porosity and Permeability of the Biscayne Aquifer, Florida: U.S. Geological Survey Open-File Report 2011-1037, 8 p.

Cunningham, K.J. and Sukop, M.C., 2012, Megaporosity and Permeability of *Thalassinoides*-Dominated Ichnofabrics in the Creataceous Karst-Carbonate Edwards-Trinity Aquifer System, Texas: U.S. Geological Survey Open-File Report 2012-1021, 4 p.

Cunningham, K.J., Sukop, M.C., Huang, H., Alvarez, P.F., Curran, H.A., Renken, R.A., and Dixon, J.F., 2009, Prominence of Ichnologically Influenced Macroporosity in the Karst Biscayne aquifer: Stratiform "super-K" zones, Geological Society of America Bulletin, vol. 121, no. 1/2; p. 164–180.

Droser, M.J. and Bottjer, D.J., 1986, A Semiquantitative Field Classification of Ichnofabric: Journal of Sedimentary Petrology, vol. 56, no. 4, p. 558–559.

Dunham, R.J., 1962, Classification of Carbonate Rocks According to Depositional Textures: in American Association of Petroleum Geologists Memoir 1: Classification of Carbonate Rocks—A Symposium, p. 108–121.

Ekdale, A.A. and Bromley, R.G., 1984a, Comparative Ichnology of Shelf-Sea and Deep-Sea Chalk: Journal of Paleontology, vol. 58, p. 322–332.

Ekdale, A.A. and Bromley, R.G., 1984b, Sedimentology and Ichnology of the Cretaceous-Tertiary Boundary in Denmark: Implications for the Causes of the Terminal Cretaceous Extinction: Journal of Sedimentary Petrology, vol. 54, p. 681–703.

Embry, A.F. and Klovin, J.E., 1971, A Late Devionian Reef Bank on Northeastern Banks Island, N.W.T.: Bulletin of Canadian Petroleum Geology, vol. 19, no. 4, p. 730–781.

Faith, J.R., 2004, Strain and Fractures in an Extensional Relay Ramp, Sierra del Carmen, Black Gap Wildlife Management Area, Brewster County, Texas—Implications for Determining Structural Controls on Groundwater Flow Pathways in the Edwards Aquifer, South-central Texas: University of Texas at San Antonio, M.S. thesis, 88 p.

Fisher, W.L. and Rodda, P.U., 1969, Edwards Formation (Lower Cretaceous), Texas: Dolomitization in a Carbonate Platform System: American Association of Petroleum Geologists Bulletin, vol. 55, no. 1, p. 55–72.

Gary, M.O., Rucker, D.F., Smith, B.D., Smith, D.V., and Befus, K., 2013, Geophysical Investigations of the Edwards-Trinity Aquifer System at Multiple Scales: Interpreting Airborne and Direct-Current Resistivity in Karst: NCKRI Symposium 2, 13th Sinkhole Conference, p. 195–206.

George, W.O., 1952, Geology and Ground-water Resources of Comal County, Texas: U.S. Geological survey Water-Supply Paper 1138, 126 p.

Gingras, M.K., Baniak, G., Gordon, J., Hovikoski, J., Konhauser, K.O., La Croix, A.D., Lemiski, R., Mendoza, C., Pemberton, S.G., Polo, C., and Zonneveld, J., 2012, Porosity and Permeability in Bioturbated Sediments: Developments in Sedimentology, vol. 64, p. 837–868.

Gingras, M.K., Pemberton, S.G., Mendoza, C.A., and Henk, F., 1999, Assessing the Anisotropic Permeability of *Glossifungites* Surfaces: Petroleum Geoscience, vol. 5, p. 349–357.

Gingras, M.K., Mendoza, C.A., and Pemberton, S.G., 2004, Fossilized Worm Burrows Influence the Reservoir Quality of Porous Media: American Association of Petroleum Geologists Bulletin, vol. 88, no. 7, p. 875–883.

Golab, J.A., Clark, A.K., and Hasiotis, S.T., 2015, Bioturbation-Influenced Fluid Pathways within a Carbonate Platform System: The Aptian–Albian Glen Rose Limestone: GSA Annual Meeting, Baltimore, MD, 1–4 November.

Grimshaw, T. W., and Woodruff Jr., C.M., 1986, Structural Style in an *En Echelon* Fault System, Balcones Fault Zone, Central Texas: Geomorphologic and Hydrologic Implications, in Abbott, P. L. and Woodruff, Jr., C.M., eds., The Balcones Escarpment—Geology, Hydrology, Ecology and Social Development in Central Texas: Guidebook published for the 1986 Geological Society of America Annual Meeting, San Antonio, Texas, p. 71–75.

Hanson, J.A., and Small, T.A., 1995, Geologic Framework and Hydrogeologic Characteristics of the Edwards Aquifer Outcrop, Hays County, Texas: U.S. Geological Survey Water-Resources Investigations Report 95–4265, 10 p.

Hasiotis, S.T. and Mitchell, C.E., 1993, A Comparison of Crayfish Burrow Morphologies: Triassic and Holocene Fossil, Paleo- and Neo-ichnological Evidence, and the Identification of Their Burrowing Signatures: Ichnos, vol. 2, p. 291–314.

Hasiotis, S.T. and Platt, B.R., 2012, Exploring the Sedimentary, Pedogenic, and Hydrologic Factors that Control the Occurrence and Role of Bioturbation in Soil Formation and Horizonation in Continental Deposits: An Integrative Approach: The Sedimentary Record, vol. 10, p. 4–9.

Horvorka, S.D., Dutton, A.R., Ruppel, S.C., and Yeh, J., 1994, Sedimentologic and Diagenetic Controls on Aquifer Properties, Lower Cretaceous Edwards Carbonate Aquifer, Texas: Implications for Aquifer Management: Transactions of the Gulf Coast Association of Geological Societies, vol. 44, p. 277–284.

Hunt, B.B. and Smith, B.A., 2010, Spring 2009 Potentiometric Map of the Middle Trinity Aquifer in Groundwater Management Area 9, Central Texas: Barton Springs/Edwards Aquifer Conservation District Report of Investigations 2010-0501, 31 p.

Inden, R. F., 1974, Lithofacies and Depositional Model for a Trinity Cretaceous Sequence, Central Texas: in Aspects of Trinity Geology: Geoscience and Man, vol. 8, p. 37–52.

Imlay, R.W., 1945, Subsurface Lower Cretaceous Formations of South Texas: American Association of Petroleum Geologists Bulletin, vol. 29, p. 1416–1469.

Kerans, C., 1988, Karst-controlled Reservoir Heterogeneity in Ellenburger Group Carbonates of West Texas: American Association of Petroleum Geologists Bulletin, vol. 72, no. 10, p. 1160–1183.

Keswani, A. D. and Pemberton, S. G., 2007, Applications of Ichnology in Exploration and Exploitation of Mississippian Carbonate Reservoirs, Midale Beds, Weyburn Oilfield, Saskatchewan. In Alberta, Canada, Canadian Society of Petroleum Geologists and Canadian Society of Exploration Geophysicists Conference, p. 14–17.

Kraus, M. J. and Hasiotis, S.T., 2006, Significance of Different Modes of Rhizolith Preservation to Interpreting Paleoenvironmental and Paleohydrologic Settings: Examples from Paleogene Paleosols, Bighorn Basin, Wyoming, U.S.A.: Journal of Sedimentary Research, vol. 76, no. 4, p. 633–646.

La Croix, A.D., Gingras, M.K., Dashtgard, S.E., and Pemberton, S.G., 2012, Computer Modeling Bioturbation: The Creation of Porous and Permeable Fluid-Flow Pathways: American Association of Petroleum Geologists Bulletin, vol. 96, no. 3, p. 545–556.

Loucks, R.G., 1977, Porosity Development and Distribution in Shoal-Water Carbonate Complexes—Subsurface Pearsall Formation (Lower Cretaceous) South Texas, in Bebout,

D.G. and Loucks, R.G., eds., Cretaceous carbonates of Texas and Mexico—Applications to subsurface exploration: University of Texas at Austin, Bureau of Economic Geology Report of Investigation 89, p. 97–126.

Loucks, R.G., 1999, Paleocave Carbonate Reservoirs: Origins, Burial-Depth Modifications, Spatial Complexity, and Reservoir Implications: American Association of Petroleum Geologists Bulletin, vol. 83, no. 11, p. 1795–1834.

Lozo, F.E., and Stricklin Jr., F.L., 1956, Stratigraphic Notes on the Outcrop Basal Cretaceous, Central Texas: Gulf Coast Association of Geological Societies Transactions, vol. 6, p. 67–78.

Mace, R.E., Chowdhury, A.H., Anaya, H., Way, S., 2000, Groundwater Availability of the Trinity Aquifer, Hill Country Area, Texas: Numerical Simulations through 2050: Texas Water Development Board Report 353, 117 p.

Maclay, R.W., 1989, Edwards Aquifer in the San Antonio Region: Its Hydrology and Management: South Texas Geological Society Bulletin, vol. 30, no. 4, p. 11–28.

Maclay, R.W., 1995, Geology and Hydrology of the Edwards Aquifer in the San Antonio Area, Texas: U.S. Geological Survey Water Resources Investigations Report 95-4186, 64 p.

Maclay, R.W., and Small, T.A., 1976, Progress Report on Geology of the Edwards Aquifer, San Antonio Area, Texas, and Preliminary Interpretation of Borehole Geophysical and Laboratory Data on Carbonate Rocks: U.S. Geological Survey Open-File Report 76–627, 65 p.

Maclay, R.W., and Small, T.A., 1986, Carbonate Geology and Hydrology of the Edwards Aquifer in the San Antonio Area, Texas: Texas Water Development Board, Report 296, p. 90.

Mancini, E.A. and Scott, R.W., 2006, Sequence Stratigraphy of Comanchean Cretaceous Outcrop Strata of Northeast and South-Central Texas: Implications for Enhanced Petroleum Exploration: Gulf Coast Association of Geological Societies Transactions, vol. 56, p. 539–550.

Matthews, R.K., 1967, Diagenetic fabrics in biosparites from the Pleistocene of Barbados, West Indies: Journal of Sedimentary Petrology, vol. 36, no. 4, p. 1147–1153.

Maxey, G.B., 1964, Hydrostratigraphic Units: Journal of Hydrology, vol. 2, p. 124–129.

Mazzullo, S.J. and Chilingarian, G.V., 1996, Hydrocarbon Reservoirs in Karsted Carbonate Rocks: Developments in Petroleum Science, vol. 44, no. 2, p. 797–865.

Mylroie, J.E. and Carew, J.L., 1990, The Flank Margin Model for Dissolution Cave Development in Carbonate Platforms: Earth Surface Processes and Landforms, vol. 15, p. 413–424.

Myrow, P.M., 1995, *Thalassinoides* and the Enigma of Early Paleozoic Open-Framework Burrow Systems: PALAIOS, vol. 10, no. 1, p. 58–74.

Pantea, M.P., Blome, C.D., and Clark, A.K. 2014, Three-Dimensional Model of the Hydrostratigraphy and Structure in and around the U.S. Army–Camp Stanley Storage Activity Area, Northern Bexar County, Texas: USGS Scientific Investigations Report 2014–5074.

Pantea, M.P., Cole, J.C., Smith, B.D., Faith, J.R., and Blome, C.D., 2008, Three-Dimensional Geologic Model of Complex Fault Structures in the Upper Seco Creek Area, Medina and Uvalde Counties, South-Central Texas: U.S. Geological Survey Scientific Investigations Report 2008–5131, DVD-ROM, 9 p.

Pemberton, S.G. and Frey, R.W., 1982, Trace Fossil Nomenclature and the *Planolites*-*Palaeophycus* Dilemma: Journal of Paleontology, vol. 56, no. 4, p. 843–881.

Perkins, B.F., 1974, Paleoecology of a Rudist Reef Complex in the Comanche Cretaceous, Glen Rose Limestone, Central Texas, in Perkins, B.F., ed., Aspects of Trinity Division Geology—A Symposium: Louisiana State University: Geoscience and Man, vol. 8, p. 131–173.

Petta, T.J., 1977, Diagenesis and geochemistry of a Glen Rose patch reef complex, Bandera County, Texas, in Bebout, D.G., and Loucks, R.G., eds., Cretaceous carbonates of Texas and Mexico—Applications to subsurface exploration: University of Texas at Austin, Bureau of Economic Geology Report of Investigation 89, p. 138–165.

Pittman, J.G., 1989, Stratigraphy of the Glen Rose Formation, Western Gulf Coast Plain: Gulf Coast Associations of Geological Societies Transactions, vol. 39, p. 247–264.

Puckette, J., Halihan, T., and Faith, J.R., 2009, Characterization of the Arbuckle-Simpson Aquifer—Final Report for the Arbuckle-Simpson Hydrology Study: Sillwater, Oklahoma, Oklahoma State University, School of Geology, for the Oklahoma Water Resources Board, 53 p.

Riding, R., 2007, *Girvanella* and Other Algae as Depth Indicators: Lethaia, vol. 8, p. 173–179.

von Roemer, C.F., 1852, Die Kreidebildungen von Texas und Ihre Organischen Einschliisse: Bonn, 100 p.

Rose, P.R., 1972, Edwards Group, Surface and Subsurface, Central Texas: University of Texas at Austin, Bureau of Economic Geology Report of Investigations 74, 198 p.

Schlager,W., 1989, Drowning Unconformities on Carbonate Platforms: Controls on Carbonate Platform and Basin Development, SEPM Special Publication No. 44, p. 15–25.

Scanlon, B.R., Mace, R.E., Barrett, M.E., and Smith, B., 2003, Can We Simulate Regional Groundwater Flow in a Karst System Using Equivalent Porous Media Models? Case study, Barton Springs Edwards aquifer, USA: Journal of Hydrology, vol. 276, p.137–158.

Scott, R.W., Molineux, A.M., and Mancini, E.A., 2007, Lower Albian Sequence Stratigraphy and Coral Buildups—Glen Rose Formation, Texas, USA, in Scott, R.W., ed., Cretaceous Rudists and Carbonate Platforms—Environmental feedback: Society for Sedimentary Geology, v. 87, p. 181–191.

Sheehan, P.M. and Schiefelbein, D.R.J., 1984, The Trace Fossil *Thalassinoides* from the Upper Ordovician of the Eastern Great Basin: Deep Burrowing in the Early Paleozoic: Journal of Paleontology, vol. 58, no. 2, p. 440–447.

Small, T.A. and Lambert, R.B., 1998, Geologic Framework and Hydrogeologic Characteristics of the Outcrops of the Edwards and Trinity Aquifers, Medina Lake Area, Texas: U.S. Geological Survey Water-Resources Investigations Report 97–4290, 21 p.

Smith, B.D., Cain, M.J., Clark, A.K., Moore, D.W., Faith, J.R., Hill, P.R., 2005, Helicopter Electromagnetic and Magnetic Survey Data and Maps, Northern Bexar County, Texas: U.S. Geological Survey Open-File Report 05-1158, 24 p.

Smith. D.V. and Pratt, D. 2003, Advanced Processing and Interpretation of the High Resolution Aeromagnetic Survey Data Over the Central Edwards Aquifer, Texas: Proceedings from the Symposium on the Application of Geophysics to Engineering and Environmental Problems, Environmental and Engineering Society, 11p.

Smith, J.J., Hasiotis, S.T., Kraus, M.J., and Woody, D.T., 2008, Relationship of Floodplain Ichnocoenoses to Paleopedology, Paleohydrology, and Paleoclimate in the Willwood

Formation, Wyoming, During the Paleocene–Eocene Thermal Maximum: PALAIOS, vol. 23, p. 683–699.

Stricklin, F. L. and Amsbury, D.L., 1974, Depositional Environments on a Low-Relief Carbonate Shelf, Middle Glen Rose limestone, Central Texas: Geoscience and Man, vol. 8, p. 53–66.

Stricklin, F.L., Jr., Smith, C.I., and Lozo, F.E., 1971, Stratigraphy of Lower Cretaceous Trinity Deposits of Central Texas: University of Texas at Austin, Bureau of Economic Geology Report of Investigations 71, 63 p.

Tonkin, N.S., McIlroy, D., Meyer, R., and Moore-Turpin, A., 2010, Bioturbation Influence on Reservoir Quality: A Case Study from the Cretaceous Ben Nevis Formation, Jeanne d'Arc Basin, Offshore Newfoundland, Canada: American Association of Petroleum Geologists Bulletin, vol. 94, p. 1059–1078.

Uchman, A., 1995, Taxonomy and Palaeoecology of Flysch Trace Fossils: The Marnosoarenacea Formation and Associated Facies (Miocene, Northern Apennines, Italy): Beringeria, vol. 15, p. 3.

Uchman, A., 1998, Taxonomy and Ethology of Flysch Trace Fossils: A Revision of the Marian-Książkiewicz Collection and Studies of Complementary Material: Annales Societatis Geologorum Poloniae, vol. 68, p. 105–218.

Vaziri, S.H. and Fürsich, F.T., 2007, Middle to Upper Triassic Deep-Water Trace Fossils from the Ashin Formation, Nakhlak Area, Central Iran, Journal of Sciences, Islamic Republic of Iran, vol. 18, no. 3, p. 253–268.

Vinn, O., Hove, H.A.T., Mutvei, H., and Kirsimäe, K., 2008, Ultrastructure and Mineral Composition of Serpulid Tubes (Polychaeta, Annelida): Zoological Journal of the Linnean Society, vol. 154, p. 633–650.

Ward, W.C. and Ward, B.W., 2007, Stratigraphy of Middle Part of the Glen Rose Formation (Lower Albian), Canyon Lake Gorge, Central Texas, U.S.A.: Cretaceous Rudists and Carbonate Platforms: Environmental Feedback: SEPM Special Publication 87, p. 193–210.

Wentworth, C.K., 1922, A Scale of Grade and Class Terms for Clastic Sediments: Journal of Geology, vol. 31, p. 377–392.

Whitney, M.I., 1952, Some Zone Marker Fossils of the Glen Rose Formation of Central Texas: Journal of Paleontology, vol. 26, no. 1, p. 65–73.

Winter, J.A., 1961, Stratigraphy of the Lower Cretaceous (Subsurface) of South Texas: Gulf Coast Association of Geological Societies Transactions, vol. 11, p.15–24.

Winters, W.J., Dallimore, S.R., Collett, T.S., Katsube, T.J., Jenner, K.A., Cranston, R.E., Wright, J.F., Nixon, F.M., and Uchida, T., 1999, Physical Properties of Sediments from the JAPEX/JNOC/GSC Mallik 2L-38 Gas Hydrate Research Well: in Dallimore, S.R., Uchida, T., and Collett, T.S., eds., Scientific Results from JAPEX/JNOC/GSC Mallik 2L-38 Gas Hydrate Research Well, Mackenzie Delta, Northwest Territories, Canada: Geological Survey of Canada Bulletin 544, p. 95–100.

Wright, V.P., Baceta, J.I., Lapointe, P.A., 2014, Paleokarstic Macroporosity Development at Platform Margins: Lessons from the Paleocene of North Spain: Interpretation, vol. 2, p. 1–16.

Zhou, W., Beck, B.F., Adams, A.L., 2002, Effective Electrode Array in Mapping Karst Hazards in Electrical Resistivity Tomography: Environmental Geology, vol. 42, p. 922–928.

Appendix I

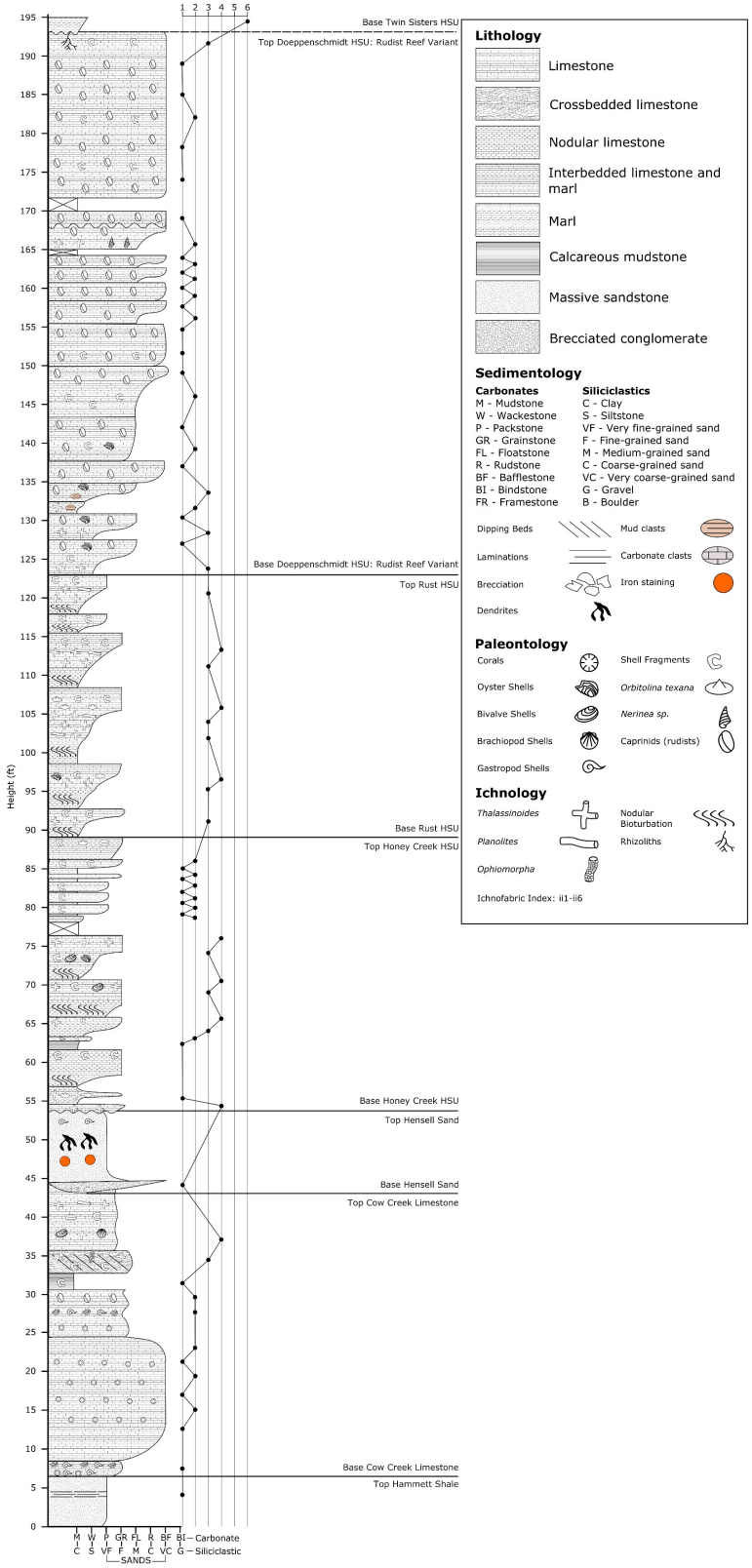
Base Twin Sisters HSU
Top Doeppenschmidt HSU: Rudist Reef Variant
Base Doeppenschmidt HSU: Rudist Reef Variant
Top Rust HSU
Base Rust HSU
Top Honey Creek HSU
Base Honey Creek HSU
Top Hensell Sand
Base Hensell Sand
Top Cow Creek Limestone
Base Cow Creek Limestone
Top Hammett Shale
Height (ft)
Carbonate
Siliciclastic
SANDS
Lithology
Limestone
Crossbedded limestone
Nodular limestone
Interbedded limestone and marl
Marl
Calcareous mudstone
Massive sandstone
Brecciated conglomerate
Sedimentology
Carbonates
M - Mudstone
W - Wackestone
P - Packstone
GR - Grainstone
FL - Floatstone
R - Rudstone
BF - Bafflestone
BI - Bindstone
FR - Framestone
Siliciclastics
C - Clay
S - Siltstone
VF - Very fine-grained sand
F - Fine-grained sand
M - Medium-grained sand
C - Coarse-grained sand
VC - Very coarse-grained sand
G - Gravel
B - Boulder
Dipping Beds
Laminations
Brecciation
Dendrites
Mud clasts
Carbonate clasts
Iron staining
Paleontology
Corals
Oyster Shells
Bivalve Shells
Brachiopod Shells
Gastropod Shells
Shell Fragments
Orbitolina texana
Nerinea sp.
Caprinids (rudists)
Ichnology
Thalassinoides
Planolites
Ophiomorpha
Nodular Bioturbation
Rhizoliths
Ichnofabric Index: ii1-ii6

Supplemental Figure 1. Stratigraphic column from along the Blanco River, western Hays County, Texas. Section includes the Honey Creek, Rust, Doeppenschmidt, and base of the Twin Sisters hydrostratigraphic units. The underlying Hammett Shale, Cow Creek Limestone, and Hensel Sand of the Pearsall Formation are also included. Ichnofabric index for individual beds shown.

Appendix II

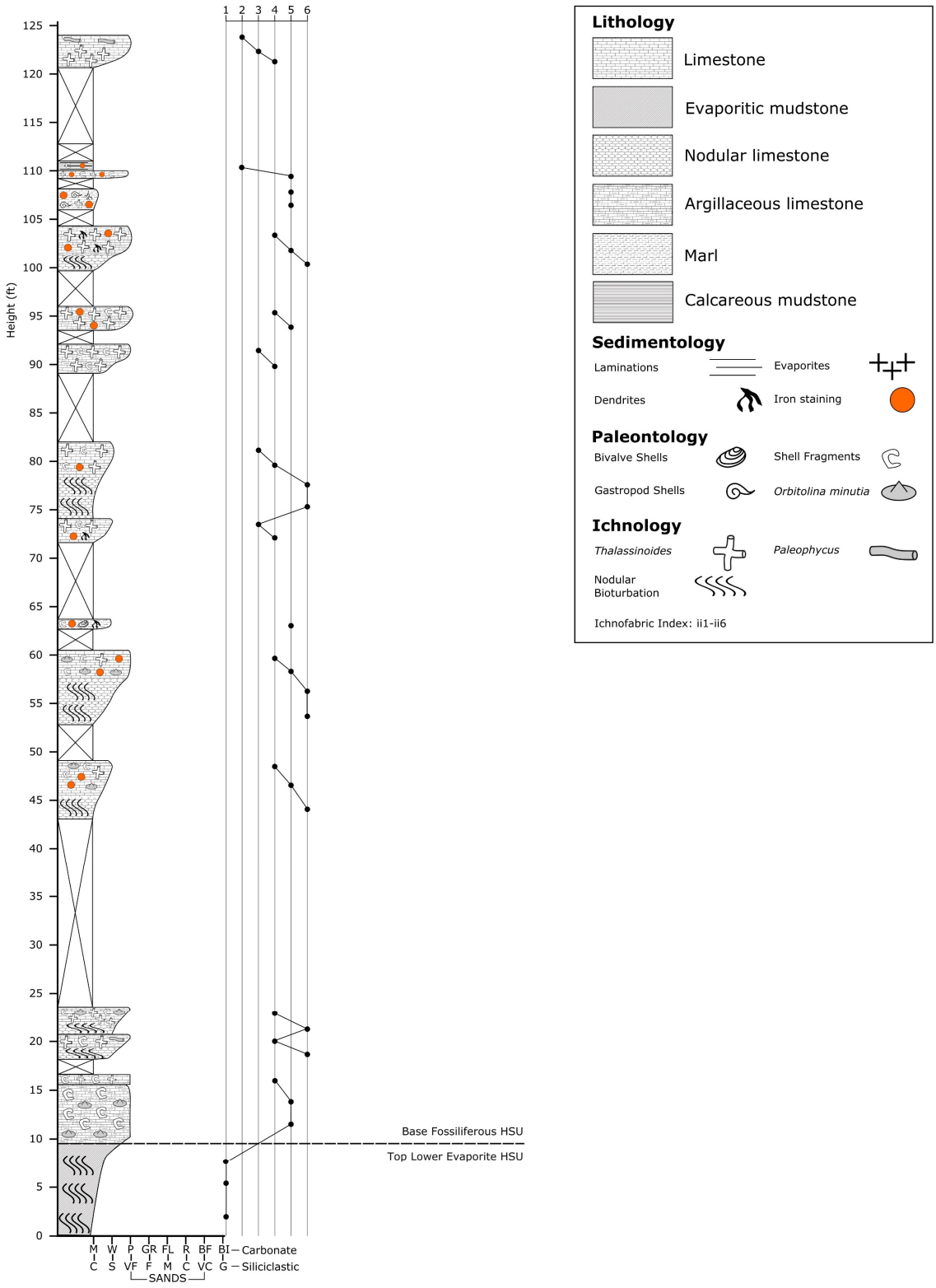
1 2 3 4 5 6
Height (ft)
125
120
115
110
105
100
95
90
85
80
75
70
65
60
55
50
45
40
35
30
25
20
15
10
5
0
Base Fossiliferous HSU
Top Lower Evaporite HSU
M C
W S
P VF
GR F
FL M
R C
BF VC
BI G
Carbonate
Siliciclastic
SANDS
Lithology
Limestone
Evaporitic mudstone
Nodular limestone
Argillaceous limestone
Marl
Calcareous mudstone
Sedimentology
Laminations
Evaporites
Dendrites
Iron staining
Paleontology
Bivalve Shells
Shell Fragments
Gastropod Shells
Orbitolina minutia
Ichnology
Thalassinoides
Paleophycus
Nodular Bioturbation
Ichnofabric Index: ii1-ii6

Supplemental Figure 2. Stratigraphic column from central Blanco County, Texas. Section includes the Lower Evaporite and Fossiliferous HSUs. Ichnofabric index for individual beds shown.

Appendix III

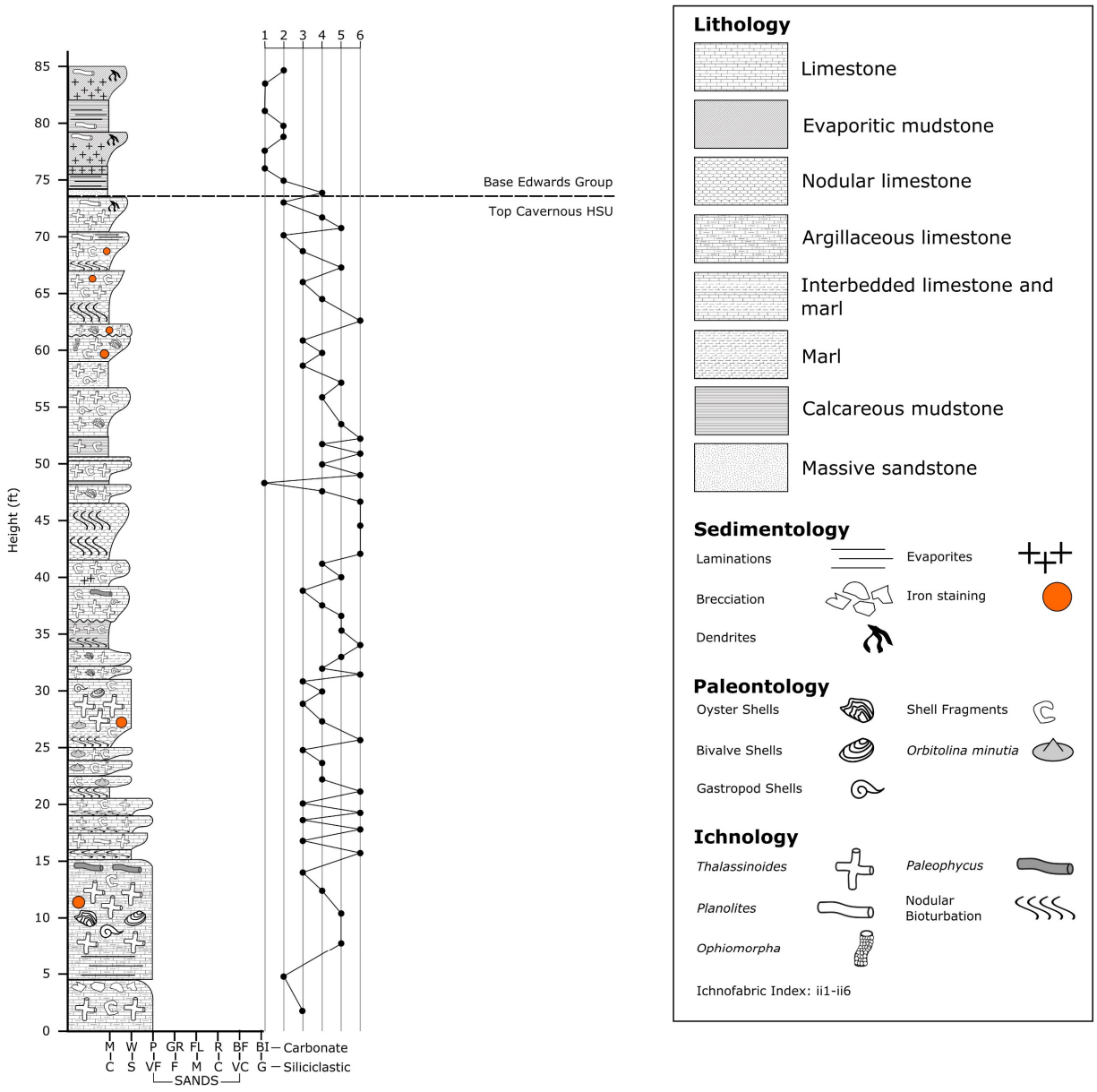

Supplemental Figure 3. Stratigraphic column from northern Bexar County, Texas. Section includes the Cavernous HSU and the base of the Basal Nodular member of the Kainer Formation of the Edwards Group. Ichnofabric index for individual beds shown.

Appendix IV

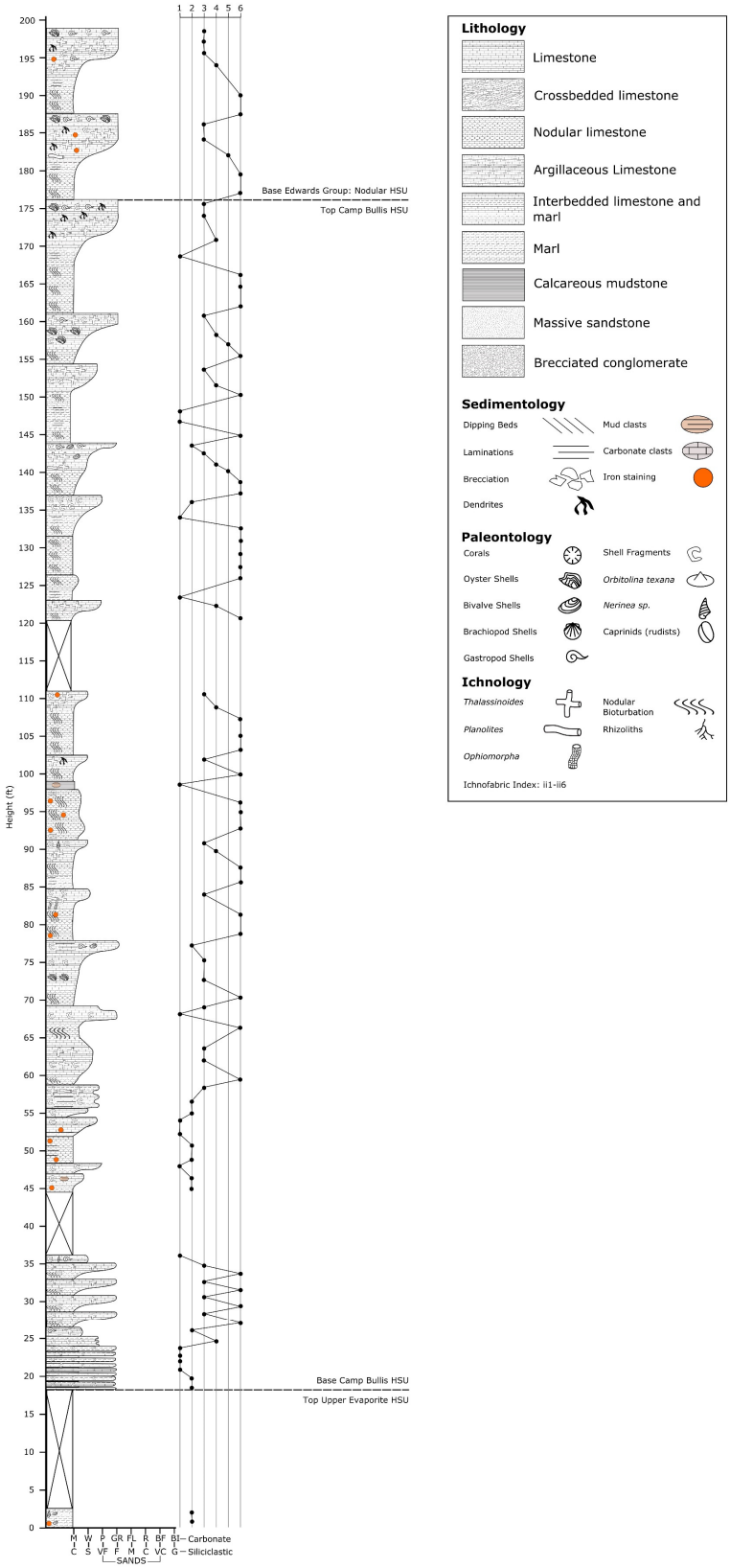
1 2 3 4 5 6
Base Edwards Group: Nodular HSU
Top Camp Bullis HSU
Base Camp Bullis HSU
Top Upper Evaporite HSU
Height (ft)
M W P GR FL R BF BI — Carbonate
C S VF F M C VC G — Siliciclastic
SANDS
Lithology
Limestone
Crossbedded limestone
Nodular limestone
Argillaceous Limestone
Interbedded limestone and marl
Marl
Calcareous mudstone
Massive sandstone
Brecciated conglomerate
Sedimentology
Dipping Beds
Laminations
Brecciation
Dendrites
Mud clasts
Carbonate clasts
Iron staining
Paleontology
Corals
Oyster Shells
Bivalve Shells
Brachiopod Shells
Gastropod Shells
Shell Fragments
Orbitolina texana
Nerinea sp.
Caprinids (rudists)
Ichnology
Thalassinoides
Planolites
Ophiomorpha
Nodular Bioturbation
Rhizoliths
Ichnofabric Index: ii1-ii6

Supplemental Figure 4. Stratigraphic column from western Bandera County, Texas. Section includes the Upper Evaporite and Camp Bullis hydrostratigraphic units. The base of the overlying Edwards Group (VIII) is also included. Ichnofabric index for individual beds shown.

Appendix V

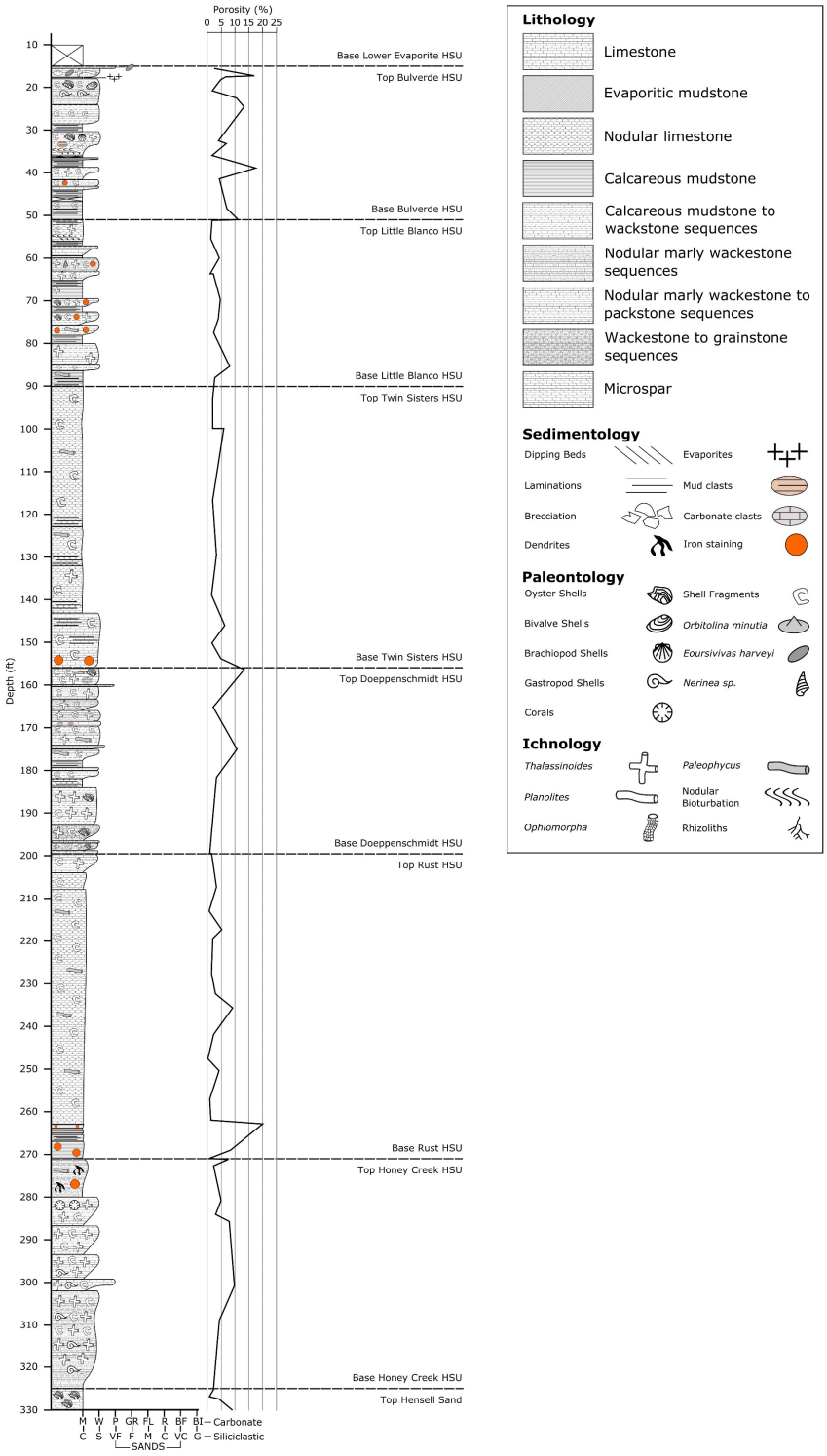
Porosity (%)
0 5 10 15 20 25
Depth (ft)
10
20
30
40
50
60
70
80
90
100
110
120
130
140
150
160
170
180
190
200
210
220
230
240
250
260
270
280
290
300
310
320
330
Base Lower Evaporite HSU
Top Bulverde HSU
Base Bulverde HSU
Top Little Blanco HSU
Base Little Blanco HSU
Top Twin Sisters HSU
Base Twin Sisters HSU
Top Doeppenschmidt HSU
Base Doeppenschmidt HSU
Top Rust HSU
Base Rust HSU
Top Honey Creek HSU
Base Honey Creek HSU
Top Hensell Sand
M C
W S
P VF
GR F
FL M
R C
BF VC
BI G
Carbonate
Siliciclastic
SANDS
Lithology
Limestone
Evaporitic mudstone
Nodular limestone
Calcareous mudstone
Calcareous mudstone to wackstone sequences
Nodular marly wackestone sequences
Nodular marly wackestone to packstone sequences
Wackestone to grainstone sequences
Microspar
Sedimentology
Dipping Beds
Evaporites
Laminations
Mud clasts
Brecciation
Carbonate clasts
Dendrites
Iron staining
Paleontology
Oyster Shells
Shell Fragments
Bivalve Shells
Orbitolina minutia
Brachiopod Shells
Eoursivivas harveyi
Gastropod Shells
Nerinea sp.
Corals
Ichnology
Thalassinoides
Paleophycus
Planolites
Nodular Bioturbation
Ophiomorpha
Rhizoliths

Supplemental Figure 5. Core analysis from MW9-CC, central Bexar County, Texas. Section includes the Honey Creek, Rust, Twin Sisters, Doeppenschmidt, Little Blanco, Bulverde and base of the Lower Evaporite hydsrostratigraphic units (HSUs). The underlying Hammett Shale, Cow Creek Limestone, and Hensel Sand of the Persall Formation are also included. Matrix porosity is recorded for the Glen Rose Limestone HSUs

Appendix VI

Supplemental Table 1. Point counted matrix porosity taken from core MW9-CC in northern Bexar County, Texas.

Sample	Location	Hydrostratigraphic Unit	Matrix Porosity (%)
MW9 15.15	MW9-CC	Bulverde	2.77
MW9 16.9	MW9-CC	Bulverde	17.33
MW9 17.2	MW9-CC	Bulverde	6.49
MW9 17.8	MW9-CC	Bulverde	4.75
MW9 20.3	MW9-CC	Bulverde	1.68
MW9 22.1	MW9-CC	Bulverde	10.70
MW9 23.85	MW9-CC	Bulverde	13.18
MW9 24.4	MW9-CC	Bulverde	13.61
MW9 32.3	MW9-CC	Bulverde	3.77
MW9 32.8	MW9-CC	Bulverde	7.51
MW9 35.8	MW9-CC	Bulverde	1.38
MW9 38.5	MW9-CC	Bulverde	18.09
MW9 41.2	MW9-CC	Bulverde	4.42
MW9 47.8	MW9-CC	Bulverde	7.12
MW9 50.65	MW9-CC	Bulverde	11.41
MW9 50.9	MW9-CC	Bulverde	1.69
MW9 55.15	MW9-CC	Little Blanco	1.37
MW9 59.7	MW9-CC	Little Blanco	4.48
MW9 63.3	MW9-CC	Little Blanco	1.01
MW9 63.5	MW9-CC	Little Blanco	2.41
MW9 69.25	MW9-CC	Little Blanco	4.76
MW9 73.75	MW9-CC	Little Blanco	4.10
MW9 77.1	MW9-CC	Little Blanco	2.37

MW9 85.15	MW9-CC	Little Blanco	8.25
MW9 87.7	MW9-CC	Little Blanco	2.75
MW9 92.55	MW9-CC	Twin Sisters	2.03
MW9 99.7	MW9-CC	Twin Sisters	2.03
MW9 99.7	MW9-CC	Twin Sisters	6.10
MW9 116.55	MW9-CC	Twin Sisters	2.03
MW9 129.3	MW9-CC	Twin Sisters	3.39
MW9 138.65	MW9-CC	Twin Sisters	1.70
MW9 145.75	MW9-CC	Twin Sisters	6.44
MW9 149.9	MW9-CC	Twin Sisters	1.71
MW9 153.7	MW9-CC	Twin Sisters	5.08
MW9 156.15	MW9-CC	Doeppenschmidt	13.65
MW9 165.05	MW9-CC	Doeppenschmidt	2.03
MW9 174.95	MW9-CC	Doeppenschmidt	10.85
MW9 181.55	MW9-CC	Doeppenschmidt	3.33
MW9 199.1	MW9-CC	Doeppenschmidt	1.01
MW9 199.3	MW9-CC	Doeppenschmidt	1.67
MW9 207.1	MW9-CC	Rust	3.41
MW9 212.75	MW9-CC	Rust	0.68
MW9 217.2	MW9-CC	Rust	5.44
MW9 219.2	MW9-CC	Rust	2.05
MW9 227.6	MW9-CC	Rust	1.70
MW9 232.2	MW9-CC	Rust	3.04
MW9 235.55	MW9-CC	Rust	9.34
MW9 241.45	MW9-CC	Rust	2.41
MW9 247.4	MW9-CC	Rust	0.34
MW9 250.2	MW9-CC	Rust	4.41
MW9 256.95	MW9-CC	Rust	1.02
MW9 261.8	MW9-CC	Rust	1.37

MW9 262.7	MW9-CC	Rust	20.54
MW9 268.65	MW9-CC	Rust	8.87
MW9 270.7	MW9-CC	Rust	0.67
MW9 271.2	MW9-CC	Honey Creek	8.11
MW9 272.55	MW9-CC	Honey Creek	2.35
MW9 280.6	MW9-CC	Honey Creek	5.05
MW9 283.95	MW9-CC	Honey Creek	3.06
MW9 285.5	MW9-CC	Honey Creek	8.00
MW9 300.8	MW9-CC	Honey Creek	9.93
MW9 308.8	MW9-CC	Honey Creek	4.38
MW9 325.1	MW9-CC	Honey Creek	2.36
MW9 326.65	MW9-CC	Honey Creek	0.67
MW9 327.2	MW9-CC	Honey Creek	4.39
MW9 330.15	MW9-CC	Honey Creek	9.38
MW9 332.45	MW9-CC	Honey Creek	9.12
MW9 333.3	MW9-CC	Honey Creek	5.76

Supplemental Table 2. Porosity and permeability results for plugs from core MW5-LGR in northern Bexar County, Texas.

Sample	Location	Hydrostratigraphic Unit	Porosity (%)	Permeability (mD)
MW5 75.55	MW5-LGR	Fossiliferous	15.5	0.049
MW5 92.15	MW5-LGR	Fossiliferous	17.3	0.091
MW5 96.95	MW5-LGR	Fossiliferous	18.5	0.121
MW5 104.2	MW5-LGR	Fossiliferous	26.2	406
MW5 113.35	MW5-LGR	Fossiliferous	17.1	0.103
MW5 115.4	MW5-LGR	Fossiliferous	16.0	0.022
MW5 124.35	MW5-LGR	Fossiliferous	6.0	0.0043
MW5 125.15	MW5-LGR	Lower Evaporite	22.8	0.083
MW5 136.2	MW5-LGR	Lower Evaporite	14.7	0.07
MW5 142.65	MW5-LGR	Bulverde	10.9	0.137
MW5 154.35	MW5-LGR	Bulverde	24.5	0.446
MW5 168.5	MW5-LGR	Bulverde	14.2	0.017
MW5 171.2	MW5-LGR	Bulverde	18.4	0.095
MW5 173.3	MW5-LGR	Little Blanco	27.0	1.36
MW5 178.7	MW5-LGR	Little Blanco	15.0	0.082
MW5 189.25	MW5-LGR	Little Blanco	14.1	0.013
MW5 196.65	MW5-LGR	Little Blanco	2.72	N/A
MW5 202.7	MW5-LGR	Little Blanco	24.8	56.8
MW5 205.7	MW5-LGR	Little Blanco	2.71	N/A
MW5 207.4	MW5-LGR	Little Blanco	20.0	0.385
MW5 215	MW5-LGR	Twin Sisters	16.2	0.432
MW5 225.25	MW5-LGR	Twin Sisters	16.6	0.049
MW5 232.4	MW5-LGR	Twin Sisters	17.3	0.046
MW5 245.1	MW5-LGR	Twin Sisters	22.9	0.485
MW5 257.5	MW5-LGR	Twin Sisters	20.5	0.195

MW5 269.55	MW5-LGR	Twin Sisters	14.8	0.02
MW5 279.55	MW5-LGR	Twin Sisters	2.69	N/A
MW5 286.4	MW5-LGR	Doeppenschmidt	14.6	1.15
MW5 296.55	MW5-LGR	Doeppenschmidt	22.2	8.12
MW5 297.6	MW5-LGR	Doeppenschmidt	16.6	1.62
MW5 304.65	MW5-LGR	Doeppenschmidt	15.1	0.0091
MW5 318.8	MW5-LGR	Doeppenschmidt	2.7	N/A
MW5 323.4	MW5-LGR	Doeppenschmidt	2.71	N/A
MW5 324.7	MW5-LGR	Doeppenschmidt	14.8	0.965
MW5 329.3	MW5-LGR	Rust	15.0	0.277
MW5 332.75	MW5-LGR	Rust	2.71	N/A
MW5 347.4	MW5-LGR	Rust	12.1	0.07
MW5 359.3	MW5-LGR	Rust	14.6	0.23
MW5 365.6	MW5-LGR	Rust	19.8	0.938
MW5 381.5	MW5-LGR	Rust	18.9	3.75
MW5 391.5	MW5-LGR	Rust	13.9	0.132
MW5 394.6	MW5-LGR	Rust	24.1	4.14
MW5 395.7	MW5-LGR	Honey Creek	24.6	2.38
MW5 396.9	MW5-LGR	Honey Creek	21.4	3.15
MW5 407.3	MW5-LGR	Honey Creek	30.2	91.6
MW5 414.8	MW5-LGR	Honey Creek	2.71	N/A
MW5 431.2	MW5-LGR	Honey Creek	2.71	N/A
MW5 440.9	MW5-LGR	Honey Creek	2.71	N/A
MW5 449	MW5-LGR	Honey Creek	2.71	N/A

Supplemental Table 3. Porosity and permeability results for plugs from outcrops in Hays and Kendall counties, Texas.

Sample	Location	Hydrostratigraphic Unit	Porosity (%)	Permeability (mD)
ABK-A	Bandera County	Camp Bullis	9.2	0.090
ABK-B	Bandera County	Camp Bullis	20.1	1.93
ABK-C	Bandera County	Camp Bullis	10.0	0.023
ABK-D	Bandera County	Camp Bullis	21.3	2.07
ABK-E	Bandera County	Camp Bullis	8.3	0.014
ABK-F	Bandera County	Camp Bullis	11.9	0.095
ABK-G	Bandera County	Camp Bullis	11.3	0.0076
ABK-H	Bandera County	Camp Bullis	22.6	0.697
ABK-1	Bandera County	Camp Bullis	35.9	1.91
ABK-2	Bandera County	Camp Bullis	34.6	130.
ABK-3	Bandera County	Camp Bullis	23.6	37.5
ABK-4	Bandera County	Camp Bullis	28.4	8.39
ABK-7	Bandera County	Camp Bullis	32.1	54.7
ABK-8	Bandera County	Camp Bullis	8.2	0.0010
ABK-9	Bandera County	Camp Bullis	9.0	0.0037
ABK-10	Bandera County	Camp Bullis	13.5	2.48
ABK-11	Bandera County	Camp Bullis	3.4	0.00
Narrows	Hays County	Honey Creek	27.7	7.26

CHAPTER 3. EFFECTS OF *THALASSINOIDES* ICHNOFABRICS ON THE PETROPHYSICAL PROPERTIES OF THE LOWER CRETACEOUS LOWER GLEN ROSE LIMESTONE, MIDDLE TRINITY AQUIFER, NORTHERN BEXAR COUNTY, TEXAS

Currently in review as:

Golab, J.A., Smith, J.J., Clark, A.K., and Blome, C.D., 2016, Effects of *Thalassinoides* Ichnofabrics on the Petrophysical Properties of the Lower Cretaceous Lower Glen Rose Limestone, Middle Trinity Aquifer, Northern Bexar County, Texas: Journal of Sedimentary Geology.

Abstract

The combined Edwards and Trinity aquifer system is the primary source of freshwater for the rapidly growing San Antonio and Austin metropolitan areas. The karstic Lower Cretaceous (Aptian–Albian) Lower Glen Rose Limestone (GRL) contains the middle Trinity aquifer and has been subdivided into six hydrostratigraphic units (HSUs) with distinct hydrologic characteristics. These HSUs were first identified in the subsurface via core examination at the Camp Stanley Storage Activity (CSSA) in northern Bexar County, Texas and were then correlated to associated gamma-ray and resistivity logs. The Trinity aquifer system is a telogenetic karst and fluid flow is directed primarily through solution-enhanced faults, fractures, and pervasive *Thalassinoides* networks because matrix porosity of both transmissive and confining HSUs is very low. Meteoric water infiltrates the Trinity aquifer through vertically-oriented faults and likely moves laterally through biogenic pores. Two 7.62 cm diameter GRL cores and well logs from

monitoring wells CS-MW9-CC and CS-MW5-LGR recovered from the CSSA were used to characterize the effect such large-scale *Thalassinoides* networks have on the petrophysical properties (resistivity and natural gamma-ray) of four HSUs (Honey Creek, Rust, Doeppenschmidt, and Twin Sisters HSUs). Resistivity logs show that resistance values greater than 300 Ω-m correlate with well-developed biogenic porosity and values greater than 650 Ω-m are associated with solution enhancement of the *Thalassinoides* networks. These high resistivity zones are cyclical and are identified in muddy confining units, even when no changes in lithology or karstic development are identified. Pervasive biogenic networks are also likely the starting point for karstic development along faults. Natural gamma-ray logs do not reflect hydrologic characteristics directly, but are inversely correlated to resistivity logs and display m-scale cyclicity. Resistivity logs can be used to identify interconnected *Thalassinoides* networks within GRL strata and when coupled with natural gamma-logs, the lateral distribution of these networks within HSUs can be correlated. Identifying such fluid pathways is of particular importance for wells not located in proximity to major faults and karstic features.

1.0 Introduction

The combined Edwards and Trinity aquifers are contained within the Lower Cretaceous carbonate and siliciclastic strata of the Central Texas Platform and are the primary source of fresh water for the cities of San Antonio and Austin, Texas. The Trinity aquifer system is contained within the Trinity Group and subdivided into the upper, middle, and lower Trinity aquifers (Barker and Ardis, 1996). The Lower Glen Rose Limestone (GRL), a major highstand carbonate system within the Trinity Group, contains the majority of the middle Trinity aquifer and has been subdivided into six hydrostratigraphic units (HSUs; Blome and Clark, 2014; Clark

et al. 2014). These HSUs have distinct hydrologic characteristics (Choquette and Pray, 1970) and were first identified in the subsurface using gamma-ray and resistivity logs from the Camp Stanley Storage Activity (CSSA) in northern Bexar County, Texas (Fig. 1; Clark, 2004; Parsons 2006; Blome and Clark, 2014).

Resistivity logs are commonly used to determine relative porosity and permeability; with higher resistivity values associated with higher hydrologic connectivity (Zhou et al., 2002; Angulo et al., 2011). Traditionally, high resistivity values in the Lower GRL have been attributed to karstic development along faults (e.g., Wierman et al., 2010). While meteoric waters enter the Lower GRL along a system of nearly vertical normal faults and fractures (Horvorka et al., 1994; Maclay, 1995), lateral movement of ground water is within beds containing networks of the trace fossil *Thalassinoides* (Golab et al., 2016). Most of these biogenic fluid pathways have been enhanced by meteoric and groundwater flow and it is likely that most Lower GRL karstic features are the result of water moving away from faults through these interconnected burrow networks.

This study focuses on resistivity and natural gamma-ray responses to the presence of *Thalassinoides* networks within the Lower GRL HSUs and shows that the biogenic fluid pathways identified in outcrop can be correlated into the subsurface via geophysical logs and have the potential to be correlated over the entire extent of the Edwards and Trinity aquifers. *Thalassinoides* networks identified in outcrop are likely the primary reason behind cyclic high resistivity values seen in logs from the transmissive Honey Creek and Doeppenschmidt HSUs. Identifying laterally continuous zones of biogenic porosity in the subsurface will be valuable for developing a three-dimensional geologic framework for the Trinity aquifer.

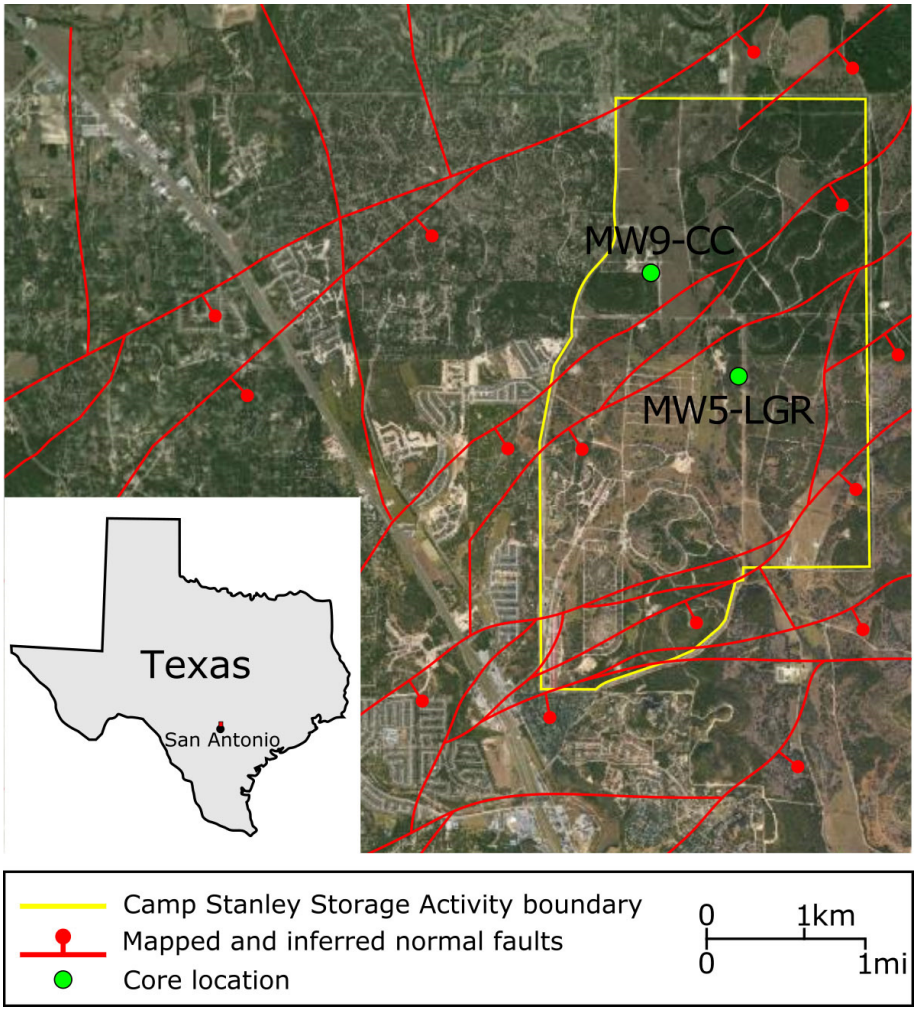

Figure 1. Area map showing the location of the two cores (CS-MW9-CC and CS-MW5-LGR) in northern Bexar County, Texas and the boundary of the Camp Stanley Storage Activity Area. Faults are shown in red with downthrown block indicated. Fault and core locations modified from Clark (2004) and Pantea et al. (2014). Satellite imagery from Google Earth (2016).

2.0 Geologic background

The Lower GRL is ~70–90 m thick in northern Bexar County, Texas and is laterally extensive (Fig. 2; Imlay, 1945; George, 1952; Stricklin et al., 1971; Pittman, 1989). The Lower GRL, in addition to most of the underlying Pearsall Formation, contains the middle Trinity aquifer and acts as a catchment for the overlying Edwards and upper Trinity aquifers (Small and Lambert 1998). The Lower GRL has been subdivided into six HSUs from outcrop studies using a

porosity-based classification system first defined by Maxey (1964) and Choquette and Pray (1970). These HSUs are, in ascending order, the Honey Creek, Rust, Doeppenschmidt, Twin Sisters, Little Blanco, and Bulverde HSUs (Blome and Clark, 2014; Clark et al., 2014). The Honey Creek, Doeppenschmidt, and Little Blanco HSUs are defined as transmissive units; the Rust and Twin Sisters are defined as confining units; and the Bulverde is defined as a semi-confining unit (Clark et al., 2014; Blome and Clark, 2014; Golab et al., 2016). In the subsurface, these HSUs were first identified in cores from the CSSA (Clark, 2004; Parsons, 2006; Blome and Clark, 2014). Geophysical logs from these boreholes were then used to correlate natural gamma-ray and resistivity response to the HSU contacts identified in the cores.

Changes in well-log response are related to stratigraphic variability in mud content with respect to natural gamma and permeability as recorded by resistivity (Zhou et al., 2002; Angulo et al., 2011). Geophysical logs, particularly natural gamma-ray logs, have since been used to correlate Lower GRL strata containing the middle Trinity aquifer throughout the extent of the Trinity aquifer system into the subsurface (e.g., Small and Lambert, 1998; Blome et al., 2005; Broun, 2011; Pantea et al., 2014). The middle Trinity aquifer is of particular importance because it produces better quality water than the upper Trinity aquifer which often contains high amounts of dissolved evaporitic minerals (Parsons, 2006; Pantea et al., 2014; Golab et al., 2016).

Previous studies of ichnofossils in Trinity aquifer strata have focused on outcrops (Cunningham and Sukop, 2012; Golab et al., 2016; Clark et al., 2016). The sedimentological and ichnological characteristics of the six Lower GRL HSUs have been described in detail from outcrop and core (e.g., Blome and Clark, 2014; Clark and Morris, 2015; Golab et al., 2016; Clark et al., 2016). All of these HSUs—transmissive, confining, and semi-confining—generally consist of argillaceous mudstone–packstone successions with abundant *Thalassinoides*-dominated

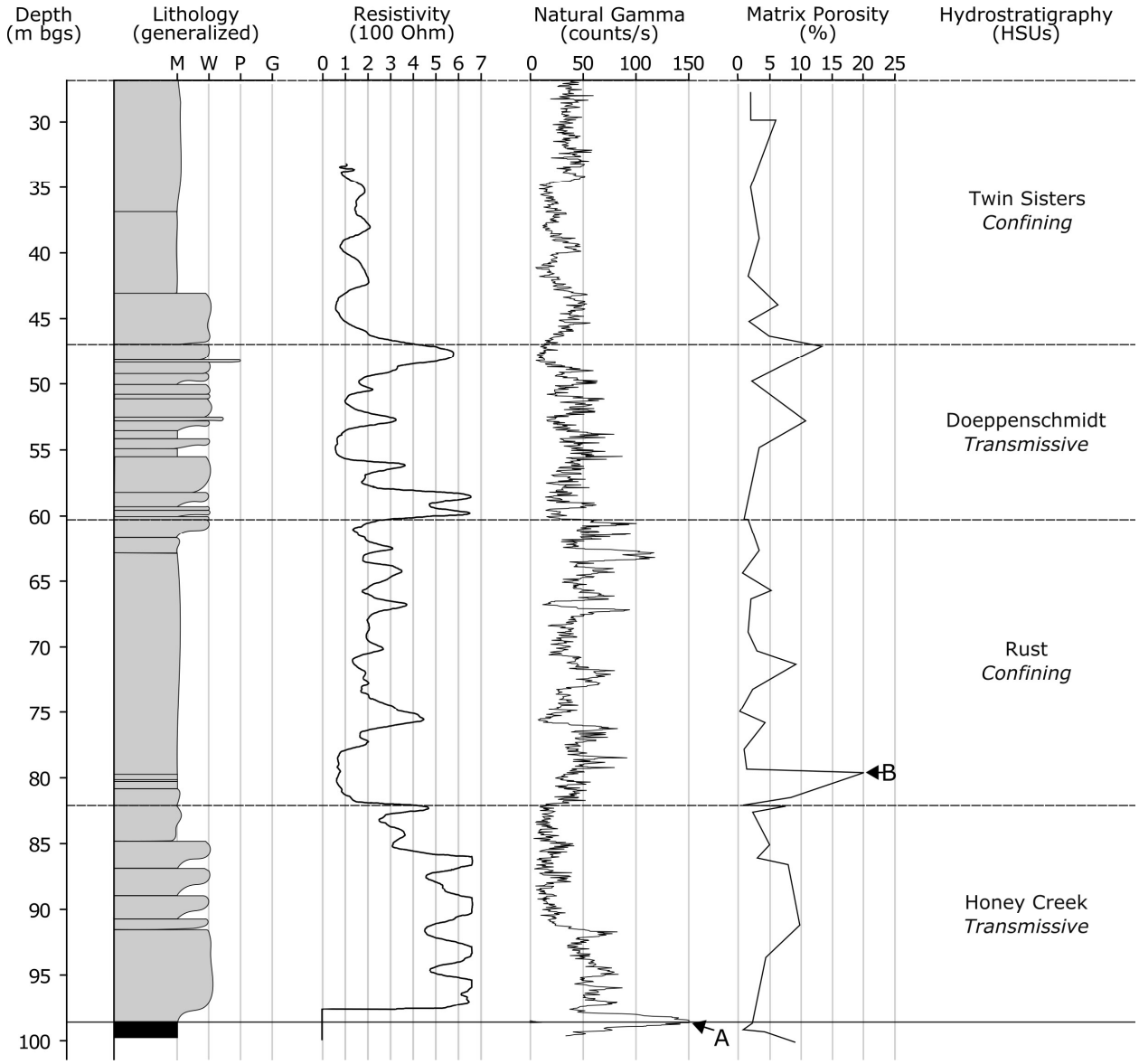

Figure 2. Section showing the Glen Rose Limestone in MW9-CC. Figure includes generalized lithology at depth below land surface, resistivity logs, natural gamma, matrix porosity from point counts and hydrostratigraphic unit contacts. A) High gamma-ray value (>150 CPS) associated with the shalely top of the Bexar Shale member of the Pearsall Formation. B) High matrix porosity value associated with a thin wackestone bed near the base of the confining Rust hydrostratigraphic unit.

ichnofabrics (Golab et al., 2016; Clark et al., 2016). Commonly, Lower GRL HSUs are characterized by m-scale cyclic successions of mudstone and wackestone grading upsection to packstone, with laterally discontinuous rudist bioherms (Behrens, 1965; Clark, 2003; Golab et

al., 2016 Clark and Morris, 2015). These successions are interpreted as high-frequency (5^{th}-order), shallowing-upward sequences (Ward and Ward, 2007). Additionally, most Lower GRL strata have been extensively bioturbated and are dominated by three-dimensional, boxwork *Thalassinoides* networks (Cunningham and Sukop, 2012; Golab et al., 2016). Lower GRL strata also contain lesser amounts of *Palaeophycus*, *Planolites*, rhizoliths, Serpulid traces, and *Cruziana* (Golab et al., 2016). Generally, transmissive and semi-confining HSUs contain well-developed biogenic porosity whereas confining HSUs have been homogenized due to pervasive bioturbation (Golab et al., 2016; Clark et al., 2016).

Within the m-scale mudstone–packstone successions that compose the transmissive Lower GRL HSUs, ichnofabric indices (ii) tend to decrease upsection (Golab et al., 2016). Ichnofabric indices are used to estimate the volumetric amount of bioturbation within strata (Droser and Bottjer, 1986) and are used as proxy for hydrology within strata. In many cases, beds at the base of successions lack obvious sedimentary structures or ichnofossils and were likely completely homogenized by bioturbation (ii6; Golab et al., 2016). Middle portions of successions commonly have ii3–4 and are likely the most transmissive intervals within the sequences (Golab et al., 2016). The tops of most successions have ii1–ii2 and fluid movement is restricted to very low intergranular flow (Golab et al., 2016). Additionally, most of the biogenic porosity in the Lower GRL has been solution enhanced by meteoric water. In contrast, confining HSUs generally lack coarsening upwards trends and are commonly pervasively bioturbated throughout (Golab et al., 2016).

Solution-enhancement features are prominent in carbonate systems (e.g., Mylroie and Carew, 1990), and karstic development in the Lower GRL is primarily along faults and fractures (Horvorka et al., 1994; Maclay, 1995; Faith, 2004). The Lower GRL is normally faulted by the

Miocene Balcones Fault Zone, which extends from central to north Texas with displacements as high as 61 m within the study area (Fig 1; Horvorka et al., 1994; Pantea et al., 2014). Conjugate fractures between these faults further facilitated the infiltration of meteoric water into the subsurface (Kastning, 1986). The abundant *Thalassinoides* networks in the Lower GRL act as the primary fluid pathways between these major faults and karstic features and it is likely that the Lower GRL karstic features are the result of water moving laterally away from faults through these networks (Golab et al., 2016).

This study focuses on resistivity and natural gamma-ray response to the presence of *Thalassinoides* networks within the Honey Creek, Rust, Doeppenschmidt, and Twin Sisters HSUs within two wellbores (CS-MW9-CC and CS-MW5-LGR; Fig. 1) and associated cores from the CSSA. These cores contain most of the typical lithological, sedimentological, and ichnological features of the Lower GRL described from outcrop (e.g., Clark and Morris, 2015; Golab et al., 2016; Clark et al., 2016). All HSUs are fossiliferous and bioclasts may include whole and fragmentary shells of bivalves, echinoids, foraminifera, and gastropods.

The electrical resistivity of strata depends on several factors that include lithology, porosity, permeability, and fluid composition within pores (Angulo, 2011). Resistivity logs are commonly used to determine relative porosity and permeability between units; and higher resistivity values from well logs have commonly been interpreted as karstic development in the Lower GRL (Broun, 2011). Bioturbation and karstic development add additional complexity to these logs, as extensive bioturbation will homogenize sediment and reduce fluid flow.

Natural gamma-ray logs from both wellbores used in this study are variable due to small-scale changes in mud and siliciclastic content. Generally, Lower GRL gamma-ray logs display high (40–60 CPS) values within relatively homogeneous mudstone and marl units. There is an

overall inverse correlation between high gamma-ray values and low resistivity values caused by increased mud content preventing fluid flow. However, this correlation is not consistent due to the presence of *Thalassinoides* burrows that crosscut lithologies. Additionally, karstic development removes carbonate material and concentrates clays and siliciclastics leading to high gamma-ray values (Boero and Schwertmann, 1989; Wierman et al., 2010). Although gamma-ray logs cannot be used directly as hydrologic indicators, they can be used to correlate lithology throughout the aquifer.

3.0 Methods

This study used two 7.62 cm diameter GRL cores, from monitoring wells CS-MW9-CC and CS-MW5-LGR (Fig. 1), recovered from the CSSA and stored at the U.S. Geological Survey's Core Research Center in Denver, Colorado. Both of these boreholes were part of the hydrological characterization of the CSSA by Parsons Engineering and the U.S. Geological Survey (Parsons, 2006), and CS-MW9-CC was designated the type section for the U.S. Geological Survey's interdisciplinary Trinity aquifer remapping project (Clark, 2003, 2005; Clark et al., 2009; Blome and Clark, 2014; Pantea et al., 2014). Both boreholes were logged for gamma-ray, spontaneous potential, and resistivity. Gamma-ray logs were measured in counts per second (CPS) and spontaneous potential logs were measured in millivolts. Resistivity logs were measured in Ohm-meters (Ω-m) and calculated for 8, 16, 32, and 64 in diameters around the well bore (Blome and Clark, 2014). A preliminary analysis of these two cores was published by Blome and Clark (2014) showing revised subsurface contacts for the HSUs and lithologic descriptions.

CS-MW9-CC is ~147 m long and includes the Lower GRL and the Hensel Sand, Cow Creek Limestone, and top of the Hammett Shale members of the underlying Pearsall Formation (Parsons, 2006; Blome and Clark, 2014). For this study, ichnofabric index (ii) and porosity characteristics (Choquette and Pray, 1970) are described. Well logs for CS-MW9-CC included gamma-ray from 0–147 m in depth and spontaneous potential and resistivity from ~32–147 m in depth (Fig. 2).

CS-MW5-LGR is ~142 m long and includes ~38 m of the Upper GRL, Lower GRL, and the top ~4.5 m of the Pearsall Formation (Parsons, 2006; Blome and Clark, 2014). MW5-LGR is a full-diameter core and 52 plug samples were drilled with a diamond-tipped, 2.54 cm-diameter core bit and sent to Weatherford International for helium expansion testing of porosity and permeability (Appendix I). Well logs for CS-MW5-LGR included gamma ray from 0–142 m in depth and from ~68.6–142 m in depth for spontaneous potential and resistivity.

One hundred petrographic thin sections were produced from CS-MW9-CC by Wagner Petrographic, Lindon, Utah. These thin sections were used for lithologic descriptions (see Dunham, 1962) and point counted to determine the relative abundance of bioclasts, mud and cement, and porosity (Fig. 3 and Appendix II). Point counting was conducted using an Olympus BX53 microscope with an automated stepper stage controlled by PetrogLite 3.0 software (Conwy Valley Systems Ltd., 2011). Microphotographs were taken with an Olympus SC100 microscope camera using Olympus Stream 1.9.3 imaging software (Olympus Software Imaging Solutions, 2014).

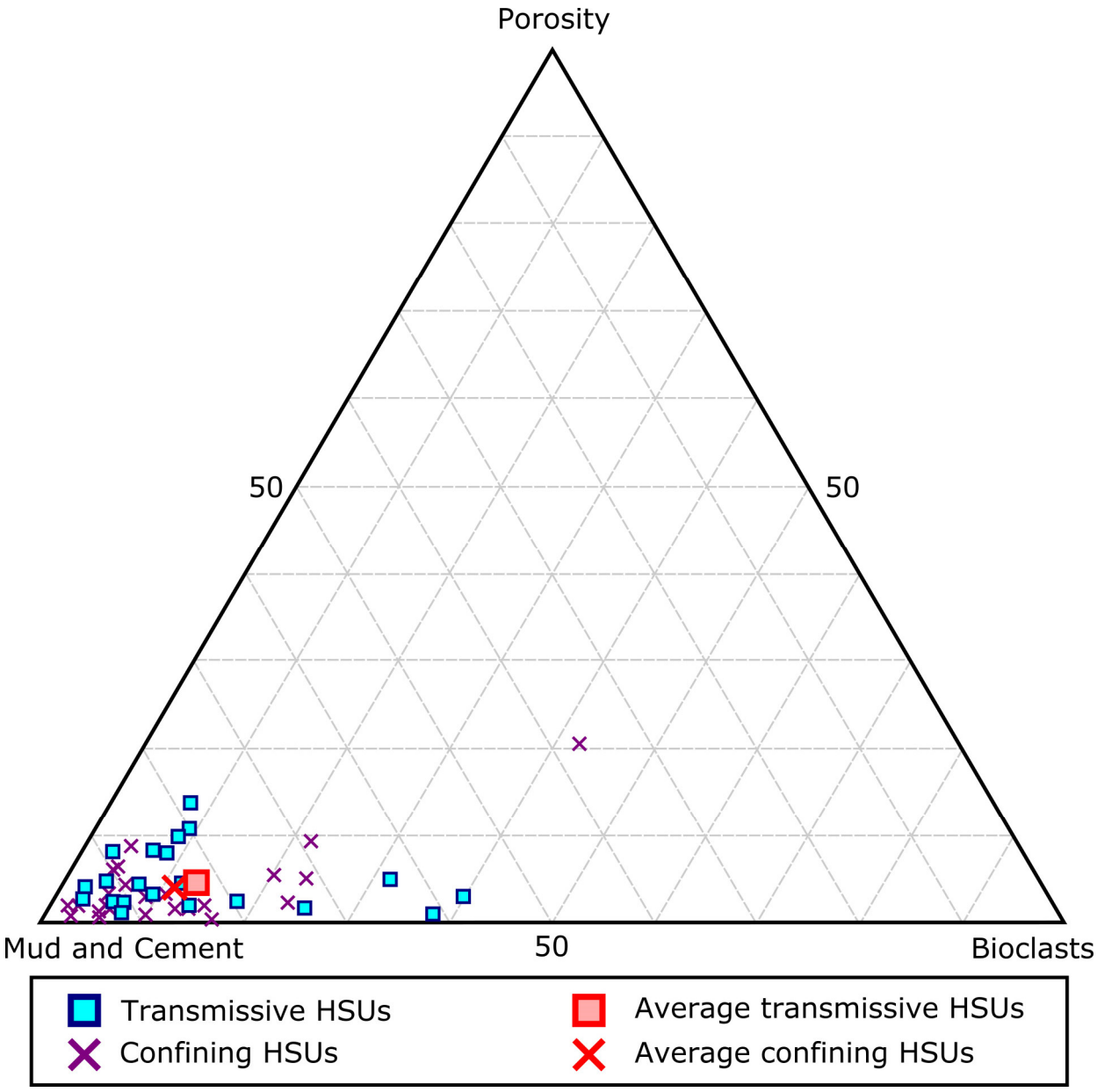

Figure 3. Ternary Diagram showing point count data from thin-sections of MW9-CC. Figure shows relative abundance of biolasts, mud and cement, and porosity. Samples are grouped by hydrostratigraphic characteristics and include transmissive hydrostratigraphic units (HSUs; Honey Creek and Doeppenschmidt) and confining HSUs (Rust and Twin Sisters).

4.0 Results

4.1 Transmissive HSUs

Generally, Lower GRL transmissive HSUs (Honey Creek and Doeppenschmidt) consist of m-scale, coarsening-upward successions of argillaceous fossiliferous wackestone–packstone

(Ward and Ward, 2007; Golab et al., 2016). The ii within these successions commonly decreases upsection and most fluid flow is directed laterally through macro-scale biogenic networks between major faults and karstic features (Golab et al., 2016). Additionally, postdepositional solution-enhancement of *Thalassinoides* networks further increased connectivity within these transmissive units.

4.1.1 Resistivity of transmissive HSUs

Resistivity values for the Honey Creek HSU in CS-MW9-CC range from 245 Ω-m to > 650 Ω-m. CS-MW9-CC values from 85–98 meters below ground surface (mbgs) are generally high (> 440 Ω-m) and contain intervals with a maximum resistivity of > 650 Ω-m (Fig. 2). The majority of the Honey Creek HSU is typical of Lower GRL transmissive units and consists of m-scale successions of argillaceous mudstone transitioning upsection to wackestone with interconnected *Thalassinoides* networks (ii3–4). These successions show resistivity values that shift from ~440 Ω-m to > 650 Ω-m as they transition upsection from mudstone to wackestone. The top ~3 m of the Honey Creek HSU has two maximum resistivity values of ~350 and 475 Ω-m; less than seen lower in the unit. Outcrop and core observations show this upper interval of the Honey Creek HSU is primarily interbedded laminated calcareous mudstone and nodular wackestone lacking interconnected *Thalassinoides* networks and having an ii1–2 (Golab et al. 2016).

The Doeppenschmidt HSU in CS-MW9-CC ranges from ~60–640 Ω-m. The basal ~2 m of the Doeppenschmidt HSU (58–60 mbgs) has high resistivity values that range from ~470 Ω-m to > 650 Ω-m, similar to most Honey Creek HSU strata (Fig. 2). This zone of high resistivity is characterized by argillaceous wackestone with well-developed *Thalassinoides* networks (ii3–4).

The top ~2.5 m of the Doeppenschmidt HSU (47–49.5 mbgs) also displays high resistivity values of with a maximum value of ~580 Ω-m and is similarly characterized by argillaceous wackestone with well-developed *Thalassinoides* networks (ii3–4). In contrast, the middle portion of the Doppenschmidt HSU (50–57 mbgs) is distinct and displays lower resistivity with values that range from ~60–360 Ω-m. Most of this section consists of argillaceous wackestone with some mudstone and is nearly completely homogenized by pervasive bioturbation (ii5–6), leaving little biogenic porosity. In thin section, most moldic porosity in this middle section is occluded by sparry cement. The relatively higher resistivity zones in excess of ~300 Ω-m correlate with core intervals showing ii5 and some distinct *Thalassinoides.*

4.1.2 Natural gamma-ray logs of transmissive HSUs

Generally, transmissive HSUs have lower natural gamma-ray measurements than confining HSUs because they contain beds with less mud and have not been completely homogenized by bioturbation. The contact of the Honey Creek HSU with the underlying Pearsall Formation is characterized by a thin, regional shale bed that can be seen in gamma-ray logs as a spike of ~150 CPS (Fig. 2A; Blome and Clark, 2014). The high gamma-ray value of this organic shale is distinct from Lower GRL strata which are composed mostly of interbedded carbonate muds.

The Honey Creek HSU in CS-MW9-CC contains natural gamma-ray values that range from ~3–83 CPS. The basal ~8m of the Honey Creek HSU (~91–98.5 mbgs) has natural gamma-ray values ranging from ~34–83 CPS (Fig. 2). Values in this basal section that are < 50 CPS correlate with high resistivity values that are > 650 Ω-m. This section of the Honey Creek HSU has the highest average gamma-ray values for the entire core, indicating high mud content. The

overlying ~9 m of the Honey Creek HSU (~82–91 mbgs) have gamma-ray values lower than the underlying strata that range from ~3–40 CPS. Similar to the basal strata of the Honey Creek HSU, there is an inverse correlation between low gamma-ray values and high resistivity response. There is not, however, a distinct gamma-ray log response to the muddy interbedded units seen at the top ~3 m of the Honey Creek HSU.

The Doeppenschmidt HSU in CS-MW9-CC contains natural gamma-ray values that generally range from ~5–70 CPS with maximum values as high as 87 CPS. Similar to the Honey Creek HSU, there is a distinct inverse correlation between high gamma-ray values and low resistivity. The gamma-ray log from the middle portion (~50–57 mbgs) of the Doeppenschmidt HSU shows only a subtle shift toward higher average values and does not closely mirror the shift toward lower resistivity in this section. The relatively consistent nature of Doeppenschmidt HSU gamma-ray values indicates that mud content is consistent throughout the unit and therefore not related directly to these lower resistivity values

4.1.3 Porosity characteristics of transmissive HSUs

Thin sections from the Honey Creek HSU show most m-scale successions transition upsection from argillaceous mudstone (Fig. 4A) to fossiliferous wackestone (Fig. 4B). All samples from the Honey Creek HSU are dominated by mud containing sparry infill of molds (Fig, 4C). Matrix porosity of thin sections averaged 5.8% porosity and samples contained an average of 79% mud and spar (Fig. 3). On the macroscale, the Honey Creek HSU commonly contains well-developed *Thalassinoides* networks, particularly within the middle portions of m-scale coarsening-upward successions. These *Thalassinoides* networks are commonly solution-enhanced from meteoric and ground water and interconnected. Within the Honey Creek, these

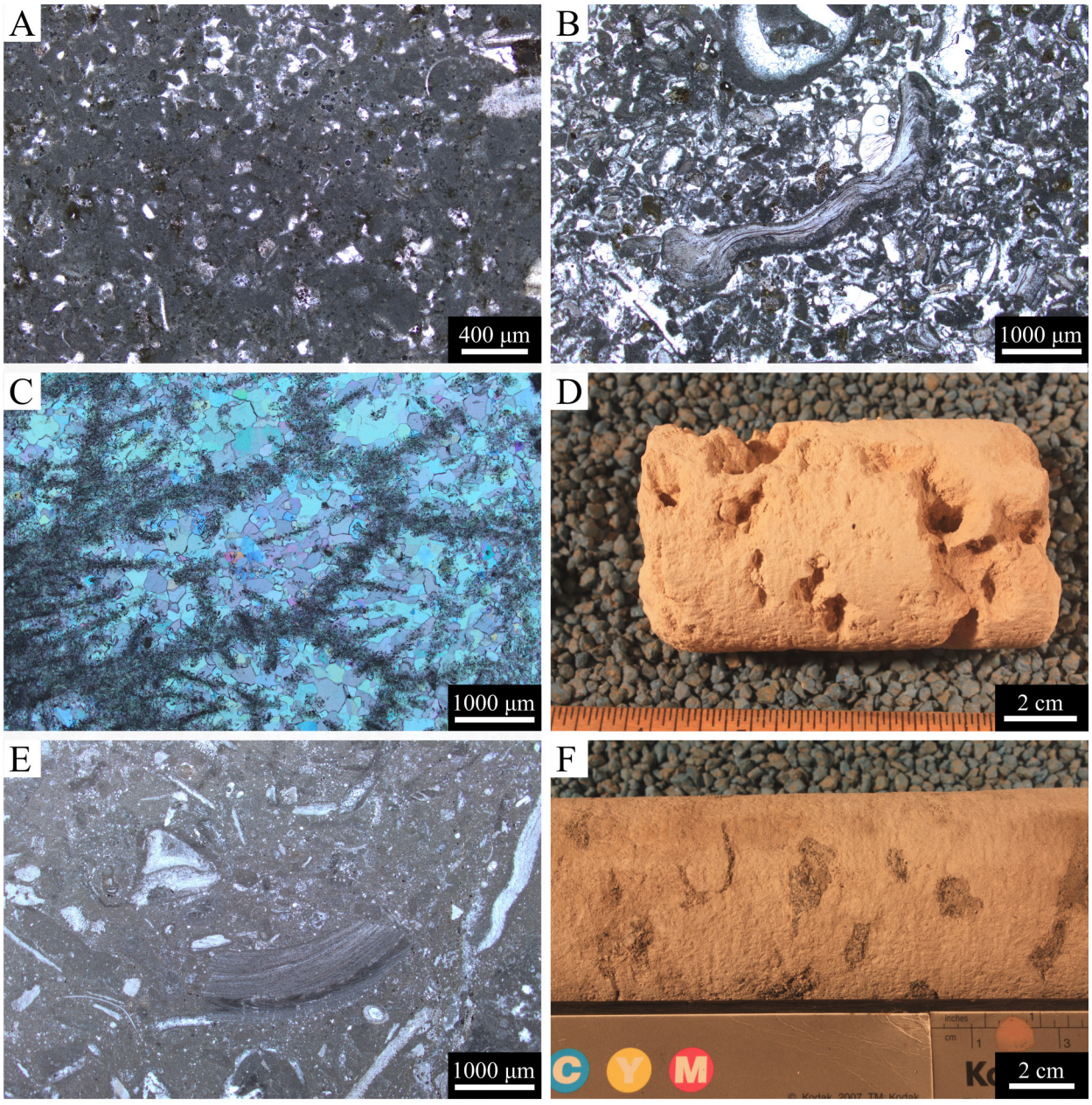

Figure 4. Photographs of common transmissive hydrostratigraphic unit (HSU) features. A) Photomicrograph of an argillaceous mudstone with some shell fragments from the Honey Creek HSU under 40x magnification and plain-polarized light (PP). B) Photomicrograph of an argillaceous fossiliferous wackestone from the Honey Creek HSU at 20x magnification and PP. C) Photomicrograph of an isolated coral head molds infilled with postdepositional spar from the Honey Creek HSU at 20x magnification and under cross-polarized light. D) Solution-enhanced, open *Thalassinoides* network in the Honey Creek HSU. E) Photomicrograph of argillaceous fossiliferous wackestone from the Doeppenschmidt HSU at 20xmagnification and PP. F) *Thalassinoides* network with packstone fill in the Doeppenschmidt HSU.

Thalassinoides networks are commonly open, as groundwater has dissolved any permeable burrow fill (Fig. 4D).

Thin-sections from the Doeppenschmidt HSU have an average of 5.4% matrix porosity and contain 77.5% mud and spar, similar to the Honey Creek HSU. Both the Doeppenschmidt and the Honey Creek HSU averaged between 15–17% biogenic clasts within matrix material (Fig. 4E) and most molds and intergranular porosity were infilled with sparry cement. On the macroscale, the Doeppenschmidt HSU contains well-developed *Thalassinoides* networks within the middle portions of coarsening-upward successions. Unlike the Honey Creek HSU, many of the Doeppenschmidt *Thalassinoides* contain permeable packstone infill (Fig. 4F). In the middle of the Doeppenschmidt HSU, *Thalassinoides* networks have muddier wackestone infill and corresponding generally lower resistivity values, (Fig. 4B). Some of this infill may be coarser material moving through the aquifer after deposition.

4.2 Confining HSUs

Lower GRL confining HSUs (Rust and Twin Sisters) contain more mud and fewer fractures than transmissive HSUs. Confining HSUs generally consist of m-scale successions of pervasively bioturbated nodular mudstone to marly wackestone with ii5–6 (Fig. 2; Golab et al. 2016). Some beds have identifiable *Thalassinoides* networks (ii5), however, these networks are typically mud-filled and do not enhance fluid flow (Golab et al., 2016; Clark et al., 2016). Moldic porosity is common in these units although these molds are generally not solution enhanced or interconnected (Golab et al., 2016; Clark et al., 2016). Most confining successions do not coarsen upward, although some units show this trend in outcrop (Golab et al., 2016; Clark

et al., 2016). Fluid flow within these units is confined to fractures and some *Thalassinoides* with coarser-grained infill, but permeability is relatively low overall.

4.2.1 Resistivity of confining HSUs

Resistivity values for the Rust HSU in CS-MW9-CC range from 60–420 Ω-m. The basal ~2.5 m of this HSU (79.5–82 mbgs) are consistently low (~60 Ω-m) and associated with thinly interbedded mudstones and wackestone with ii1–2 (Fig. 2). The majority of the overlying beds within the Rust HSU (~60–79.5 mbgs) are characterized by resistivity values that fluctuate between ~130 Ω-m and 420 Ω-m. Despite these fluctuations in resistivity, this interval of the core is dominated by relatively homogeneous marly mudstone and wackestone with a nodular, mottled appearance (ii6). Few *Thalassinoides* networks can be identified within beds with ii5, and are associated with resistivity values of up to >400 Ω-m. Outcrop studies show that the Rust HSU contains coarsening-upward successions north of Bexar County (Golab et al., 2016; Clark et al., 2016). Lithologically, such successions are difficult to identify in core; however, resistivity kicks within this section indicate nine potential successions (Fig. 2). Some of these high resistivity zones also correlate to increased matrix porosity from point-counts (see Porosity characteristics of confining HSUs).

The Twin Sisters HSU in CS-MW9-CC has resistivity values that range from ~60–210 Ω-m. The basal ~4 m of this HSU (~43–47 mbgs) is characterized by resistivity values that range from ~50–200 Ω-m upsection. This basal section consists of marly wackestone with some moldic porosity. The overlying beds of the Twin Sisters HSU from ~27–43 mbgs are characterized by ~5 m cycles of resistivity that increase from 60 Ω-m to 210 Ω-m upsection. These beds consist of homogeneous marly mudstone with ii5–6 and few biogenic clasts. The Twin Sisters HSU

contains more mud than the Rust HSU and has lower resistivity on average. Although evidence of cyclicity is difficult to identify lithologically, kicks within the resistivity values for the Twin Sisters HSU are associated with some identifiable *Thalassinoides* networks in the core.

4.2.2 Natural gamma-ray logs of confining HSUs

Nautral gamma-ray values for the Rust HSU range from ~7–116 CPS. The basal ~6 m of this HSU (~76–82 mbgs) is characterized by gamma-ray values that commonly range from ~25–70 CPS with a single kick at ~92 CPS. These relatively high zones are associated with interbedded mudstones and some clay horizons identified in core CS-MW9-CC (Blome and Clark 2014). The overlying beds of the Rust HSU (~60–76 mbgs) have more variable gamma-ray values that range from ~7–95 CPS with values >75 CPS inversely correlated with low resistivity values. Outcrop studies show that the Rust HSU contains some coarsening-upward successions with wackestone to packstone filled *Thalassinoides* in some locations north of Bexar County (Golab et al., 2016; Clark et al., 2016).

Natural gamma-ray values for the Twin Sisters HSU (27–47 mbgs) are not as variable as logs from the Rust HSU and range from ~5–58 CPS. Values in this HSU >25 CPS inversely correlate with low resistivity values < 100 Ω-m. The Twin Sisters HSU contains few identifiable *Thalassinoides* networks and generally has ii6. The cyclic trend seen in the gamma-ray and resistivity logs correlate to the m-scale coarsening-upwards sequences seen in most strata, although this trend is difficult to observe in core. Overall, little fluid flow is possible within the Twin Sisters HSU outside of faults and fractures.

4.2.3 Porosity characteristics of confining HSUs

Point counts from the Rust HSU had an average of 4.3% porosity and contained 81.9% mud and spar (Fig. 5A). One sample had 20.5 % porosity from a single, thin (<1cm) wackestone bed. Most of the Rust HSU in CS-MW9-CC consisted of relatively homogenized wackestone with a nodular appearance (Fig 5B). On the macroscale, few *Thalassinoides* networks were identified and most were mud-filled. Moldic porosity was also very low and existing molds were not interconnected (Fig 5C). The basal ~5 m of the Rust HSU also contained interbedded clayey horizons with ii1.

The Twin Sisters HSU had an average of 3.4 % porosity and contained ~89.4% mud and spar (Fig. 5D). On the macroscale, most of the Twin Sisters HSU was relatively homogenous and contained few identifiable *Thalassinoides*. Generally, beds were ii5–6 and some beds were so heavily bioturbated that the existing *Thalassinoides* networks were collapsed, creating a brecciated horizon (Fig. 5E). Some shaley horizons were identified in the basal ~3 m of the section interbedded with wackestone. The upper ~17 m of the Twin Sisters was predominately mudstone and contained little to no sedimentary structures (Fig. 5F).

5.0 Discussion

5.1 Carbonate pore systems

Although carbonate systems are common aquifers and hydrocarbon reservoirs globally, characterization of their porosity in the subsurface is difficult (e.g., Choquette and Pray, 1970; Ahr et al., 2005; Lønøy, 2006). Carbonate pore systems are complex, and chemical weathering processes such as solution-enhancement of pores via meteoric water are more pronounced in carbonate strata when compared to siliciclastic aquifers and reservoirs (Ramakrishnan et al.,

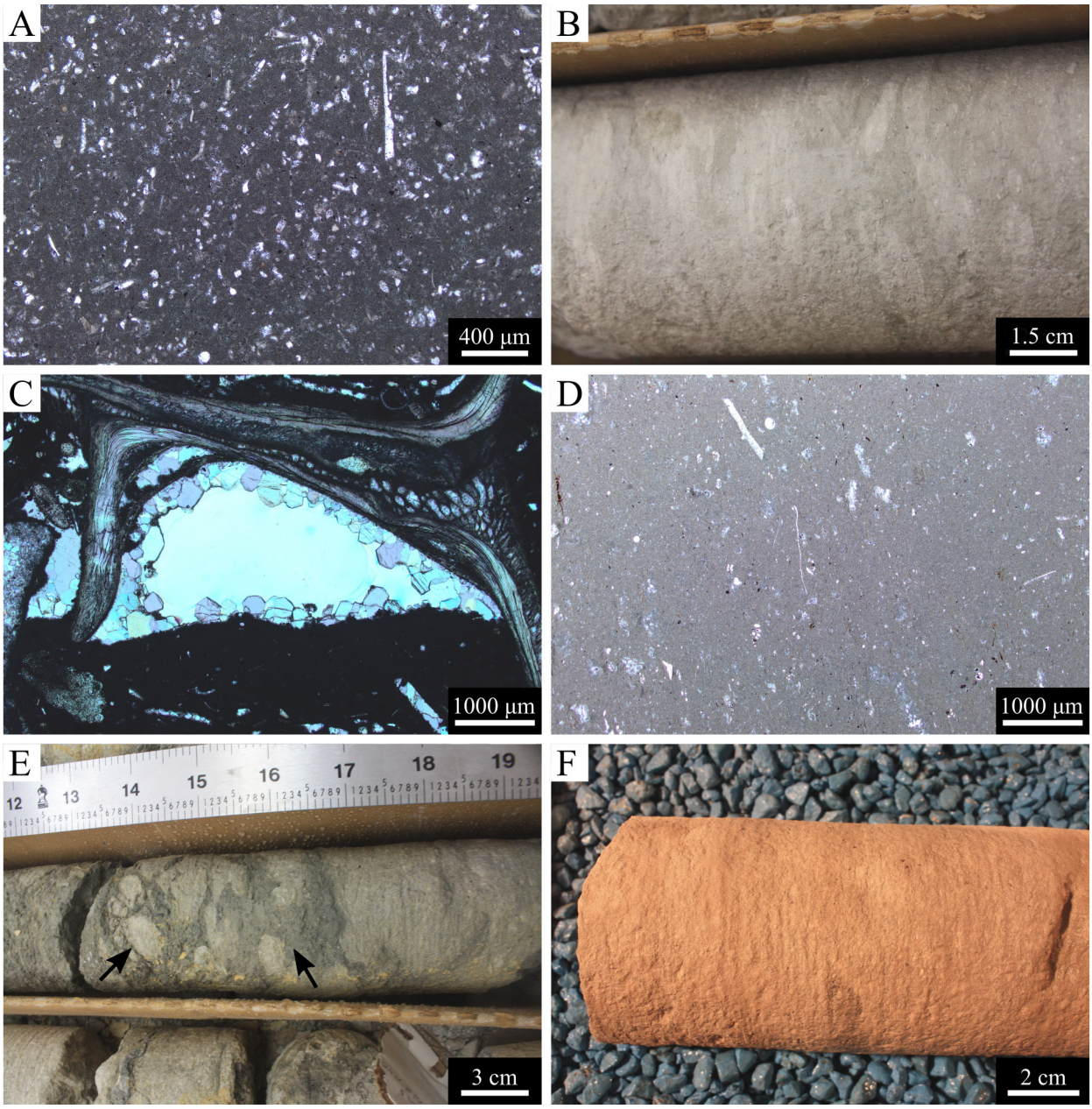

Figure 5. Photographs of common confining hydrostratigraphic unit (HSU) features. A) Photomicrograph of an argillaceous wackestone with shell fragments from the Rust HSU under 40x magnification and plain-polarized light (PP). B) Photograph of core segment of argillaceous mudstone from the Rust HSU with a nodular appearance due to pervasive bioturbation. C) Photomicrograph of a shelter pore with some sparry infill from the Rust HSU under 20x magnification and cross-polarized light. D) Photomicrograph of an argillaceous mudstone with shell fragments from the Twin Sisters HSU under 20x magnification and PP. E) Brecciated horizon due to collapse following solution enhancement of a *Thalassinoides* network from the Twin Sisters HSU. F) Argillaceous mudstone lacking sedimentary structures from the Twin Sisters HSU.

2000; Ahr et al., 2005). The middle Trinity aquifer is primarily a telogenetic karstic aquifer, as most fluid flow in the aquifer is directed through faults and solution-enhanced biogenic pores (Vacher and Mylroie, 2002). The porosity characteristics within telogenetic karsts, such as the Edwards and Trinity aquifers, is particularly difficult to characterize, as there is little to no intergranular flow and fluid pathways crosscut original bedding (White, 1999, 2002; Vacher and Mylroie, 2002; Gingras et al., 2012).

Traditional methods such as point-counting and helium-expansion porosity and permeability testing were developed to measure porosity in siliciclastic systems and carbonate strata with predominately intergranular porosity (Cunningham et al., 2009). Additionally, even in eogenetic karstic aquifers, which contain interganular flow in addition to large-scale fluid pathways, these methods will underestimate fluid flow (Cunningham et al., 2009). These techniques measure the porosity and permeability of the matrix material between cm-scale, interconnected biogenic pores or fractures and do not accurately reflect the true hydrologic properties of the system (Lønøy. 2006; Cunningham et al., 2009).

Some studies have been conducted on both telogenetic and eogenetic aquifers and reservoirs to resolve the problem of fluid-flow characterization of karstic systems (e.g., Vacher and Mylroie, 2002; Ahr et al., 2005; Cunningham et al., 2009; Wright et al., 2014). X-ray tomography scans of cores and hand samples have been used in some cases such as the Biscayne aquifer in southern Florida (Cunningham et al., 2009; Cunningham and Sukop, 2012); but such datasets are currently unavailable for the Edwards and Trinity aquifers. Additionally, although pump tests have been performed on GRL strata by Parsons Engineering at the CSSA (Parsons, 2006), absent direct measurements of fluid flow in individual HSUs, empirically analyzing the hydraulic effects of *Thalassinoides* networks from these measurements is not possible. The

datasets that are currently available for the Edwards and Trinity aquifers includes outcrop studies (e.g., Small and Lambert, 1998; Clark and Morris, 2015; Golab et al., 2016; Clark et al., 2016) and traditional wireline logs (e.g., Wierman et al., 2010; Broun, 2011; Blome and Clark, 2014).

5.2 Trinity aquifer petrophysical properties

The Edwards and Trinity aquifers are relatively unusual as they can be observed in outcrop and subsurface within the same region. Offsets caused by the Miocene Balcones Fault Zone in south-central Texas make it possible to study outcrops of the same strata that contain the Trinity aquifer system. Ichnological and lithological patterns that have been identified in these outcrops can be directly correlated to wireline log data (e.g., Blome and Clark, 2014; Clark and Morris, 2015; Golab et al., 2016). Postdepositional dissolution within biogenic pores has increased the porosity and permeability of most beds within transmissive HSUs of the Lower GRL by interconnecting *Thalassinoides* networks throughout the strata and widening fluid pathways. Additionally, the complete dissolution of the matrix around these *Thalassinoides* networks in close proximity to faults has resulted in the formation of karstic features (Golab et al., 2016). This study shows that the fluid pathways created by these widespread *Thalassinoides* networks can be identified in the subsurface through the use of traditional wireline logs and have the potential to be correlated over the lateral extent of the combined Edwards and Trinity aquifer system.

Resistivity logs, and natural gamma logs to a lesser extent, reflect the amount of interconnected biogenic porosity throughout the subsurface of the Edwards and Trinity aquifers. Pervasive *Thalassinoides* networks are the primary factor in the movement of infiltrating meteoric water laterally away from major faults and associated karstic features in all Lower GRL

strata (Golab et al., 2016; Clark et al., 2016). The m-scale, cyclic nature of high resistivity zones observed from well-logs at the CSSA correlates to the cycles in *Thalassinoides* networks that have been identified in the associated cores and outcrop (e.g., Golab et al., 2016). High resistivity values > 300 Ω-m correlate with *Thalassinoides* networks in core and solution enhancement of these networks is characterized by resistivity values > 650 Ω-m. Although previous studies commonly correlate karstic development with high resistivity (e.g., Wierman et al., 2010), all wells within the Edwards and Trinity aquifers display these cyclical kicks, even when not located in proximity to major faults and associated karstic features. Additionally, these cyclic resistivity kicks can be identified in muddy confining units, even when no changes in lithology or karstic development can be identified. Pervasive *Thalassinoides*-dominated ichnofabrics identified in outcrop and core are therefore the most likely cause of these patterns.

Previous studies have used natural gamma-ray logs to correlate HSUs identified in cores from Bexar County, Texas northward (e.g., Wierman et al., 2010; Broun, 2011; Clark and Morris, 2015). These correlations are based on differences in overall mud content between the HSUs, as well as amount of karstic development observed in outcrop and core. Lower GRL strata are typically argillaceous and contain significant amounts of mud and cement; therefore, most beds have a moderately high and variable gamma-ray signature. Generally, zones with particularly high gamma-ray values, such as the top of the Pearsall Formation, have been used as correlative marker beds and HSUs have been interpreted via thickness observed from outcrop (e.g., Clark, 2003; Braun, 2011; Blome and Clark, 2014).

Natural gamma-ray logs associated with resistivity logs provide additional evidence linking subsurface *Thalassinoides* networks to petrophysical response. Gamma-ray logs are useful for correlating lithology in the subsurface and identifying offset caused by faulting in the

study area (e.g., Parsons, 2006; Broun, 2011; Blome and Clark, 2014). These logs, however, are of limited use in determining hydrostratigraphic characteristics without associated outcrop or core data (e.g., Clark et al., 2009; Clark and Morris, 2015; Golab et al., 2016; Clark et al., 2016). Commonly, gamma-ray logs from the GRL are inversely correlated to resistivity logs with high values correlating to coarse-grained matrix material. Outcrop studies show that the bases of m-scale successions are extensively bioturbated and have ii5–6 (Golab et al., 2016). This extensive bioturbation homogenizes the sediment and results in the relatively high, but variable gamma-ray values that are observed throughout the well-logs. These values, however, are not high enough to be indicative of pure mudstone such as seen at the top of the Pearsall Formation in northern Bexar County (see Fig. 2A).

5.3 Application to analogous karstic units

Cunningham et al. (2009) and Cunningham and Sukop (2011) used digital image logs, caliper logs, conductivity and temperature logs, and borehole flowmeters to evaluate fluid flow in the karstic Biscayne aquifer of southern Florida. These studies used lattice Boltzmann equations to estimate vertical and lateral permeability within core and outcrop samples (Cunningham et al., 2009; Cunningham and Sukop, 2011). The overall permeability within the bioturbated strata of the Biscayne aquifer calculated using these methods was over five orders of magnitude higher than had been previously reported (Cunningham et al., 2009). Similar studies were performed on karstic reservoir strata from the Thamama Formation in Saudi Arabia, where visual imagining of boreholes was combined with nuclear magnetic resonance logging tools to characterize pore systems and flow paths (e.g., Ramakrishnan et al., 2000; Ahr et al., 2005).

Such methods are particularly useful if there are no associated outcrop or core data, but are costly and unavailable for most hydrostratigraphic studies.

More traditional wireline logs, such as gamma-ray and resistivity are commonly taken from aquifer strata, particularly if a groundwater conservation district has been established. If available, such traditional logs can be coupled with detailed hydrostratigraphic analysis from outcrop and core to correlate macroscale biogenic porosity in the subsurface. The use of traditional wireline logs also acts as a method to check the hydrologic properties of the burrow fill and the lateral connectivity of burrow networks. Studies from the Upper Devonian Wabamun Group in Alberta, Canada show that *Thalassinoides* networks become interconnected laterally when over 10% of a stratum is bioturbated but commonly only become vertically connected across strata when over 60% of the sediment is bioturbated (La Croix et al., 2012; Baniak et al., 2013). The difference in permeability between the matrix and the burrow fill will also impact flow paths (Gingras et al., 1999). The ability to verify the permeability of interpreted biogenic networks is important, as the weathered surfaces of outcrops may only provide some information on the connectivity and properties of the burrows.

Identifying ichnofossils and characterizing bioturbation within a sedimentary unit is important, but further data is needed to verify their impact on fluid flow. For example, ichnofossils lined with fine-grained sediment (*Palaeophycus*) or pellets (*Ophiomorpha*) introduce preferred flowpaths, but they may decrease the overall permeability of a stratum by confining and directing groundwater transmission (Cunningham et al., 2009; Tonkin et al., 2010). Passively-filled burrows such as *Thalassinoides* networks may act as megapermeability (Cunningham et al., 2009) if cementation occurs early and the burrows remain open in the subsurface (Tonkin et al., 2010; Golab et al., 2016). Burrow fill that is coarser grained than the

surrounding matrix will maintain this property and act as significant fluid pathways (Cunningham et al., 2009; Tonkin et al., 2010; Golab et al., 2016). If these *Thalassinoides* networks are filled with mud or silt, the permeability of the stratum will be significantly decreased (Tonkin et al., 2010). These changes in interconnectivity and burrow fill will be visible on wireline logs, leading to more accurate interpretations of fluid pathways.

6.0 Conclusions

The Lower GRL in Bexar County, Texas has been divided in to six HSUs which have been defined as transmissive, confining, or semi-confining (Clark et al., 2014; Blome and Clark, 2014; Golab et al., 2016). Generally, transmissive HSUs are composed of m-scale successions of carbonate mudstone and argillaceous wackestone to packstone and these successions can be identified in the subsurface from well logs in the absence of core data. Previous outcrop and core studies have identified pervasive *Thalassinoides*-dominated biogenic networks throughout most of the GRL strata. These networks provide the primary fluid pathways for Trinity aquifer water between major faults and karstic development. Generally, the ichnofabric indices of these networks decrease upsection within the GRL successions. The fluid flow within these networks can be identified in the subsurface as areas of high (>300 Ω-m) resistivity.

When coupled with lithologic interpretations from associated gamma-ray logs, changes in the vertical and lateral distribution of *Thalassinoides* networks observed in core and outcrop can be correlated across several counties north of Bexar County and may be used to correlate these high permeability strata. This will be valuable for developing a three-dimensional geologic framework for the Trinity aquifer. Using traditional wireline logs for hydrostratigraphic interpretations will help develop a better understanding of the lateral extent of *Thalassinoides*

networks within the GRL, but this depends on detailed outcrop studies and does not provide direct measurements of subsurface hydrologic characteristics.

Gaining a complete understanding of the subsurface hydrology of the Edwards and Trinity aquifers will require additional datasets. Studies by Cunningham et al. (2009, 2011) used digital image logs, caliper logs, conductivity and temperature logs, and borehole flowmeters to evaluate fluid flow in the similar Biscayne aquifer of southern Florida. Such detailed techniques are similar to studies performed on karstic reservoir strata from the Thamama Formation (Ahr et al., 2005). Although these techniques are commonly considered cost-prohibitive, their application to Trinity aquifer strata could greatly improve the understanding of aquifer quality and flow paths in south-central TX.

This study shows that resistivity logs can be used to identify well-developed biogenic porosity within GRL strata. This is particularly important for wells not located near major faults and karstic features. When coupled with gamma-logs, an accurate interpretation of the lateral distribution of biogenic porosity within each HSU will be possible. Such an understanding of the vertical and lateral variability of high-permeability *Thalassinoides* networks within Edwards and Trinity aquifer strata is vital for planning future development of central Texas, as the metropolitan areas of San Antonio and Austin continue to grow in population and expand outward from the city centers.

References

Ahr, W.M., Allen, D., Boyd, A., Bachman, H.N., Smithson, A., Clerke, E.A., Gzara, K.B.M., Hassall, J.K., Murty, C.R.K., Zubari, H., and Ramamoorthy, R., 2005, Confronting the Carbonate Conundrum: Oilfield Review, vol. 17, no. 1, p. 18–29.

Angulo, B., Morales, T., Uriarte, J.A., and Antigüedad, I., 2011, Hydraulic Conductivity Characterization of a Karst Recharge Area Using Water Injection Tests and Electrical Resistivity Logging: Engineering Geology, vol. 117, p. 90–96.

Baniak, G.M., Gingras, M.K., and Pemberton, S.G., 2013, Reservoir Characterization of Burrow-Associated Dolomites in the Upper Devonian Wabamun Group, Pine Creek Gas Field, Central Alberta, Canada: Marine and Petroleum Geology, vol. 48, p. 275–292.

Barker, R.A., and Ardis, A.F., 1996, Hydrogeological Framework of The Edwards-Trinity Aquifer System, West-Central Texas: U.S. Geological Survey Professional Paper 1421–B, 61 p.

Behrens, E.W., 1965, Environment Reconstruction for a Part of The Glen Rose Limestone, Central Texas: Sedimentology, v. 4, p. 65–111.

Blome, C.D., Faith, J.R., Pedraza, D.E., Ozuna, G.B., Cole, J.C., Clark, A.K., Small, T.A., and Morris, R.R., 2005, Geologic Map of the Edwards Aquifer Recharge Zone, South-Central Texas: U.S. Geological Survey Scientific Investigations Map 2873.

Blome, C.D., and Clark, A.K., 2014, Key Subsurface Data Help to Refine Trinity Aquifer Hydrostratigraphic Units, South-Central Texas: U.S. Geological Survey Data Series 768, 1 sheet, http://dx.doi.org/10.3133/ds768.

Boero, V. and Schwertmann, U., 1989, Iron Oxide Mineralogy of Terra Rossa and Its Genetic Implications: Geoderma, v. 44, p. 319–327.

Broun, A.S., 2011, East to West Stratigraphic Cross Section, Northern Hays County: In Surface to Subsurface Trinity Lithostratigraphy: Implications for Groundwater Availability in The Hill County, Eastern Blanco and Northern Hays Counties, Texas: Austin Geological Society, Guidebook 33, p. 14–16.

Choquette, P.W., and Pray, L.C., 1970, Geologic Nomenclature and Classification of Porosity in Sedimentary Carbonates: American Association of Petroleum Geologists Bulletin, v. 54, no. 2, p. 207–250.

Clark, A.K., 2003, Geologic Framework and Hydrogeologic Features of the Glen Rose Limestone, Camp Bullis Training Site, Bexar County, Texas: U.S. Geological Survey Scientific Investigations Report 03–4081, 9 p., 1 pl., scale 1:24,000.

Clark, A.K., 2004, Geologic Framework and Hydrogeologic Characteristics of the Glen Rose Limestone, Camp Stanley Storage Activity, Bexar County, Texas: U.S. Geological Survey Scientific Investigations Map 2831, 1 pl., scale 1: 25,000.

Clark, A.R., Blome, C.D., and Faith, J.R., 2009, Map Showing Geology and Hydrostratigraphy of the Edwards Aquifer Catchment Area, Northern Bexar County, South-Central Texas: U.S. Geological Survey Open-File Report 2009-1008.

Clark, A.K., Golab, J.A., and Morris, R.R., 2016, Geologic Framework, Hydrostratigraphy, and Ichnology of the Blanco, Payton, and Rough Hollow 7.5-minute Quadrangles, Blanco, Comal, Hays, and Kendall Counties, Texas: U.S. Geological Survey Scientific Investigations Map 3363, 21 p., 1 sheet, scale 1:24,000.

Clark, A.K., and Morris, R.R., 2015, Geologic and hydrostratigraphic map of the Anhalt, Fischer, and Spring Branch 7.5-minute quadrangles, Blanco, Comal, and Kendall Counties,

Texas: U.S. Geological Survey Scientific Investigations Map 3333, 13 p., 1 sheet, scale 1:50,000.

Clark, A.K., and Morris, R.R., 2015, Geologic and Hydrostratigraphic map of the Anhalt, Fischer, and Spring Branch 7.5-minute Quadrangles, Blanco, Comal, and Kendall Counties, Texas: U.S. Geological Survey Scientific Investigations Map 3333, 13 p., 1 sheet, scale 1:50,000.

Conwy Valley Systems Ltd., 2011, PetrogLite Version 3.0 for MS Windows OS. Conway, United Kingdom.

Cunningham, K.J. and Sukop, M.C., 2011, Multiple Technologies Applied to Characterization of the Porosity and Permeability of the Biscayne Aquifer, Florida: U.S. Geological Survey Open-File Report 2011-1037, 8 p.

Cunningham, K.J. and Sukop, M.C., 2012, Megaporosity and Permeability of *Thalassinoides*-Dominated Ichnofabrics in the Creataceous Karst-Carbonate Edwards-Trinity Aquifer System, Texas: U.S. Geological Survey Open-File Report 2012-1021, 4 p.

Cunningham, K.J., Sukop, M.C., Huang, H., Alvarez, P.F., Curran, H.A., Renken, R.A., and Dixon, J.F., 2009, Prominence of Ichnologically Influenced Macroporosity in the Karst Biscayne aquifer: Stratiform “super-K” zones, Geological Society of America Bulletin, vol. 121, no. 1/2; p. 164–180.

Droser, M.J. and Bottjer, D.J., 1986, A Semiquantitative Field Classification of Ichnofabric: Journal of Sedimentary Petrology, vol. 56, no. 4, p. 558–559.

Dunham, R.J., 1962, Classification of Carbonate Rocks According to Depositional Textures: in American Association of Petroleum Geologists Memoir 1: Classification of Carbonate Rocks—A Symposium, p. 108–121.

Faith, J.R., 2004, Strain and Fractures in an Extensional Relay Ramp, Sierra del Carmen, Black Gap Wildlife Management Area, Brewster County, Texas—Implications for Determining Structural Controls on Groundwater Flow Pathways in the Edwards Aquifer, South-central Texas: University of Texas at San Antonio, M.S. thesis, 88 p.

George, W.O., 1952, Geology and Ground-water Resources of Comal County, Texas: U.S. Geological survey Water-Supply Paper 1138, 126 p.

Gingras, M.K., Baniak, G., Gordon, J., Hovikoski, J., Konhauser, K.O., La Croix, A.D., Lemiski, R., Mendoza, C., Pemberton, S.G., Polo, C., and Zonneveld, J., 2012, Porosity and Permeability in Bioturbated Sediments: Developments in Sedimentology, vol. 64, p. 837–868.

Gingras, M.K., Pemberton, S.G., Mendoza, C.A., and Henk, F., 1999, Assessing the Anisotropic Permeability of *Glossifungites* Surfaces: Petroleum Geoscience, vol. 5, p. 349–357.

Golab, J.A., Smith, J.J., Clark, A.K., and Morris, R.R., 2016, Bioturbation-Influenced Fluid Pathways within a Carbonate Platform System: The Lower Cretaceous (Aptian–Albian) Glen Rose Limestone: Palaeogeography, Palaeoclimatology, Palaeoecology, doi: 10.1016/j.palaeo.2016.10.025.

Horvorka, S.D., Dutton, A.R., Ruppel, S.C., and Yeh, J., 1994, Sedimentologic and Diagenetic Controls on Aquifer Properties, Lower Cretaceous Edwards Carbonate Aquifer, Texas: Implications for Aquifer Management: Transactions of the Gulf Coast Association of Geological Societies, vol. 44, p. 277–284.

Imlay, R.W., 1945, Subsurface Lower Cretaceous Formations of South Texas: AAPG Bulletin, vol. 29, p. 1416–1469.

Kastning, E.H., 1986, Cavern Development in the New Braunfels Area, Central Texas: in The Balcones Escarpment-Geology, Hydrology, Ecology and Social Development in Central Texas: Geological Society of America, p. 91–100.

Lønøy, A., 2006, Making Sense of Carbonate Pore Systems: AAPG Bulletin, vol. 90, no. 9, p. 1381–1405.

Maclay, R.W., 1995, Geology and Hydrology of the Edwards Aquifer in the San Antonio Area, Texas: U.S. Geological Survey Water Resources Investigations Report 95-4186, 64 p.

Maclay, R.W., and Small, T.A., 1976, Progress Report on Geology of The Edwards Aquifer, San Antonio Area, Texas, And Preliminary Interpretation of Borehole Geophysical and Laboratory Data on Carbonate Rocks: U.S. Geological Survey Open-File Report 76–627, 65 p.

Maxey, G.B., 1964, Hydrostratigraphic Units: Journal of Hydrology, vol. 2, p. 124–129.

Mylroie, J.E. and Carew, J.L., 1990, The Flank Margin Model for Dissolution Cave Development in Carbonate Platforms: Earth Surface Processes and Landforms, vol. 15, p. 413–424.

Olympus Software Imaging Solutions, 2014, Olympus Stream Version 1.9.3 for Windows 7 and Windows 8. Münster, Germany.

Pantea, M.P., Blome, C.D., and Clark, A.K. 2014, Three-Dimensional Model of The Hydrostratigraphy and Structure in and Around the U.S. Army–Camp Stanley Storage Activity Area, Northern Bexar County, Texas: USGS Scientific Investigations Report 2014–5074.

Parsons Engineering, 2006, Hydrogeologic Conceptual Site Model for Camp Stanley Storage Activity: Prepared for Camp Stanley Storage Activity, Boerne, Texas: Volume 5: Groundwater, http://www.stanley.army.mil/Volume5/HCSM/TOC.htm.

Pittman, J.G., 1989, Stratigraphy of the Glen Rose Formation, Western Gulf Coast Plain: Transactions of the Gulf Coast Associations of Geological Societies, vol. 39, p. 247–264.

Ramakrishnan, T.S., Ramamoorthy, R., Saito, N., Flaum, C., 2000, Method for Interpreting Carbonate Reservoirs: United States Patent 6,088,656, 10 p.

Small, T.A, and Lambert, R.B., 1998, Geologic Framework and Hydrogeologic Characteristics of The Outcrops of The Edwards and Trinity Aquifers, Medina Lake Area, Texas: U.S. Geological Survey Water-Resources Investigations Report 97–4290, 21 p.

Stricklin, F.L., Jr., Smith, C.I., and Lozo, F.E., 1971, Stratigraphy of Lower Cretaceous Trinity Deposits of Central Texas: University of Texas at Austin, Bureau of Economic Geology Report of Investigations 71, 63 p.

Vacher, H.L. and Mylroie, J.E., 2002, Eogenetic Karst from The Perspective of an Equivalent Porous Medium: Carbonates and Evaporites, v. 17, no. 2, p. 182–196.

Ward, W.C. and Ward, B.W., 2007, Stratigraphy of Middle Part of the Glen Rose Formation (Lower Albian), Canyon Lake Gorge, Central Texas, U.S.A.: Cretaceous Rudists and Carbonate Platforms: Environmental Feedback: SEPM Special Publication 87, p. 193–210.

Wierman, D.A., Broun, A.S., and Hunt, B.B., 2010, Hydrogeologic Atlas of the Hill Country Trinity Aquifer: Blanco, Hays, and Travis Counties, Central Texas: Prepared by the Hays-Trinity, Barton Springs/Edwards Aquifer, and Blanco -Perdenales Groundwater Conservation Districts, 17 p.

White, W.B., 1999, Conceptual Models for Karstic Aquifers, in Palmer, A.N., Palmer, M.V., and Sasowsky, I.D., eds., Proceedings, 5th Symposium of The Karst Waters Institute: Charlottesville, Virginia, The Karst Water Institute, p. 11–16.

White, W.B., 2002, Karst Hydrology: Recent Dvelopments and Open Questions: Engineering Geology, v. 65, p. 85–105.

Wright, V.P., Baceta, J.I., Lapointe, P.A., 2014, Paleokarstic Macroporosity Development at Platform Margins: Lessons from the Paleocene of North Spain: Interpretation, vol. 2, p. 1-16.

Zhou, W., Beck, B.F., Adams, A.L., 2002, Effective Electrode Array in Mapping Karst Hazards in Electrical Resistivity Tomography: Environmental Geology, vol. 42, p. 922–928.

Appendix I

Supplementary Table 1. Helium-expansion porosity and permeability data from MW5-LGR. Originally released under Blome and Clark (2014) and Golab et al. (2016).

Depth (m)	Porosity (%)	Permeability (mD)	Hydrostratigraphic unit
23.03	15.50	0.049	Fossiliferous
28.09	17.30	0.091	Fossiliferous
29.55	18.50	0.121	Fossiliferous
31.76	26.20	406.000	Fossiliferous
34.55	17.10	0.103	Fossiliferous
35.17	16.00	0.022	Fossiliferous
37.90	6.00	0.004	Fossiliferous
38.15	22.80	0.083	Lower Evaporite
41.51	14.70	0.070	Bulverde
43.48	10.90	0.137	Bulverde
47.05	24.50	0.446	Bulverde
51.36	14.20	0.017	Bulverde
52.18	18.40	0.095	Bulverde
52.82	27.00	1.360	Little Blanco
54.47	15.00	0.082	Little Blanco
57.68	14.10	0.013	Little Blanco
59.94	26.70	N/A	Little Blanco
61.78	24.80	56.800	Little Blanco
62.70	23.60	N/A	Little Blanco
63.22	20.00	0.385	Little Blanco
65.53	16.20	0.432	Twin Sisters
68.66	16.60	0.049	Twin Sisters
70.84	17.30	0.046	Twin Sisters
74.71	22.90	0.485	Twin Sisters
78.49	20.50	0.195	Twin Sisters
82.16	14.80	0.020	Twin Sisters
85.21	13.90	N/A	Twin Sisters
87.30	14.60	1.150	Doeppenschmidt
90.39	22.20	8.120	Doeppenschmidt
90.71	16.60	1.620	Doeppenschmidt
92.86	15.10	0.009	Doeppenschmidt
97.17	14.60	N/A	Doeppenschmidt
98.57	11.00	N/A	Doeppenschmidt
98.97	14.80	0.965	Rust
100.37	15.00	0.277	Rust
101.42	12.20	N/A	Rust
105.89	12.10	0.070	Rust
109.52	14.60	0.230	Rust
111.44	19.80	0.938	Rust
116.28	18.90	3.750	Rust

119.33	13.90	0.132	Rust
120.28	24.10	4.140	Rust
120.61	24.60	2.380	Honey Creek
120.98	21.40	3.150	Honey Creek
124.15	30.20	91.600	Honey Creek
126.43	20.50	N/A	Honey Creek
131.43	17.20	N/A	Honey Creek
134.39	16.00	N/A	Honey Creek
136.86	9.20	N/A	Honey Creek
137.31	9.90	N/A	Pearsall Formation
139.23	17.20	0.801	Pearsall Formation

Appendix II

Supplementary Table 2. Thin-section point count data from MW9-CC.

Depth (m)	Bioclasts	Micrite and cement	Pore space	Total counts	Hydrostratigraphic unit
4.62	62	219	8	289	Bulverde
5.15	59	170	48	277	Bulverde
5.24	38	207	17	262	Bulverde
5.43	56	225	14	295	Bulverde
6.19	90	203	5	298	Bulverde
6.74	114	153	32	299	Bulverde
7.27	177	80	39	296	Bulverde
7.44	110	144	40	294	Bulverde
9.85	80	201	11	292	Bulverde
10.00	34	237	22	293	Bulverde
10.91	34	251	4	289	Bulverde
11.73	80	160	53	293	Bulverde
12.56	47	234	13	294	Bulverde
14.57	57	217	21	295	Bulverde
15.44	49	215	34	298	Bulverde
15.51	51	239	5	295	Bulverde
16.81	21	267	4	292	Little Blanco
18.20	34	243	13	290	Little Blanco
19.29	22	271	3	296	Little Blanco
19.36	17	267	7	291	Little Blanco
21.11	12	268	14	294	Little Blanco
22.48	7	274	12	293	Little Blanco
23.50	53	235	7	295	Little Blanco
25.95	20	247	24	291	Little Blanco
26.73	8	275	8	291	Little Blanco
28.21	8	282	6	296	Twin Sisters
30.39	5	284	6	295	Twin Sisters
30.39	12	265	18	295	Twin Sisters
35.52	16	273	6	295	Twin Sisters
39.41	15	270	10	295	Twin Sisters
42.26	17	272	5	294	Twin Sisters
44.43	13	263	19	295	Twin Sisters
45.69	36	252	5	293	Twin Sisters
46.85	69	211	15	295	Twin Sisters
47.60	23	230	40	293	Doeppenschmidt
50.31	40	249	6	295	Doeppenschmidt
53.33	27	236	32	295	Doeppenschmidt
55.34	28	262	10	300	Doeppenschmidt
60.69	112	181	3	296	Doeppenschmidt
60.75	75	219	5	299	Doeppenschmidt

63.12	31	252	10	293	Rust
64.85	16	274	2	292	Rust
66.20	59	219	16	294	Rust
66.81	44	243	6	293	Rust
69.37	40	249	5	294	Rust
70.78	26	261	9	296	Rust
71.80	63	199	27	289	Rust
73.59	67	217	7	291	Rust
75.41	49	246	1	296	Rust
76.26	18	264	13	295	Rust
78.32	29	263	3	295	Rust
79.80	15	272	4	291	Rust
80.07	126	110	61	297	Rust
81.89	13	254	26	293	Rust
82.51	8	287	2	297	Rust
82.66	9	263	24	296	Honey Creek
83.07	21	270	7	298	Honey Creek
85.53	94	188	15	297	Honey Creek
86.55	117	168	9	294	Honey Creek
87.02	25	251	24	300	Honey Creek
91.68	25	238	29	292	Honey Creek
94.12	22	262	13	297	Pearsall Formation
99.09	33	257	7	297	Pearsall Formation
99.56	65	230	2	297	Pearsall Formation
99.73	46	237	13	296	Pearsall Formation
100.63	148	113	27	288	Pearsall Formation
101.33	166	103	27	296	Pearsall Formation
101.59	50	228	17	295	Pearsall Formation

CHAPTER 4. PALEOENVIRONMENTAL AND PALEOGEOGRAPHIC IMPLICATIONS OF PALEOSOLS AND ICHNOFOSSILS IN THE UPPER PENNSYLVANIAN–PERMIAN HALGAITO FORMATION, SOUTHEASTERN UTAH

Currently in preparation as:

Golab, J.A., Smith, J.J., and Hasiotis, S.T., 2017, Paleoenvironmental and Paleogeographic Implications of Paleosols and Ichnofossils in the Upper Pennsylvanian–Permian Halgaito Formation, Southeastern Utah: PALAIOS.

Abstract

The Upper Pennsylvanian–Permian (Virgilian–Wolfcampian) Halgaito Formation (HF) is an ~125–155-m-thick succession of carbonate and carbonate-cemented siliciclastic strata exposed along the Cedar Mesa on the Colorado Plateau in southeastern Utah. Defining the stratigraphic standing of the HF has been problematic due to differing paleoenvironmental and paleogeographic interpretations by various authors. This complication is likely because the HF lies at the interface between the underlying, predominately marine carbonate Hermosa Group and the overlying, alluvial–eolian siliciclastic Cutler Group. This study refines the depositional history of the HF using a combined iconological, paleopedological, and sedimentological approach in order to rectify some of the competing interpretations of this system and verify its position within the stratigraphic nomenclature. Five stratigraphic sections were measured along the Cedar Mesa. The depositional history of the HF can be divided into a lower, predominately marine section and an upper predominately eolian section. The marine section contains carbonate intertidal foreshore to nearshore deposits with simple carbonate entisols. These entisols are

poorly developed and contain large root fossils. This marine portion of the HF generally shallows upsection, but is highly punctuated and was flooded by small-scale transgressions four times. The continental section contains predominately eolian siltstone deposits with siliciclastic entisols and mottled inceptisols. Paleosol development generally increases upsection from the underlying marine beds. Water tables also become deeper upsection as indicated by depths of rhizoliths. The uppermost ~40 m of strata is laminated and crossbedded and contains little to no paelopedogenic development or rhizoliths. These eolian beds are carbonate cemented and likely sourced from the underlying marine strata of the Hermosa Group as the Elephant Canyon Seaway regressed to the north during the Upper Pennsylvanian. Thin, crossbedded fluvial strata can be observed throughout the HF and contain the coarsest material in the HF and were likely sourced from the highlands of the Uncompagre uplift, similar to the strata within the overlying Cutler Group units. Such fluvial beds are thin, not laterally extensive, and compose very little of the HF volumetrically. This suggests that the HF is stratigraphically related to the underlying marine units, rather than the overlying continental units and this study considers the HF the uppermost formation of the Hermosa Group.

1.0 Introduction

The Upper Pennsylvanian–Permian (Virgilian–Wolfcampian) Halgaito Formation (HF) is an ~125–155-m-thick succession of interbedded carbonate and siliciclastic strata exposed on the Colorado Plateau in southeastern Utah (UT; Fig. 1). Mixed carbonate and siliciclastic systems are common in the geologic record and are potentially productive hydrocarbon reservoirs (McNeal et al., 2004). Such mixed systems are often vertically and laterally complex and are characterized by rapidly changing facies that are challenging to interpret. The nomenclature and

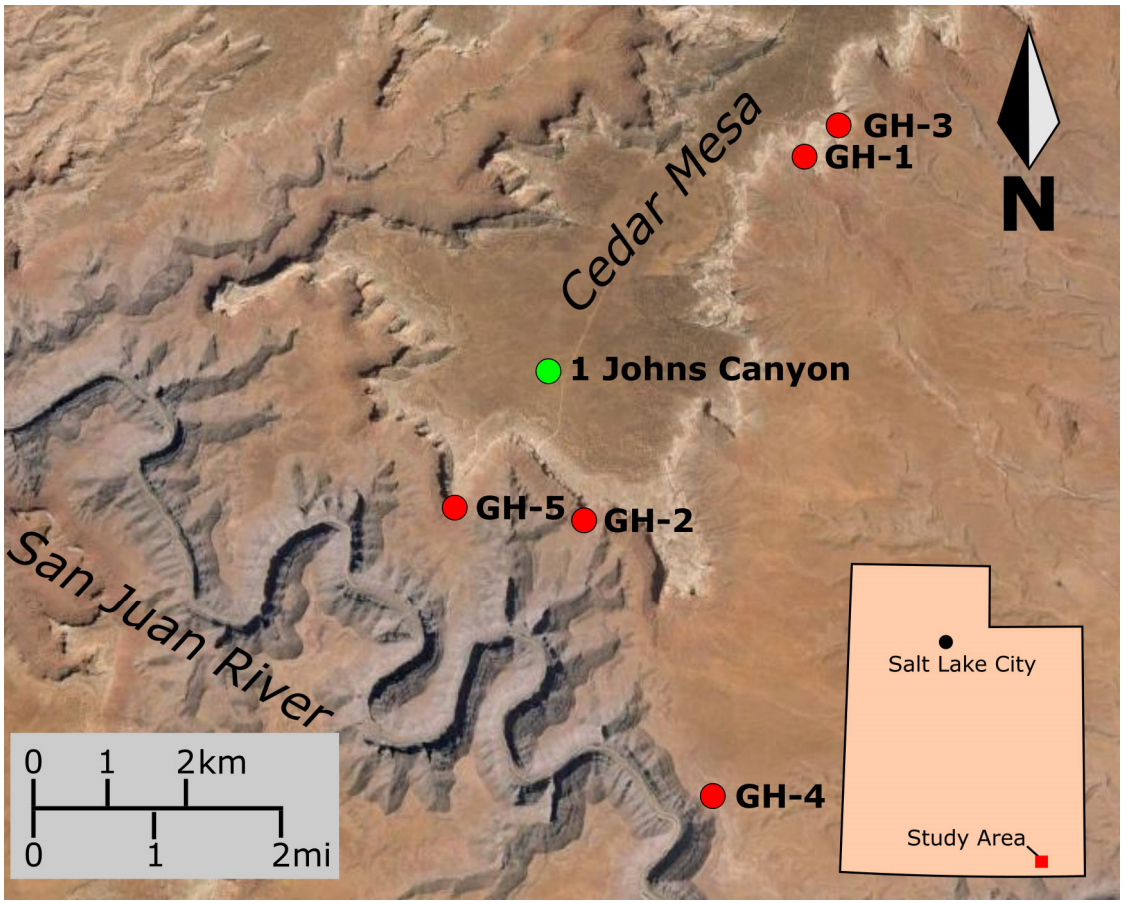

Figure 1. Map showing the study area surrounding the Cedar Mesa and San Juan River in southeast Utah. Approximate locations of five measured sections (red; GH-1–5) as well as the location of Texaco test well 1 Johns Canyon (green) are indicated. Satellite imagery from Google Earth (2016).

stratigraphic standing of the HF, in particular, has been problematic due to differing paleoenvironmental and paleogeographic interpretations by various authors (e.g., Baars, 1962; Ohlen and McIntyre, 1965; Condon, 1997; Murphy, 1987). These competing interpretations are likely because the HF lies at the interface between the predominately marine Hermosa Group and the alluvial–eolian Cutler Group and has characteristics common to both systems.

The lower ~40 m of the HF is characterized by marine limestone and carbonate cemented sandstones interbedded with red siltstone. Most of these red siltstones are interpreted to be eolian in origin and were likely reworked by both fluvial and marine processes (Baars, 1962; Murphy,

1987; Scott, 2005). These lowermost beds of the HF have previously been referred to as the Rico Formation (e.g., Baars, 1962; Condon, 1997; Loope, 1984; Murphy, 1987; Scott, 2005). Upsection, the HF is characterized by reduced marine influence and pervasive beds of red siltstone with simple and composite paleosols. Fluvial reworking of these eolian-sourced siltstones is common and increases upsection. The HF grades laterally northwest into and is laterally equivalent with the marine carbonates and arkosic sandstones of the Elephant Canyon Formation (Baars, 1962; Murphy, 1987; Dubiel et al., 1996; Condon, 1997).

The retreat of the Elephant Canyon seaway northward out of the Paradox basin likely exposed underlying carbonate strata and eolian processes deposited sand-sized particles near the coast and silt-sized grains further inland to the south. Alluvial reworking of these eolian-sediments likely occurred after primary deposition (Fig. 2; Murphy 1987). This interpretation is supported by previous provenance studies that show most siltstone within the HF is carbonaceous, eolian-sourced and likely derived from carbonates underlying the Hermosa Group (e.g., Murphy, 1987; Scott, 2005). The interbedded carbonate and siltstone beds observed at the base of the HF indicate that this retreat was relatively slow and punctuated over time. Well-developed composite and compound paleosols and fluvial sedimentary structures within the upper beds of the HF suggest that the water table was relatively high throughout deposition, and climate was likely not as arid compared to previous interpretations (Scott, 2005). Plants and soil dwelling organisms played a part in trapping the eolian sediment from the north and incorporating it into the soil (e.g., Scott, 2005).

This study uses a combined ichnological, paleopedological, and sedimentological approach to refine the paleoenvironmental and paleogeographic history of the northern Paradox basin during the deposition of the HF. We also interpret paleoecologic and paleohydrologic

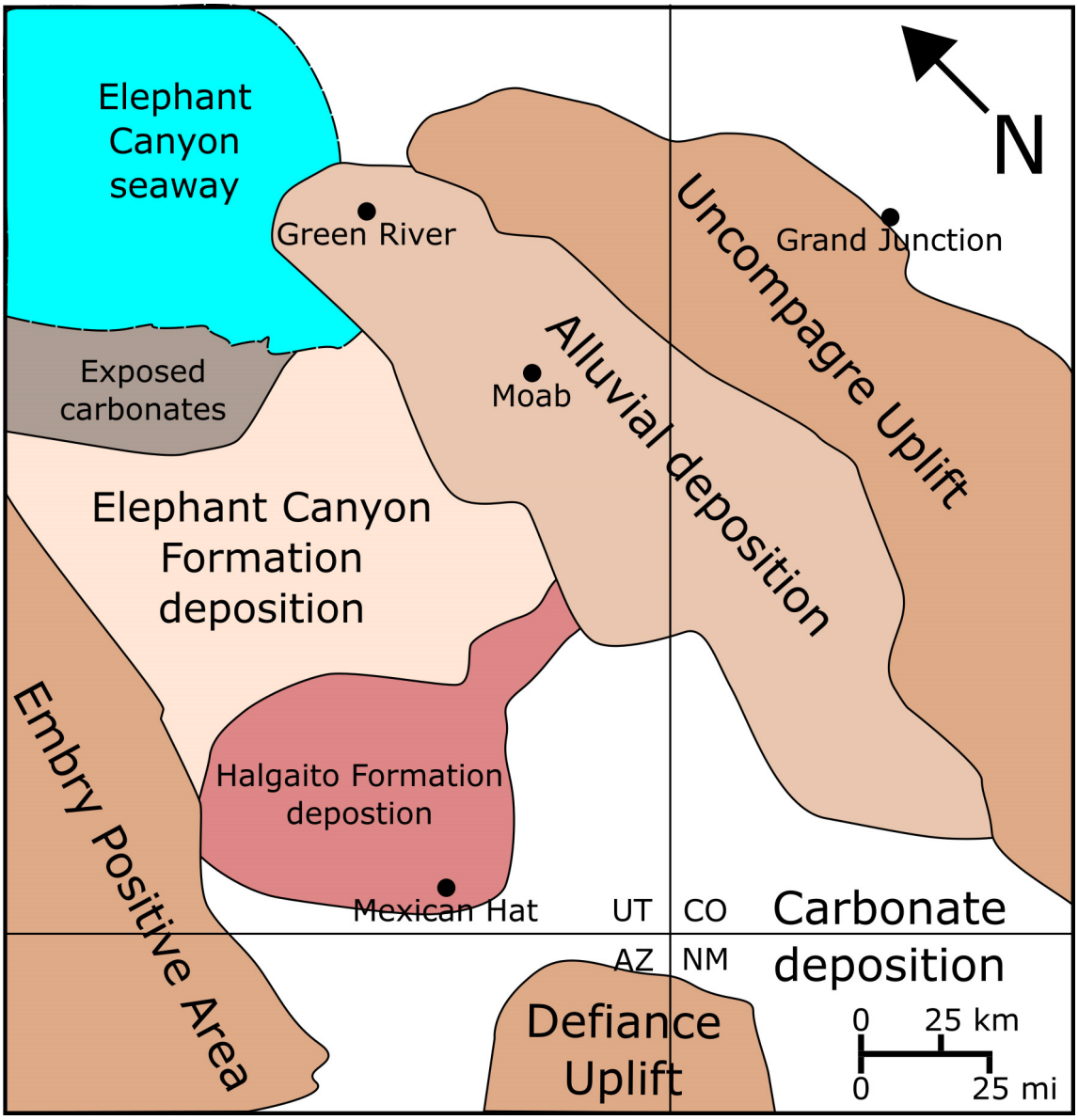

Figure 2. Paleogeographic reconstruction of the northern Paradox basin during deposition of the Halgaito formation. The northwestern retreat of the Elephant Canyon seaway exposed underlying carbonate ramp strata and allowed the development of eolian sandstone (Elephant Canyon Formation) and eolian loessite (Halgaito Formation) deposits. Highland areas bounding the Paradox basin include the Uncompagre uplift, the Embry positive area, and the Defiance uplift. Modified from Murphy (1987), Condon (1997), and Scott (2013).

trends during the deposition from ichnofossils and paleopedogenic development in the strata. The rapidly changing marine and continental facies contained in the HF provide the opportunity to examine organism behavior and soil development associated with rapid sea-level fluctuations.

Additionally, the HF is one of the few examples of a thick (>30 m) silty loess deposit in the ancient rock record (Murphy, 1987; Scott, 2005).

2.0 Geological background

2.1 Regional structure and stratigraphy

Prior to the development of the Paradox basin, the four corners region was covered by an extensive heterozoan-dominated carbonate platform from the Middle Devonian to the Late Mississippian depositing the Elbert Formation and the Quray and Leadville limestones (Ohlen and McIntyre, 1965; Nuccio and Condon, 1996; Whidden et al., 2014). The development of the the Uncompagre uplift initiated by the collision of Gondwana and Laurentia during the Late Mississippian created a regional unconformity and began the development of the Paradox basin (Fig. 2; Kluth and Coney, 1982; Nuccio and Condon, 1996; Barbeau, 2003; Kluth and DuChene, 2009; Whidden et al., 2014). The Paradox basin spans most of the four corners region and is bounded by the Uncompagre uplift to the northeast and east, the Embry positive area and San Rafael Swell to the west, and San Luis and Defiance uplifts to the south (Fig.2; Wengerd, 1955; Wengerd and Matheny, 1958; O'Sullivan, 1965; Scott, 2013).

The Paradox basin is an asymmetrical, extensional basin that contains Middle Pennsylvanian through early Permian (Cisuralian) sediments (Fig. 2; Wengerd, 1962; Ohlen and McIntyre, 1965; Lemke, 1985; Barbeau, 2003). Within the basin, the Middle to Upper Pennsylvanian Hermosa Group, which conformably overlies the carbonate Molas Formation, consists of the Pinkerton Trail, Paradox, Honaker Trail, and Halgaito formations (Fig. 3; Baars, 1962; Ohlen and McIntyre, 1965; Nuccio and Condon, 1996: Whidden et al., 2014).

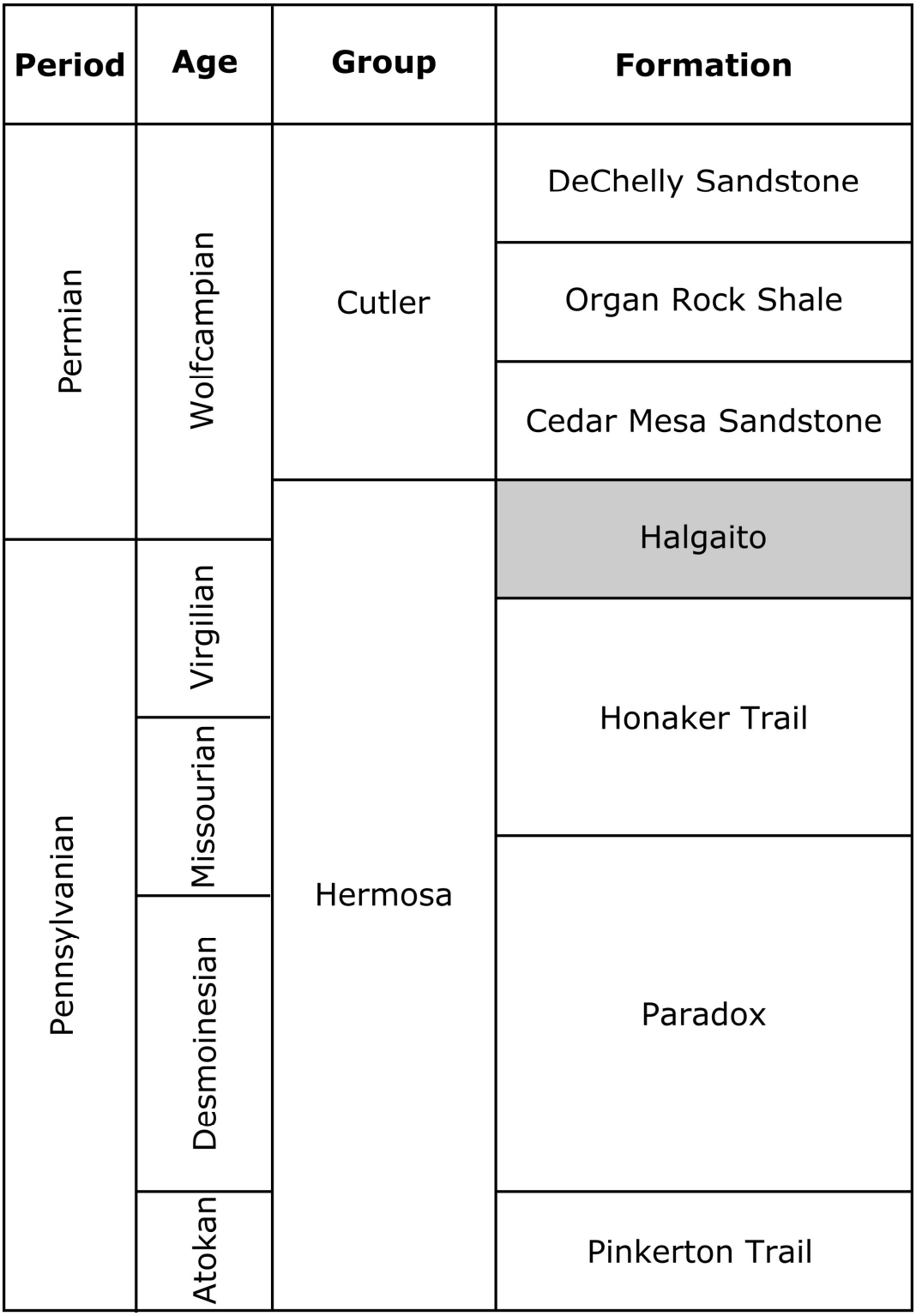

Figure 3. Generalized stratigraphic column of the field area showing the exposed formations of the Hermosa and Cutler Groups in the study area. The stratigraphic standing of the Halgaito Formation has been debated by several authors and this study places it at the top of the Hermosa Group modified from Rasmussen (2014).

Hermosa Group units are heterogeneous and are dominated by marine carbonates, evaporites, and siliciclastic siltstone and sandstone sourced primarily from the Uncompagre uplift (Ohlen and McIntyre, 1965; Nuccio and Condon, 1996). These units were deposited by the regional Elephant Canyon seaway in the northern portion of the Paradox basin. The Middle Pennsylvanian (Atokan) Pinkerton Trail Formation is a heterogeneous unit that transitions from red, siliciclastic siltstone to interbedded fossiliferous limestone and organic-rich shale (Peterson and Ohlen, 1963; Ohlen and McIntyre, 1965; Nuccio and Condon, 1996; Whidden et al., 2014). The overlying Upper Pennsylvanian (Desmoinesian–Missourian) Paradox Formation is a heterogeneous carbonate and evaporite unit with extensive algal mud deposits capped by evaporites in the southwest portion of the basin that grade into bedded evaporites toward the center of the basin (Peterson and Ohlen, 1963; Ohlen and McIntyre, 1965; Whidden et al., 2014). The Upper Pennsylvanian (Missourian–Virgilian) Honaker Trail Formation overlies the Paradox Formation and is characterized by a ~300-m-thick succession of carbonate strata that consist of algal mound deposits interbedded with gray shale and some siliciclastic beds (Peterson and Ohlen, 1963). The lower beds of the Honaker Trail Formation contain evaporates and are lithologically similar to the Paradox Formation (Ohlen and McIntyre, 1965). The uppermost beds of the Honaker Trail Formation are primarily shallow marine wackestone to packstone and contains some interbedded siliciclastic units. The Honaker Trail Formation is conformably overlain by the HF.

2.2 Halgaito Formation

The Upper Pennsylvanian–Permian (Virgilian–Wolfcampian) HF is a transitional mixed carbonate and siliciclastic deposit between the underlying marine units of the Honaker Trail

Formation and the dominantly continental siliciclastics of the Permian Cutler Group (Ohlen and McIntyre, 1965; Jordan and Mountney, 2012). Deposition of the HF is associated with the regression of the Elephant Canyon seaway northward (Fig. 2; Ohlen and McIntyre, 1965; Murphy, 1987; Scott, 2005). Carbonate beds within the lower strata of the HF are primarily shallow-marine tidal-flat deposits formed during the retreat of the seaway; whereas siliciclastic beds upsection in the formation are primarily eolian-sourced carbonaceous siltstones deposited by the predominately northern winds entering the Paradox basin (Ohlen and McIntyre, 1965; Murphy, 1987).

The base of the HF is characterized by fossiliferous packstone and carbonate cemented sandstones interbedded with red siltstone to very fine-grained sandstone. Most of these red siltstones are massive or laminated and have been interpreted to be eolian sourced (Murphy, 1987; Scott, 2005). This lowermost portion of the HF has previously been referred to as the Rico Formation by several authors due to the presence of marine deposits and a change in fossil content from brachiopods to bivalves (e.g., Baars, 1962; Loope, 1984; Murphy, 1987; Scott, 2005). Baars (1962) also mapped a major angular unconformity at the top of the Rico Formation, but this interpretation has been disputed (Loope, 1984; Condon, 1997). The validity of the Rico Formation as a mappable geologic unit has since been questioned by several authors and this name is no longer used in many studies (e.g., Dubiel et al., 2009; Loope et al., 1990; Sanderson and Verville, 1990; Condon, 1997).

Upsection, the HF is characterized by reduced marine influence and pervasive beds of red siltstone containing simple and composite paleosols (Murphy, 1987; Scott, 2005). Similar to the previously described lower beds, most of these siltstones are carbonaceous and eolian-sourced. Several sequence boundaries have been identified within the Hermosa and Cutler groups

associated with glacioeustatic forcing (Jordan and Mountley, 2012), and associated glaciation with the deposition of these groups likely increased the amount of eolian material entering the Paradox basin. However, loess derived directly from glacial outwash cannot account for the volume of accumulated sediments seen in the HF (Scott, 2005). These upper beds of the HF grade regionally northwest into marine carbonates and sandstones of the Elephant Canyon Formation (Baars, 1962; Murphy, 1987; Dubiel et al., 1996; Condon, 1997).

The HF is time equivalent with the undifferentiated lower Cutler Formation and has previously been identified as part of the Pennsylvanian–Permian Cutler Group (e.g., Kunkle, 1958; Baars, 1962; Peterson and Hite, 1969; Loope, 1984). Culter Group units are primarily alluvial deposits sourced from the surrounding highlands, particularly the Uncompagre uplift (Baars, 1962; Kunkle, 1958; Ohlen and McIntyre, 1965; Peterson and Hite, 1969; Cole et al., 1996). Although the HF shares some lithologic similarities with the Cutler Group, its association with the regression of the Elephant Canyon seaway and eolian-sourced sediments make it sedimentologically distinct. Recent studies are revising the stratigraphic nomenclature of the Cutler and Hermosa Groups (e.g., Loope et al., 1990; Dubiel et al., 1996; Condon, 1997; Scott, 2005) and some studies have suggested removing the designation of Cutler Group from the Paradox basin entirely (Rasmussen, 2002; 2014). This study follows Rasmussen (2002; 2014) and considers the HF the uppermost formation within the Pennsylvanian–Permian Hermosa Group.

3.0 Methods

Fieldwork consisted of measuring five stratigraphic sections along the Cedar Mesa in southeastern UT (GH-1–5; Fig. 1; Appendices I–V). These sections were measured with a 1.5 m long Jacobs staff demarcated in decimeters and were logged spatially with GPS. Beds were described sedimentologically, lithologically, and ichnologically and samples were collected along each measured section for laboratory analysis. Grain size was estimated in the field according to Dunham (1962) for carbonate units and Wentworth (1922) for siliciclastic units. Ichnofossils were examined and photographed *in situ* and some samples were collected for further laboratory analysis. All major ichnofossils localities were logged spatially with GPS. Paleosols were trenched along each stratigraphic section in order to examine morphology, pedogenic textures, remnant sedimentary structures, and associated ichnofossils. Photographs were taken of pedogenic features and samples were collected from each trench for laboratory analysis. Paleosol colors were examined using a Munsell soil color chart (Munsell, 2009) and recorded along the measured sections. A qualitative, relative sea level and water table depth curve was constructed for the HF using a combination of lithology, sedimentological structures, interpreted paleosols development, and ichnofossil assemblage. For this curve, strata was classified as either marine or continental based on lithologic and sedimentological structures. Marine strata was further subdivided into deeper foreshore and shallower nearshore deposits depending on the ichnological features and presence of paleosols. Continental strata was subdivided by depth of water table using paleosols development and depth of root penetration into the strata.

Laboratory work consisted of examining drill cuttings, thin-section descriptions, and X-ray diffraction analysis (XRD). Texaco Test Well 1 Johns Canyon is a 4,469 ft borehole at the

top of the Cedar Mesa (Fig. 1). Depths of contacts were determined using gamma-ray, neutron, resistivity, and sonic logs from this borehole. Drill cuttings from this well are located at the USGS Core Research Center in Denver, CO. Cuttings were used to describe lithology, color, and grain size throughout the HF. A total of 21 blue epoxy impregnated thin sections prepared by Wagner Petrographic in Lindon, UT, were used to examine mineralogy and grain size. Fifteen 24x46 mm thin sections were from siliciclastic samples and five 50.8x76.2 mm thin sections were from primarily carbonate samples. Analysis and photomicrographs were taken using an AmScope T490B-MT digital compound trinocular microscope.

X-ray diffraction (XRD) analysis was used to determine clay content from paleosol samples taken from measured sections. Samples were prepared by disaggregating the samples using a mortar and pestle and were run at University of Kansas Small-Molecule X-ray Crystallography Lab using a Bruker MicroSTAR diffractometer in three, one-minute runs from 5–115° 2Θ per sample. Clay mineralogy was determined by comparison of diffraction peaks according to Moore and Reynolds (1997).

4.0 Results

4.1 Lithofacies

Seven end-member lithofacies are identified in the HF from outcrop, cuttings, and thin section analysis according to grainsize, mineralogy, and sedimentary structures. The characteristics of these lithofacies are summarized in Table 1 and include, in decreasing order of relative abundance: laminated siltstone–very fine-grained sandstone (Stl), massive siltstone–very fine-grained sandstone (Stm), crossbedded siltstone–very fine-grained sandstone (Stc), mottled blocky siltstone (Stb), carbonate-cemented sandstone (Css), crinoid wackestone–packstone

(Cws), and lenticular crossbedded fine-grained sandstone (Ssc). Interpretations of depositional environment are based on original observations of HF strata and previous studies of the northern Paradox basin (see Geologic Background). Lithofacies can be grouped generally into fluvial, eolian, and marine facies (Fig. 4).

4.2 Paleosols

Three types of paleosols were identified in the field using pedogenic textures, color, grainsize, stacking pattern, and associated ichnofossils. These paleosols include, in decreasing order of relative abundance: simple and compound mottled inceptisols, simple fine-grained siliciclastic entisols, and simple carbonate entisols. Paleosols in the HF are generally characterized by increasing maturity upsection associated with a decreased carbonate input and increased siliciclastic sediments. Fluvial reworking and crosscutting of siliciclastic-sourced siltstone is common and also increases upsection.

4.2.1 Mottled inceptisols

Description: These paleosols are the most common in the HF and are associated with Stb and Stl. These paleosols are characterized by red (10R 4/6–5/8) to reddish-brown (2.5YR 4/6) matrix colors and light gray (7.5Y 7/1) to green (5G 7/1) mottles. Pedogenic features include granular to subangular-blocky peds and abundant carbonate rhizoliths, rhizocretions, and rhizohaloes (Fig. 5A). Granular peds may be associated with some original sedimentary features such as laminae, whereas horizons with blocky peds lack any original sedimentary structures. These paleosols are commonly highly bioturbated and contain the highest diversity of ichnofossils in the HF (see Ichnofossils). In some cases, red horizons are underlain by a well-cemented gleyed interval with

Table 1. Lithofacies within the Halgaito Formation

Facies	Name	Lithology	Sedimentary Structures	Ichnofossils	Interpretation
Stl	Laminated siltstone–very fine-grained sandstone	Red, very-fine-grained sandstone to siltstone. Quartz grains are well sorted, angular to subangular, and subrounded. Contains mica and few plagioclase grains. Dewatering structres are common in Stl within 10 m above and below the McKim Limetone	Cm-scale laminae that coarsen upward from silt to very fine-grained sand. Beds range from <1 m–5 m in thickness.	Rhizoliths, rhizocretions, *Scoyenia*, *Ancorichnus*, and *Naktodemasis*	Loess deposit in wet environment
Stm	Massive siltstone–very fine-grained sandstone	Red to pink siltstone to very fine grained sandstone. Quartz grains are subangular and subrounded quartz. Contains mica and some manganese nodules.	Massive with calcite cement filled fractures	Rhizoliths, rhizohaloes, *Naktodemasis*, and *Scoyenia*	Loess deposit
Stc	Crossbedded siltstone–very fine-grained sandstone	Red to pink siltstone to very fine grained sandstone. Quartz grains are subangular and subrounded quartz. Contains mica, plagioclase and microcline grains, and some manganese nodules.	Low angle crossbeds (< 30°)	Rhizoliths and rhizohaloes	Mobile dunes, loess deposits
Stb	Mottled blocky siltstone	Red and green mottled siltstone. Quartz grains are well sorted, angular to subangular, and subrounded. Contains mica and few plagioclase grains.	Generally massive with pedogenic granular to blocky texture	Rhizoliths, rhizohaloes, rhizocreations, *Naktodemasis*, and *Scoyenia*,	Pedogenically modified loess deposit
Css	Carbonate-cemented sandstone	Medium- to fine-grained, moderately-sorted, carbonate-cemented sandstone. Conatins minor amounts of plagioclase, microcline, and mud ripup clasts	Massive or crossbedded with calcite cement filled fractures	*Siphonichnus*, *Thalassinoides*, and rhizoliths	Wave-dominated foreshore to backshore deposits
Cws	Crinoid wackestone–packstone	Well-sorted, crinoid and bivalve wackestone-packstone and mudstone	Broken and angular shell fragments. Micritic with rare beds with crystalline, sparry cement. Crossbeds with mud drapes	*Siphonichnus* and *Thalassinoides*	Tidal-dominated nearshore to foreshore deposits

Table 1 (continued). Lithofacies within the Halgaito Formation

Facies	Name	Lithology	Sedimentary Structures	Ichnofossils	Interpretation
Ssc	Lenticular crossbedded fine-grained sandstone	Yellow to orange, fine-grained trough-crossbedded quartz arenite. Cemented with quartz overgrowths and mud. Quartz grains are subangular and aburounded with significant point-to-point contacts and oxidization surfaces on some grains. Also contains manganese nodules, mica, and some K-feldspar grains	High-angle crossbeds ($> 30^{o}$). Beds not laterally continuous and pinch out laterally	Rhizoliths and rhizohaloes	Fluvial channel fill

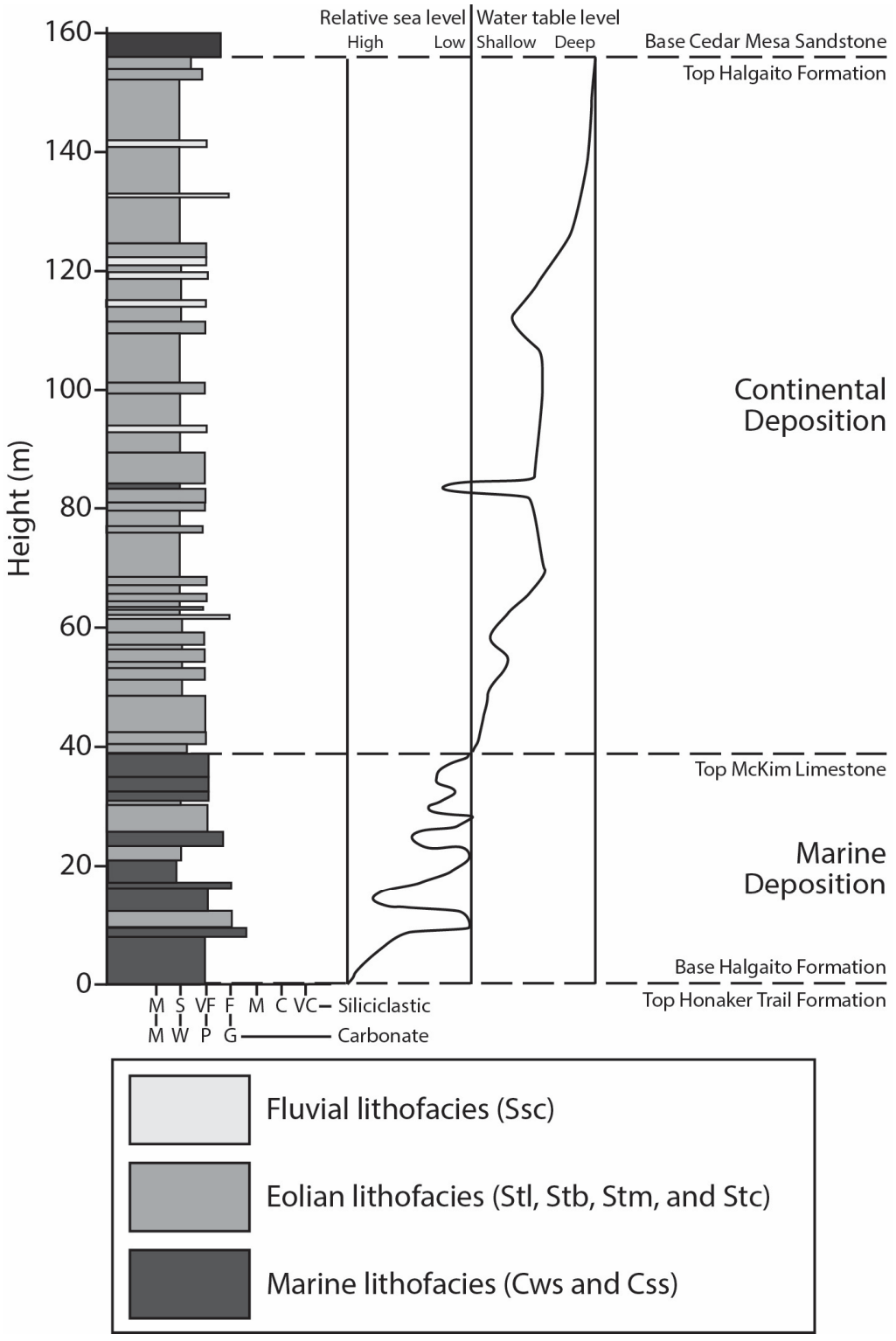

Figure 4. Generalized stratigraphic column of the Halgaito Formation showing grain-size and interpreted depositional environment. Relative sea-level and water table depth curve based on qualitative assessments of the lithology, sedimentological structures, interpreted paleosol development, and ichnofossil assemblages. See Table 1 for lithofacies descriptions.

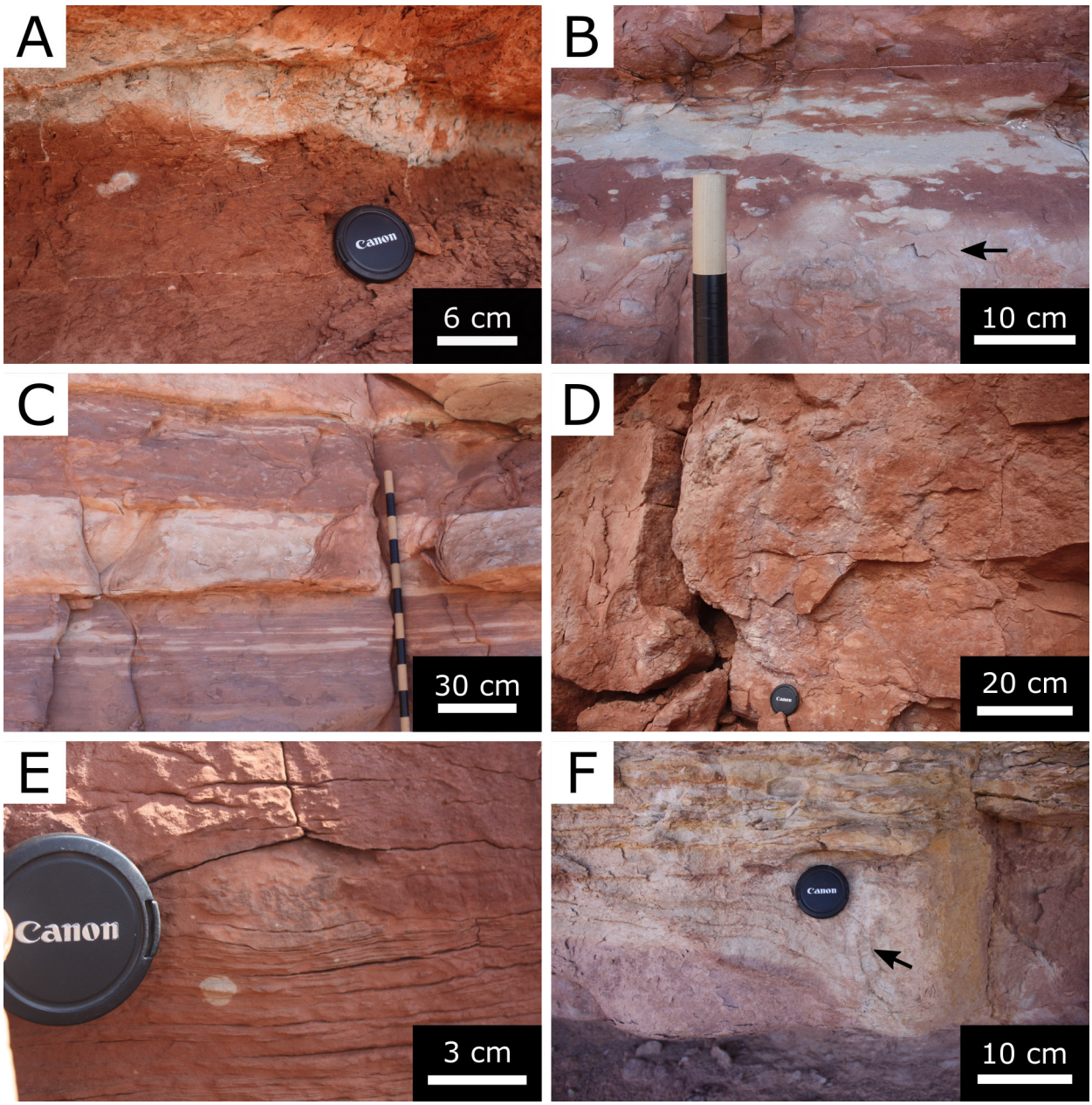

Figure 5. Paleosols present in the Halgaito Formation. A) Simple mottled inceptisol horizon showing typical subangular blocky peds, red coloration, and diagenetic gypsum. Upper gleyed horizon interpreted to be associated with subsequent waterlogging due to water table rise and increased deposition. B) Distinct gray mottling within a simple inceptisol horizon likely created by reducing conditions along root systems. Lower gleyed horizon is also visible (arrows). Compound mottled inceptisol horizons. Competent beds display less pedogenic modification than red colored incompetent beds. D) Simple siliciclastic entisol horizon with deeply penetrating large-scale depletion zone rhizohaloes. E) Calcareous rhizolith within a simple siliciclastic entisol horizon showing remnant laminations. F) Simple carbonate entisol horizon showing remnant laminations and dewatering structures (arrow); such structures are common in Stl within 10 m above and below the McKim Limestone.

distinct light green (5G 7/1) matrix colors. These underlying gleyed horizons commonly contain subangular blocky peds but may contain remnant sedimentary structures such as laminations (Fig. 5B). Inceptisol horizons with high concentrations of carbonate nodules and rhizoliths are less competent than intervals with fewer of these features. In some areas multiple horizons may be stacked to create compound successions of paleosols. Furthermore these paleosols may be characterized by thick cumulative soil horizons with a red (10R 4/6–5/8) to purple matrix with green to green-gray mottles (Fig. 5C). These cumulative successions are heavily bioturbated and distinct inchofossils can be difficult to distinguish, but red to purple rhizoliths can be observed. The rhizoliths within these horizons are significantly smaller than those observed in other simple or compound profiles. Some rhizoliths may be deeply penetrating and crosscut several horizons within such compound paleosols.

Interpretation: These paleosols are interpreted as A and AC horizons and likely formed during periods of subaerial exposure with punctuated deposition and fluctuating water table levels. Red matrix colors suggest moderately well-drained vadose zone conditions (e.g., Murphy, 1987; Schwertmann, 1993; Smith et al., 2008; Hasiotis and Platt, 2012). Purple colors and abundant calcareous rhizohaloes and carbonate nodules indicate some amount of seasonal wetting and drying (Kraus and Hasiotis, 2006; Smith et al., 2008). Cumulative horizons suggest relatively steady deposition over a long period of time creating a thick, continuous soil horizon (Kraus, 1996, 1999, 2002; Hasiotis and Platt 2012).

These paleosols were previously interpreted to have developed in arid to semiarid conditions due to the abundance of carbonate nodules and association with silt-sized eolian-sourced matrix material (e.g., Loope, 1984; Murphy, 1987). This study; however, interprets a semiarid to seasonal environment where eolian material is transported during dry seasons and

translocation of carbonate down through the soil profile occurs during periods with higher precipitation and water tables. This interpretation is further supported by the presence of underlying gleyed horizons, indicating reducing conditions due to periodic higher ground water levels (Hasiotis and Platt, 2012).

4.2.2 Simple fine-grained siliciclastic entisols

Description: These paleosols are common throughout the uppermost beds of the HF and are characterized by only incipient pedogenic development other than bioturbation with occasional granular peds. Entisols are associated with siliciclastic Stm, Stc, and Ssc. These paleosols consist of a single horizon that contains deeply penetrating rhizoliths surrounded by carbonaceous rhizohaloes and associated with carbonate nodules (Fig. 5D). These horizons are carbonate cemented and competent. Matrix colors are commonly red (10R 4/6–5/8) to reddish brown (2.5YR 4/6) and contain rare yellow (2.5Y 7/8) mottling. The rhizoliths within these horizons are typically dark red (7.5YR 3/4–3/6) to purplish gray (5RP 3/1) and often crosscut underlying strata. Many rhizoliths are associated with pervasive bioturbation (see Ichnofossils). These paleosols contain remnant sedimentary structures such as crossbedding and laminations (Fig. 5E).

Interpretation: These paleosols are interpreted as AC horizons and likely formed after periods of rapid punctuated deposition. Association of these horizons with fluvial sedimentary structures such as crossbedding indicates that these paleosols developed after fluvial reworking of sediment or during long-term periods of aridity. Depth of rhizoliths suggests water tables were relatively low and associated carbonate rhizohaloes indicate well-drained and relatively arid conditions during development of these paleosols (Smith et al., 2008; Hasiotis and Platt, 2012).

4.2.3 Simple carbonate entisols

Description: These paleosols occur in the lower portion of the HF and are associated with Cws and Css. Carbonate entisols are characterized by a single horizon with brown to red matrix colors and deeply penetrating rhizoliths with woody textures preserved in manganese (Murphy, 1987). Horizons contain some mottles that are reddish gray (7.5R 5/2) to greenish gray (10G 6/1). Rhizoliths within these paleosols are commonly dark bluish gray (10G 3/1–4/1) and may have white carbonaceous rhizohaloes (Fig 5F). These horizons juxtapose marine fossils and ichnofossils with rhizoliths and pedogenic modification.

Interpretation: Simple carbonate entisols are interpreted as single A and AC horizons associated with subaerial exposure during rapid sea-level fluctuations of the Elephant Canyon seaway. The upper portions of these paleosols may be organic rich A horizons with deeply penetrating roots into the underlying sediment, creating AC horizons. Little to no translocation of carbonate indicates these soils were likely poorly drained and were only exposed for a relatively short duration of time (Smith et al., 2008; Hasiotis and Platt, 2012).

.

4.3 Ichnofossils

Ichnofossils provide additional information about the depositional settings, relative sea-level changes, paleohydrology, and paleoclimatic histories of a unit. The HF contains both marine and continental ichnofossils due to its location between underlying marine and overlying alluvial units. The ichnofossils identified in the HF include, in descending order of relative abundance: four types of rhizoliths, two ichnospecies of *Siphonichnus*, *Naktodemasis bowni*, *Thalassinoides* isp.*, Scoyenia* isp., and *Ancorichnus ancorichnus.*

4.3.1 Rhizoliths

These are the most abundant ichnofossils in the HF and are found throughout most beds. Rhizoliths were created by terrestrial plants and generally taper downward from the tops of paleosol horizons but also crosscut underlying strata that contain no evidence of pedogenic modification. There are four types of rhizoliths observed in the HF that vary in size and morphology and include large-scale depletion zone rhizohaloes, calcareous rhizoliths, large-scale carbonaceous root fossils with rhizohaloes, and small-scale iron-oxide rhizohaloes.

4.3.1.1 Large-scale depletion zone rhizohaloes (Figs 6A–B)

Description: Large, downward branching and tapering rhizohaloes are observed in most siliciclastic units and may penetrate >3 m deep in some locations (Fig 6A). When observed at the tops of beds, these structures have a cylindrical cross-section ranging from ~3–15 cm in diameter (Fig. 6B). Rhizohaloes have dark to light purple cores that gradually fade outward to gray to light green and generally lack a distinct boundary with the surrounding matrix. A thin (~1mm) dark red to purple hypocoating is also present bordering the outside of some rhizohaloes. Many of these rhizohaloes are commonly associated with carbonate nodules and calcareous rhizoliths. These structures are often found associated with *Naktodemasis* and other ichnofossils. Rhizohaloes may crosscut multiple beds and paleosols horizons, particular within compound and cumulative successions. These rhizohaloes are particularly abundant in the middle of the HF, between 62–132 m from the base of the measured section (Fig. 4) and are commonly associated with mottled inceptisols and simple fine-grained siliciclastic entisols. Furthermore, the depths of

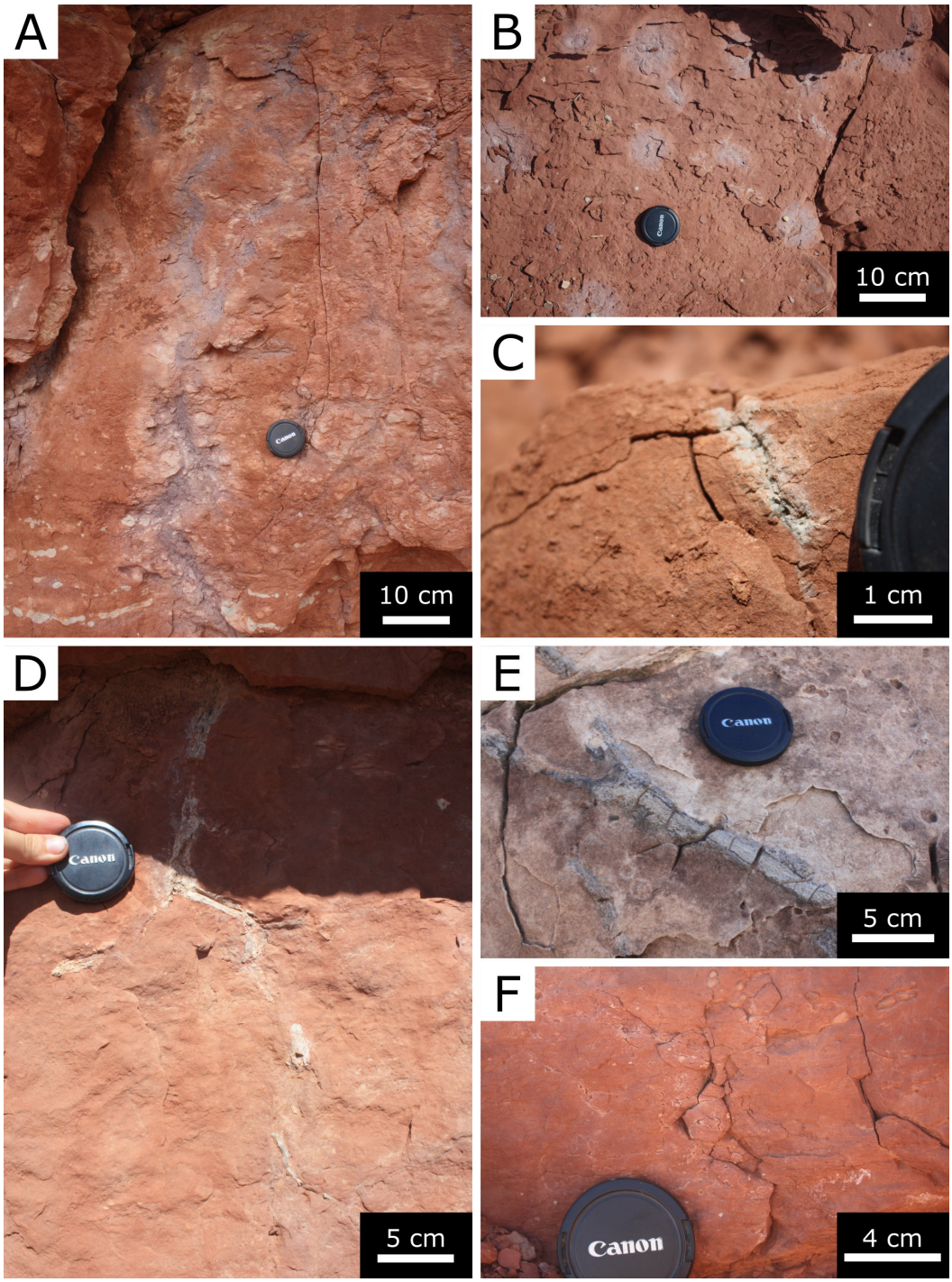

Figure 6. Rhizoliths present in the Halgaito Formation. A) Cross-section view of a deeply penetrating depletion zone rhizohalo with typical purple colored lining and gleyed exterior. Rhizohalo does not have sharp boundaries with the surrounding matrix. B) Plan view of depletion zone rhizohaloes with no distinct core visible. C) Calcareous rhizolith with some fossilized plant material and white carbonate material. D) Cross-section view of a calcareous rhizolith with no rhizohalo. E) Plan view of a large-scale carbonaceous root fossil within a marine carbonate sandstone. F) Small scale iron-oxide rhizohaloes.

depletion zone rhizohaloes tends to increase upsection, but these traces also become less abundant in the uppermost 20 m of the section

Interpretation: The cores of the rhizohaloes were likely created by deeply penetrating root systems. The size and depth of these structures indicate relatively deep water tables during plant growth and suggest well drained conditions (Kraus and Hasiotis, 2006; Smith et al., 2008). Following death of the plant, decaying organic material and infiltrating surface waters in the remnant root channels created localized reducing conditions (Kraus and Hasiotis, 2006). The purple cores of these rhizohaloes indicate the presence of goethite, a reduced form of iron-oxide. As surface water infiltrated the root systems and spread into the surrounding matrix, hematite was reduced and mobilized away from root channels leaving gray-green haloes and was concentrated in red hypocoatings at rhizohalo boundaries (Vepraskas et al., 1992; Kraus and Hasiotis, 2006). The association of these rhizohaloes with eolian deposition and mottled inceptisols and simple fine-grained siliciclastic entisols indicates that water tables were low in the middle portion of the HF (Fig. 4). The increasing depth of these rhizohaloes upsection and their absence in the top 20 m of the section suggest an overall drop in water tables and increased aridity over the course of deposition of the HF.

4.3.1.2 Calcareous rhizoliths (Figs. 6C–D)

Description: These structures consist of downward branching and tapering accumulations of white to gray calcite (Fig. 6C). Calcareous rhizoliths range from ~0.5–2 cm in diameter. The white calcite may be powdery to slightly crystalline. These rhizoliths usually lack preservation of woody textures or organic material, but some examples near the base of the HF have these features. The rhizohaloes surrounding these structures are generally thin (1–2 mm) and are

yellow to white in color. These rhizoliths are found associated within Stl and Stc. The structures may penetrate up to 1 meter and through multiple beds (Fig. 6D) and are commonly located at the tops of simple entisol horizons. Similar to depletion zone rhizohaloes, these rhizoliths are commonly associated with pervasive bioturbation with *Naktodemasis* and other ichnofossils. Additionally, calcareous rhizoliths are often located in beds with abundant fractures and associated with diagenetic gypsum (Murphy, 1987). These rhizoliths are most abundant between 40–62 m above the base of the HF in the strata overlaying the McKim Limestone bed (Fig. 4). Calcareous rhizoliths are not present within most of the middle portion of the unit but are observed in the top 12 m of the section.

Interpretation: Calcareous rhizoliths were created by relatively shallow root systems where calcite precipitated in the root channel during soil development. Calcareous rhizoliths that generally lack distinct rhizohaloes are commonly interpreted as suggesting moderately-drained soil conditions (Klappa 1980; Kraus and Hasiotis, 2006; Smith et al., 2008). The association of these rhizoliths with low-angle crossbedding suggests subaerial exposure of eolion-deposition further indicates deep water tables. However, the abundance of these rhizoliths in the strata above the McKim Limestone bed and juxtaposition with ichnofossils indicating saturated conditions (see *Scoyenia isp.* and *Ancorichnus ancorichnus*) suggests that water tables fluctuated significantly for some time after the retreat of the Elephant Canyon Seaway. Additionally, the amount of carbonate within underlying marine strata provided a source of calcareous material to precipitate these rhizoliths. The presence of calcareous rhizoliths near the top of the formation in association with thick crossbedded siltstones may indicate precipitation of carbonate around root channels in association with extremely arid conditions, which lacked enough precipitation to mobilize hematite (Kraus and Hasiotis, 2006).

4.3.1.3 Large-scale carbonaceous root fossils with rhizohaloes (Fig. 6E)

Description: Large, sub-horizontal, woody textured root fossils that are from 2–7 cm in diameter and may be > 4m in length but do not penetrate deeply and do not crosscut underlying strata (Fig. 6E). These rhizoliths are associated with marine strata including Cws and Css. Generally, these carbonaceous root fossils have horizontal orientations and can be observed at the tops of simple carbonate entisol horizons. Root material is dark gray to black and may be surrounded by a white to yellow rhizohaloes. These roots commonly overprint and crosscut *Siphonichnus* and *Thalassinoides*. These root fossils are concentrated in the basal 36 m of the formation.

Interpretation: Woody textured rhizoliths are dark gray from abundant manganese as well as preserved organic material (Murphy, 1987). Preservation of organic terrestrial root material is commonly caused by rapid deposition and possible anoxia due to extremely high water tables and poorly-drained conditions (Kraus and Hasiotis, 2006). Additionally, the location of these rhizoliths in primarily carbonate deposits further increased preservation potential due to rapid cementation. The yellow to white color of the surrounding rhizohaloes is likely due to the presence of oxidized goethite and probably developed post-depositionally (Kraus and Hasiotis, 2006). The association of these root fossils with marine carbonate sandstone and packstone and shallow penetration suggests they developed in a marine-dominated environment during the retreat of the Elephant Canyon seaway.

4.3.1.4 Small-scale iron-oxide rhizohaloes (Fig. 6F)

Description: Smaller-scale rhizohaloes (~1 mm in diameter) that are observed throughout all strata of the HF and are particularly abundant within siliciclastic Stb and Stm units and within

mottled inceptisol horizons. These small-scale traces are commonly preserved as downward tapering green or gray rhizohaloes, but some samples contain dark red to red cores (Fig. 6F). The tops of paleosol horizons commonly contain such abundant small-scale rhizohaloes and pervasive bioturbation that they become nondescript and appear as mottled colors. The rhizohaloes are commonly associated with abundant carbonate nodules. These rhizohaloes are found throughout the entire vertical extent of the HF, but are particularly abundant in the upper 100 m of the section. These small-scale rhizohaloes are observed in association with both depletion-zone rhizohaloes and carbonate rhizoliths in several locations.

Interpretation: These rhizoliths suggest the wide-spread presence of terrestrial plants during soil development and indicate well drained conditions near subaerial exposure surfaces (Kraus and Hasiotis, 2006; Hembree and Cadon, 2011; Blair, 2015). The dark red cores of these rhizohaloes indicate the presence of oxidized hematite (Kraus and Hasiotis, 2006). The green to gray haloes around these cores suggest the movement of hematite from the surrounding matrix toward the cores, causing an iron-depleted zone around the root during plant-growth. This absorption of hematite suggests well-drained conditions existed within both the A and B horizons of the developing soil (Kraus and Hasiotis, 2006; Hembree and Cadon, 2011; Blair, 2015). The plants that created these wide-spread rhizohaloes are likely the primary reason that airborne silt-sized particles were trapped during deposition (Murphy, 1987; Scott, 2005). The presence of these rhizohaloes throughout most of the entire vertical extent of the HF suggests semi-arid conditions during eolion deposition. The uppermost ~20 lack any of these rhizoliths, which further suggests an overall transition to an arid environment during deposition.

4.3.2 Siphonichnus isp.

These ichnofossils are cylindrical to elliptical, vertical to subvertical burrows with laminated infill. Some burrows contain fossil clams in life position that are similar in morphology to modern razor clams (*Ensis macha*; Molina, 1782; Márquez and van der Molen, 2011; Hasiotis and Rasmussen, 2010). The ichnofossils are most commonly associated with Css and may be crosscut by *Thalassinoides* and rhizoliths. There are two ichnospecies of these burrows in the HF: *Siphonichnus philae* and *Siphonichnus lepusaures*.

4.3.2.1 Siphonichnus philae (Fig. 7A–B)

Description: These are vertical to subvertical, straight burrows that are round to elliptical in cross-section and contain convex-upward laminae (Fig. 7A). Burrow diameters average 2.75 cm wide in the long axis and 2.28 cm wide in the short axis. Burrow diameters vary in slightly and in many cases tend to decrease upsection. Depth of burrows ranges from 3.2 to 62.3 cm depending on the thickness of the strata and amount of the burrow exposed (Fig 6B). Burrow fill is the same as the surrounding matrix and some burrows contain fossil clams in life position that are similar in morphology to modern razor clams (*Ensis macha*; Molina, 1782; Márquez and van der Molen, 2011; Hasiotis and Rasmussen, 2010).

Interpretation: These burrows are likely created by shallow marine clams in a coastal to deltaic carbonate environment with relatively rapid deposition. The convex-upward, horizontal laminations seen in burrow fill are interpreted to indicate upward movement of these clams through the bed in equilibrium with deposition (Zonneveld and Gingras, 2013). Modern razor clams live in muddy tidal-dominated environments at water depths up to 55 m (Márquez and van

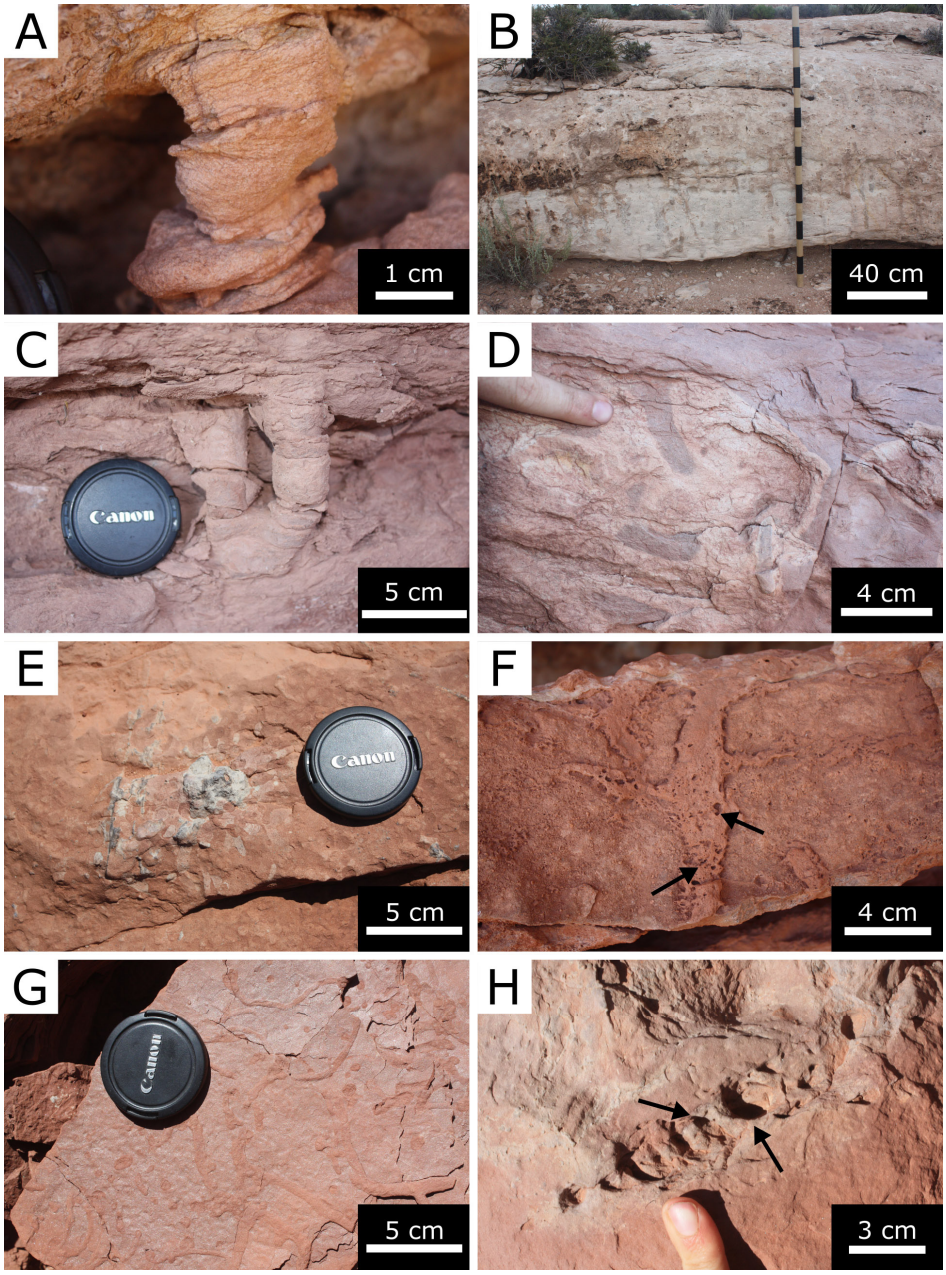

Figure 7. Ichnofossils present in the Halgaito Formation. A) *Siphonichnus philae* within a carbonate-cemented sandstone showing distinct concave-upward laminate with no burrow wall. B) Vertically-oriented *S. philae* showing >1 m depth into the strata. C) *Siphonichnus lepusaures* showing a single tube with convex-upward laminae bisecting into two tubes containing massive fill. D) *Naktodemasis bowni* within a mottled inceptisol horizon. E) *N. bowni* within a simple siliciclastic entisol in association with a carbonaceous root fossil. F) *Thalassinoides* within a carbonate cemented sandstone bed showing distinct branching morphology. Contains some evidence of a textured burrow wall (arrows). G) *Scoyenia* within a laminated siltstone bed <5 m above the McKim Limestone. Burrows are densely concentrated and crosscut each other. H) *Ancorichnus ancorichnus* within a massive siltstone bed directly above the McKim Limestone. Meniscate backfill weathers in bos-relief to the surrounding matrix.

der Molen, 2011). They are commonly found within the upper 60cm of the surface and will burrow upward in response to aggradation, but may also create subhorizontal burrows (Márquez and van der Molen, 2011; Winter and Hosoi, 2011). The vertical orientation of these ichnofossils likely suggests that the rate of deposition was rapid and the clams burrowed relatively quickly to maintain an ideal depth in the sediment.

4.3.2.1 Siphonichnus lepusaures (Fig. 7C)

Description: These are subvertical, circular to elliptical in cross-section tubes containing horizontal to convex-upward laminae that bisect upward into two tubes containing massive fill. Burrows are between 3.0 and 2.0 cm in diameter, though are commonly wider at the base below the Y-branching tubes. Burrow infill in both the lower, laminated portion and upper massive portion is the same as the surrounding matrix.

Interpretation: Similar to *S. philae*, these burrows are likely created by shallow marine clams in a coastal to deltaic environments with moderate deposition. Branching-upwards morphology is interpreted to be created by split siphons of clams (Zonneveld and Gingras, 2013). Such structures are recorded in modern intertidal environments in temperate regions (Zonneveld and Gingras, 2013). The presence of massive infill in these structures indicates that these burrows were passively infilled and likely formed in moderately low-energy depositional environments before being rapidly buried. Fluctuations in the retreat of the Elephant Canyon seaway are likely the cause of the rapid burial and infill of these burrows.

4.3.3 Naktodemasis bowni. (Figs. 7D–E)

Description: These are unlined burrows with distinct meniscate backfill that is identical to the surrounding matrix, but can be identified by differences in coloration. The menisci are perpendicular to the length of the burrow and are adhesive, meaning they do not weather in bos relief from the surrounding matrix. *Naktodemasis* average ~0.75 cm wide and may be several cm in length (Fig. 7D). These ichnofossils are commonly observed in siliciclastic paleosols, particularly within simple and compound mottled inceptisol horizons. *Naktodemasis* are abundant in association with carbonate rhizoliths in some strata and overlapping specimens gives some strata a mottled coloration (Fig. 7E).

Interpretation: These ichnofossils are created by the locomotion and habitation of soil-dwelling invertebrates such as juvenile or adult insects related to the orders *Hemiptera* and *Coleoptera* (Smith et al., 2008). The presence of *Naktodemasis* indicates non-saturated soils above the water table and generally suggests well-drained conditions (Smith et al., 2008; Hasiotis and Platt, 2012). The association of these ichnofossils with deeply-penetrating rhizoliths suggests the tracemakers were feeding on developing root systems during deposition (Smith et al., 2008). Meniscate backfill indicates the presence of some moisture in the soil (Smith et al., 2008; Hasiotis and Platt, 2012).

4.3.4 Thalassinoides isp. (Fig. 7F)

Description: Three-dimensional, branching burrows that range from 1 to 3 cm in diameter (Fig. 7F). Branches are generally oriented at ~90°. The infill of these burrows is the same as the surrounding matrix and does not contain any structure. *Thalassinoides* are found within Css and are associated with *Siphonichus isp*. These burrows may be crosscut by rhizoliths.

Interpretation: Thalassinoides are common in high-energy shallow marine depositional environments (Bromley and Ekdale, 1984; Uchman, 1995; Sheehan and Schiefelbein, 1984). Decapod crustaceans and other arthropods are common tracemakers (Sheehan and Schiefelbein, 1984; Myrow, 1995).

4.3.5 Scoyenia isp. (Fig 7G)

Description: Horizontal to subhorizontal, meandering cylindrical burrows with distinct lateral striations along the walls of the tube. No lining is present and the burrow infill is the same as the surrounding matrix. These ichnofossils range from 0.5 to 1.0 cm in diameter and may vary in width along the length of the burrow. Some burrows branch into two tubes with smaller diameters. These traces are commonly densely concentrated and individual burrows tend to crosscut each other (Fig. 7G). Some burrows are vertically oriented and appear to crosscut strata. *Scoyenia* are found in siliciclastic units and are associated with simple entisols and carbonate rhizoliths. These ichnofossils are not common throughout the HF and occur predominately in strata directly above the McKim Limestone bed and associated with calcareous rhizoliths.
Interpretation: These burrows were likely created by soil dwelling invertebrates and are generally interpreted as actively-filled locomotion structures (Frey et al., 1984; Hasiotis, 2006). Commonly, the tracemakers of *Scoyenia* are interpreted to be arthropods, including insects (Frey et al., 1984; Hasiotis and Dubiel, 1993). The textured surface of the burrow is interpreted as scratch marks from the tracemaker's limbs and the preservation of such scratch marks suggests development in fine-grained soils with a high moisture content (Hasiotis and Dubiel, 1993). *Scoyenia* has previously been found in floodplain and marginal lacustrine depositional environments and when abundant, indicate high water tables (Frey et al., 1984; Hasiotis and

Dubiel, 1993). The association of *Scoyenia* with immature soil development and carbonate rhizoliths is consistent with the interpretation that these ichnofossils were formed in poorly-drained conditions. The branching morphology observed in HF *Scoyenia* is not common for this ichnogenus and may indicate a different tracemaker than in previously described examples.

4.3.6 Ancorichnus ancorichnus (Fig. 7H)

Description: Lined, single burrows with chevron-shaped meniscate backfill (Fig. 7H). These ichnofossils are ~2 cm wide and up to ~16 cm in length. Meniscae are ~0.5 cm thick and weather differentially from the surrounding matrix material. The burrows have a thin mud lining and the internal meniscate do not cross this lining (arrows). Meniscate backfill is the same lithology as the surrounding matrix. Similar to *Scoyenia, Ancorichnus* are found associated with simple siliciclastic entisols and carbonate rhizoliths. These ichnofossils are not common and only occur associated with fluvially reworked sediment (Ssc).

Interpetation: These burrows are commonly interpreted to be created by deposit feeding, soft-bodied invertebrates such as larvae or sipunculid worms (Frey et al., 1984). *Ancorichnus* is commonly associated with wet floodplain environments (Frey et al., 1984). The preservation of distinct chevron-shaped meniscae indicates these burrows were created in relatively saturated sediments and were likely quickly cemented by carbonate dissolved in the groundwater from the surrounding matrix. The association of these burrows with immature paleosols like simple entisols and carbonate rhizoliths in the HF further suggest they were created in relatively wet soil conditions.

5.0 Discussion

The HF has a complex depositional history with multiple interpretations (e.g., Kunkle, 1958; Wengerd, 1958; Baars, 1962; Ohlen and McIntyre, 1965; Baars and Stevenson, 1987; Barbeau, 2003). This formation lies at the interface between the underlying, predominately marine units of the Hermosa Group and the overlying continental units of the Cutler Group and contains characteristics of both systems. Due to this depositional complexity the stratigraphic nomenclature of the northern Paradox basin, including the HF has been contentious (e.g., Baars, 1962; Ohlen and McIntyre, 1965; Baars and Stevenson, 1987: Murphy, 1987). This controversy can be partially explained by the interbedded marine and continental features present in the HF. This study uses a combined sedimentological, ichnological, and paleopedological approach to refine the depositional history of the HF and to help place it into a regional depositional model of the northern Paradox basin (Loope et al., 1990; Scott, 2005).

Marine deposits often contain ichnofossils from organisms reacting to a variety of physicochemical factors such as media, nutrients, salinity, turbidity, temperature, and oxygen. These ichnofossil suites are useful for interpreting depositional environments (e.g., Ekdale and Bromley, 1984; Bromley, 1996; Hasiotis, 2006). Continental deposits also contain abundant ichnofossils created by soil-dwelling organisms reacting to physicochemical factors such as soil moisture, temperature, seasonality, and precipitation (e.g., Hasiotis et al., 1993; Hasiotis and Dubiel, 1994; Hasiotis and Platt, 2012). The behavior of organisms and the distribution of ichnofossils in continental environments; however, is spatially variable and less well understood (e.g., Taylor and Goldring, 1993; Hasiotis and Platt, 2012). Due to the lateral variability of continental ichnofossil suites, associated paleosols are used to put these traces into context. (Retallack, 2001; Hasiotis, 2006; Smith et al., 2008; Hasiotis and Platt, 2012).

5.1 Stratigraphic interpretations

Five measured sections from the HF were used to correlate strata across the Cedar Mesa (Fig. 1; Supplemental Figs. 1–5). The generalized stratigraphic architecture is shown in Figure 4. Paleosol development throughout the HF is interpreted in Figure 8. Generally, the HF can be subdivided into a lower marine-dominated section and an upper eolian- and fluvial-dominated section (Fig. 4). Additionally, there is an observable trend of deepening water table levels upsection throughout the HF (Fig. 4).

5.1.1 Marine-dominated deposition

The basal ~38 m of the HF is dominated by highly bioturbated marine deposits (Cws and Css) with interbedded laminated and mottled siltstone (Stl and Stb). This section has previously been referred to as the Rico Formation by some authors (e.g., Baars, 1962; Loope, 1984; Murphy, 1987; Scott, 2005). This lowest section of the HF shares several characteristics with the underlying Honaker Trail Formation, but has been differentiated based on a transition in packstone composition from brachiopod-dominated to bivalve-dominated—possibly reflecting a shift from offshore to more nearshore conditions (Baars, 1962; Murphy, 1987). Interbedded mottled siltstones and calcareous root fossils indicate an overall transition from marine to continental deposition in this section. The laterally extensive McKim Limestone bed, a calcareous sandstone, indicates the last wide-spread marine depositional event in in the HF (Fig. 4).

Marine wackstone–packstone (Cws) beds are similar in lithology to deposits in the underlying marine Honaker Trail Formation and were deposited in a carbonate nearshore to

foreshore environment and were likely formed during fluctuations in the retreat of the Elephant Canyon Seaway. The clasts in these beds are dominated by crinoid stems, but also include brachiopod, bivalve, and gastropod shell fragments. The basal packstone bed of the HF contains trough crossbeds with mud drapes indicating a significant tidal influence on deposition. *Thalassinoides* are present in Cws, which further suggest a relatively high-energy intertidal foreshore environment. These beds contain some whole and fragmented bivalves, but lack abundant *Siphonichnus*. Rhizoliths are rare and therefore suggest that these wackestone–packstone beds were restricted to intertidal environments and only infrequently subaerially exposed.

Carbonate-cemented sandstone deposits (Css) are interbedded with wackestone-packstone units and were likely deposited in foreshore to backshore environments during the punctuated retreat of the Elephant Canyon seaway. The base of these units commonly consists of a thin, low-energy laminated green shale bed that grades quickly upsection to a thick, crossbedded to massive sandstone. These sandstone beds are heavily bioturbated and commonly contain bivalve shells and abundant *Siphonichnus philae* and *Siphonichnus lepusaures*. The depth and vertical orientation of these bivalve traces suggests rapid deposition. These carbonate-cemented sandstone beds also contain *Thalassinoides,* further suggesting high-energy shallow-marine environments. The beds are commonly capped by subaerial exposure surfaces containing well-preserved calcareous root fossils and few granular peds (Fig. 8). These root fossils do not penetrate deeply into the sediment, indicating that the water table was shallow during plant development. Paleosols horizons are classified as calcareous enitsols and were likely not exposed for long periods of time and buried rapidly. These beds suggest a shallower foreshore to

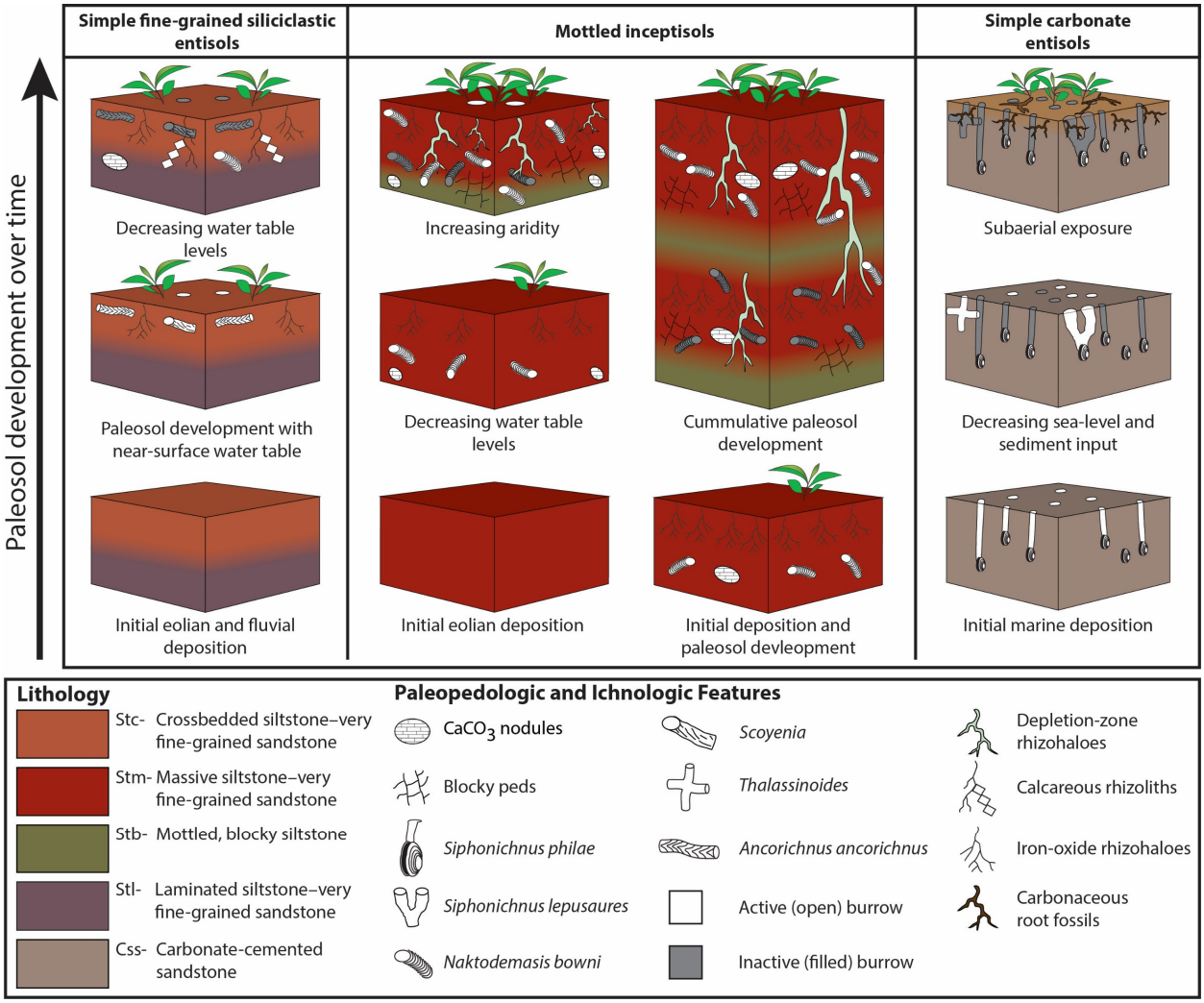

Figure 8. Box diagrams illustrating development of the three types of paleosols found in the Halgaito Formation. Initial condition of the strata is shown at the bottom of the figure and final paleosols development is shown at the top of the figure.

backshore intertidal environment than the wackestone–packstone beds and indicate increasing wave energy upsection throughout the marine portion of the HF.

Laminated and mottled siltstone deposits (Stl and Stb) interbedded within the marine-dominated section of the HF were likely deposited during short-term periods of subaerial exposure. Laminated siltstone is a common characteristic of silt-dominated eolian deposits (Murphy, 1987; Scott, 2005; 2013). Ichnologic features suggesting subaerial exposure within

these beds include small-scale iron-oxide rhizohaloes, shallow depletion-zone rhizohaloes that are > 0.4 m deep, *Scoyenia*, and *Ancorichnus ancorichnus*. Paleosol horizons containing blocky peds and carbonate nodules are classified as simple siliciclastic entisols and some mottled inceptisols. The presence of shallow rhizoliths, *Scoyenia*, and *Ancorichnus ancorichnus* suggests persistently high water table levels during deposition and paleosols development.

5.1.2 Eolian-dominated deposition

The upper ~120 m of the HF is dominated by continental siltstone deposits (Stl, Stm, and Stc) with occasional laterally discontinuous, lenticular fluvial sandstones (Ssc). Siltstone beds commonly transition from laminated (Stl) to massive or crossbedded (Stm and Stc) upsection and suggest eolian deposition of siltstone as the Elephant Canyon seaway retreated to the north. These sediments were sourced from exposed, underying Mississippian–Pennsylvanian-aged deposits as the seaway progressed northward (Murphy, 1987). This upper portion of the HF displays an overall trend of increasing aridity and deeper water table levels upsection (Fig 7).

The first ~25 m of the HF above the McKim Limestone was deposited near onshore from the Elephant Canyon seaway and contains several features that indicate predominately high water tables that were at or near the surface. These beds are characterized by 1–2 m-thick laminated siltstone–very fine-grained sandstone (Stl) with some interbedded mottled siltstone (Stb) and occasional crossbeds (Stc). Such ichnofossils as *Scoyenia* and *Ancorichnus ancorichnus* suggest poorly-drained conditions. The presence of calcareous rhizoliths indicates moderate drainage and suggests some water table fluctuation during paleosols development. Abundant dewatering structures in Stl within 10 m above and below the McKim Limestone suggest saturated conditions during deposition. Paleosol horizons within this section are

classified as simple siliciclastic entisols and were likely only exposed for relatively short-term durations.

Strata ~60–100 m above the base of the HF suggest deepening water tables upsection in association with rapid eolian deposition. The strata are characterized by 1–2 m-thick beds that commonly transition upsection from laminated siltstone (Stl) to crossbedded siltstone–very fine-grained sandstone (Stc) with rare interbedded mottled siltstone (Stb). The presence of deeply penetrating rhizohaloes, iron-oxide rhizohaloes, and *Naktodemasis bowni* indicate well-drained soils and deepening water tables compared with underlying strata. The paleosols within this section are classified as mottled inceptisols which may be simple or occasionally cumulative.

The uppermost ~50 m of the HF was likely deposited in an increasingly arid environment with very deep water tables. The lithofacies in this portion of the HF consist primarily of thick, massive and crossbedded siltstones (Stm and Stc) indicating rapid eolian deposition. Laminations may still be present in some beds (Stl) but become uncommon toward the top of the section. These strata are less bioturbated than the underlying beds in the previous sections where soil conditions were wetter and water tables were shallower. Calcareous rhizoliths and deeply-penetrating depletion-zone rhizohaloes are rare, but few other ichnological features are present. This section contains some mottled inceptisols but the uppermost 10 m shows little to no pedogenic modification with the exception of a ~0.5 m thick mottled inceptisol at the boundary with the overlying eolian Cedar Mesa Sandstone.

5.1.3 Fluvial influence

Fluvial deposits in the HF are characterized by < 1 m-thick laterally discontinuous crossbedded sandstones (Ssc) that are commonly not bioturbated but may contain some

calcareous rhizoliths. These beds occur sporadically throughout the eolian-dominated upper strata of the HF (~40–155 m), but are most abundant in the uppermost 35 m of the section (Fig 7) and are associated with the thickest cumulative inceptisol horizons. These beds are interpreted to have been deposited rapidly during flooding events and the presence of these sandstones in the uppermost beds of the HF indicates that deposition became more punctuated over time (Plink-Björklund, 2015). Unlike the eolian beds of the HF, these fluvial deposits were likely ephemeral streams sourced from the Uncompagre uplift (Murphy, 1987). These beds are volumetrically small compared to eolian strata, however, and were not the primary means of deposition within in the HF.

6.0 Conclusions

Ichnological and paleopedological studies have the potential to refine the depositional histories of mixed carbonate and siliciclastic systems, which commonly contain thin beds with rapidly changing facies. By utilizing both continental and marine ichnofossil assemblages in association with paleosol development this study has been able to interpret the depositional environment of the HF on a finer scale than previous studies (Hasiotis and Platt, 2012). Previous studies have shown a general decrease in sea-level associated with the deposition of the HF as well as the presence of paleosols (Murphy, 1987: Scott, 2005, 2013). This study, however, is the first to integrate ichnofossils with paleosol development and shows how the retreat of the Elephant Canyon Seaway affected the HF throughout its depositional history.

This study shows that the deposition of the HF was primarily related to the retreat of the Elephant Canyon Seaway to the northwest out of the Paradox basin from the Upper

Pennsylvanian to Permian. The lower, marine portion of the HF shows a trend of decreasing sea level and increasing wave influence upsection and transitions from intertidal foreshore wackestone deposits to nearshore, wave-dominated carbonate-cemented sandstone deposits with ichnofossil assemblages dominated by *Siphonichnus* and *Thalassinoides*. Paleosol development shows that the sea level decrease was punctuated with at least 4 transgressions during deposition. These paleosols are characterized by shallow, mostly horizontal carbonate impregnated rhizoliths. The McKim Limestone is the uppermost bed deposited in a marine environment and indicates the last wide-spread marine influence in the HF.

Strata above the McKim Limestone are primarily interpreted to be eolian siltstones which were sourced from underlying Mississippian–Pennsylvanian deposits to the northwest that became exposed during the retreat of the Elephant Canyon seaway (Murphy, 1987). These eolian deposits are carbonate-cemented siltstones and contain entisols and inceptisols. Beds immediately overlying the McKim Limestone contain simple paleosols and such ichnofossils as *Scoyenia* and *Ancorichnus* indicating poorly-drained conditions. Paleosol development generally increases upsection where increasing rhizolith depths and abundant *Naktodemasis* suggest better drained conditions. The uppermost beds of the HF are crossbedded, contain little paleosol development and few ichnofossils indicating a transition to more arid conditions prior to the deposition of the Cedar Mesa Formation.

Thin, crossbedded fluvial strata are also observed throughout the HF and were likely sourced from the highlands of the Uncompagre uplift. These fluvial beds are laterally discontinuous, and compose little of the HF volumetrically. This indicates that the highlands of the Uncompagre uplift did not become a significant source of sediment in the study area until the deposition of the overlying Cedar Mesa Formation. Therefore, this study supports the

interpretation that the HF should be considered the uppermost formation of the Hermosa Group (Rasmussen, 2014).

The Paradox basin contains abundant mixed carbonate and siliciclastic units, many of which are active or potential oil and gas reservoirs. The Paradox Basin has produced over 630 MMBO and 560 BCFG since drilling began (Whidden et al., 2014). Mississippian and Lower Pennsylvanian carbonate units within the basin have been the most productive (Ohlen and McIntyre, 1965; Peterson and Hite, 1969; Whidden et al., 2014); however, small reservoirs within isolated siliciclastic bodies are found in Upper Pennsylvanian (Cole et al., 1996; Whidden et al., 2014). This study helps characterize the subsurface of the northern Paradox basin at a higher resolution than possible with sedimentological techniques alone and aids in targeting the isolated reservoirs which are commonly sealed by paleosols in this region.

References

Ashley, G.M. and Driese, S.G., 2000, Paleopedology and Paleohydrology of a Volcaniclastic Paleosol Interval: Implications for Early Pleistocene Stratigraphy and Paleoclimate Record, Olduvai Gorge, Tanzania: Journal of Sedimentary Research, vol. 70, no. 5, p. 1065–1080.

Baars, D.L., 1962, Permian System of the Colorado Plateau: Bulletin of the American Association of Petroleum Geologists, v.46, no. 2, p. 149-180.

Blair, M.G., 2015, A Paleopedological and Ichnological Approach to Spatial and Temporal Variability in Pennsylvanian-Permian Strata of the Lower Dunkard Group: M.S. Thesis, The College of Arts and Sciences of Ohio University, 151 p.

Barbaeu, D.L., 2003, A Flexural Model for the Paradox Basin: Implications for the Tectonics of the Ancestral Rocky Mountains: Basin Research, vol. 15, p. 97–115.

Bottjer, D. and Droser, M.L., 1991, Ichnofabric and Basin Analysis: Palaios, v.6, p.199-205.

Bown, T.M. and Kraus, M.J., 1983, Ichnofossils of the Alluvial Willwood Formation (lower Eocene), Bighorn Basin, Northwest Wyoming, U.S.A.: Paleogeography, Paleoclimatology, Paleoecology, v.43, p.96-128.

Bromley, R.G., 1996, Trace Fossils: Biology, Taphonomy and Applications: Chapman & Hall, London, 361 p.

Bromley, R.G., and Ekdale, A.A., 1986, Composite Ichnofabrics and Tiering of Burrows: Geological Magazine, vol. 123, p. 59-65.

Brown. R.B., 1990, Soil Texture: Fact-Sheet SL-29: Soil and Water Science Department, Florida Cooperative Extension Service, Institute of Food and Agricultural Sciences, University of Florida.

Clifton, H.E., and Thompson, J.K.,1978, *Macaronichnus segregatis*: A Feeding Structure of Shallow Marine Polychaetes: Journal of Sedimentary Petrology, v. 48, p. 1293-1302

Cole, R.D., Moore, G.E., Trevena, A.S., Armin, R.A., and Morton, M.P., 1996, Lithofacies Definition in Cutler and Honaker Trail Formations, Northeastern Paradox Basin, by Sedimentologic Observation and Spectral Gamma-Ray Data: in Geology and Resources of the Paradox Basin: Utah Geological Association Guidebook 25 (ed. by A.C. Hauffman, Jr., W.R. Lund, and L.H. Godwin) Utah Geological Association, p. 161-172.

Condon, S.M., 1997, Geology of the Pennsylvanian and Permian Cutler Group and Permian Kaibab Limestone in the Paradox Basin, Southeastern Utah and Southwestern Colorado: U.S. Geological Survey Bulletin 2000-P, 38 p.

Dubiel, R.F., Huntoon, J.E., Condon, S.M., and Stanesco, J.D., 1996a, Permian Deposystems, Paleogeography, and Paleoclimate of the Paradox Basin and Vicinity: Paleozoic Systems of the Rocky Mountain Region, p. 427–443.

Dubiel, R.F., Huntoon, J.E., Stanesco, J.D., Condon, S.M., and Mickelson, D., 1996b, Permian-Triassic Depositional Systems, Paleogeography, Paleoclimate, and Hydrocarbon Resources in Canyonlands, Utah: U.S. Geological Survey Open-File Report 96-4, 24 p.

Dubiel, R.F., Huntoon, J.E., Stanesco, J.D., and Condon, S.M., 2009, Cutler Group Alluvial, Eolian, and Marine Deposystems: Permian Facies Relations and Climatic Variability in the Paradox Basin, in Houston et al., The Paradox Basin Revisited – New Developments in Petroleum Systems and Basin Analysis: Rocky Mountain Association of Geologists Special Publication, p. 265–308.

Dunham, R.J., 1962, Classification of Carbonate Rocks According to Depositional Textures: in American Association of Petroleum Geologists Memoir 1: Classification of Carbonate Rocks--A Symposium, p. 108–121.

Ekdale, A.A., and Bromley, R.G., 1984, Sedimentology and Ichnology of the Cretaceous-Tertiary Boundary in Denmark: Implications for the causes of the Terminal Cretaceous Extinction: Journal of Sedimentary Petrology, v. 54, p. 681-703.

Frey, R.W., Pemberton, G., and Fagerstrom, J.A., 1984, Morphological, Ethological, and Environmental Significance of the Ichnogenera *Scoyenia* and *Ancorichnus*: Journal of Paleontology, vol. 58, No. 2, p. 511–528.

Hasiotis, S.T., 2006, Continental Ichnology: Using Terrestrial and Freshwater Trace Fossils for Environmental and Climatic Interpretations: SEPM Short Course Notes, no.51.

Hasiotis, S.T. and Dubiel, R.F., 1993, Continental Trace Fossils of the Upper Triassic Chinle Formation, Petrified Forest National Park, in Lucas, S.G. and Morales, M., eds., The Nonmarine Triassic: New Mexico Musesum of Natural History and Science Bulletin No. 3, p. 175–178.

Hasiotis, S.T. and Dubiel, R.F., 1994, Ichnofossil Tiering in Triassic Alluvial Paleosols: Implications for Pangean Continental Rocks and Paleoclimate: Memoirs of the Canadian Society of Petroleum Geologists. v.17, p.311-317.

Hasiotis S.T., Mitchell, C.E., and Dubiel, R.F., 1993, Application of Morphologic Burrow Interpretations to Discern Continental Burrow Architects: Lungfish or Crayfish?: Ichnos, vol. 2., no. 4, p. 315–333.

Hasiotis, S.T., and Platt, B.R., 2012, Exploring the Sedimentary, Pedogenic, and Hydrologic Factors that Control the Occurrence and Role of Bioturbation in Soil Formation and

Horizonation in Continental Deposits: An integrative approach: The Sedimentary Record, v. 10, p.4-9.

Hembree, D.I. and Nadon, G.C., 2011, A Paleopedologic and Ichnologic Perspective of the Terrestrial Pennsylvanian Landscape in the Distal Appalachian Basin, U.S.A.: Palaeogeography, Palaeoclimatology, Palaeoecology, vol. 312, no. 1–2, p. 138–166.

Jordan, O.D., and Mountney, N.P., 2012, Sequence Stratigraphic Evolution and Cyclicity of an Ancient Coastal Desert System; The Pennsylvanian-Permian Lower Cutler Beds, Paradox Basin, Utah, U.S.A: Journal of Sedimentary Research, v. 82, p. 755-780.

Kluth, C.F. and Coney, P.J., 1981, Plate Tectonics of the Ancestral Rocky Mountains: Geology, vol. 9, p. 10–15.

Kluth, C.F. and DuChene, H.R., 2009, Late Pennsylvanian and Early Permian Structural Geology and Tectonic History of the Paradox Basin and Uncompahgre Uplift, Colorado and Utah, in Houston et al., The Paradox Basin Revisited – New Developments in Petroleum Systems and Basin Analysis: Rocky Mountain Association of Geologists Special Publication, p. 178–197.

Kraus, M.J., 1996, Avulsion Deposits in Lower Eocene Alluvial Rocks, Bighorn Basin, Wyoming: Journal of Sedimentary Research, vol 66, no. 2, p. 354–363.

Kraus, M.J., 1999, Paleosols in Clastic Sedimentary Rocks: Their Geologic Applications: Earth-Science Reviews, v.47, p.41-70.

Kraus, M.J., 2002, Basin-scale Changes in Floodplain Paleosols: Implications for Interpreting Alluvial Architecture: Journal of Sedimentary Research, v.72, p.500-509.

Kraus, M.J. and Aslan, A., 1993, Eocene Hydromorphic Paleosols: Significance for Interpreting Ancient Floodplain Processes: Journal of Sedimentary Petrology, vol.63, p.453-463.

Kraus, M. J., and Hasiotis, S. T., 2006, Significance of Different Modes of Rhizolith Preservation to Interpreting Paleoenvironmental and Paleohydrologic Settings: Examples from Paleogene Paleosols, Bighorn Basin, Wyoming, U.S.A.: Journal of Sedimentary Research, vol. 76, p. 633-646.

Kunkle, R.P., 1958, Permian Stratigraphy of the Paradox Basin: in Guidebook to the Geology of the Paradox Basin, Ninth Annual Field Conference: Intermountain Association of Petroleum Geologists (by the Utah Geological Association) p.163-168.

Lemke, L., 1985, Subsidence Analysis of the Paradox Basin, Utah: M.Sc Thesis, University of Arizona, Tucson, AZ.

Loope, D.B. 1984, Eolian Origin of Upper Paleozoic Sandstones, Southeastern Utah: Journal of Sedimentary Petrology, vol. 54, no. 2, p. 563–580.

Loope, D.B., Sanderson, G.A., and Verville, G.J., 1990, Abandonment of the Name "Elephant Canyon Formation: in Southeastern Utah: Physical and Temporal Implications: The Rocky Mountain Geologist, vol. 27, no. 4., p. 119–130.

Márquez, F. and van der Molen, S., 2011, Intraspecific Shell-Shape Variation in the Razor Clam *Ensis macha* Along the Patagonian Coast: Journal of Molluscan Studies, vol. 77, p. 123–128.

McNeill, D.F., Cunningham, K.J., Guertin, L.A., Anselmetti, F.S., 2004, Depositional Themes of Mixed Carbonate-siliciclastics in the South Florida Neogene: Application to Ancient Deposits, in Integration of outcrop and modern analogs in reservoir modeling: AAPG Memoir 80, p. 23-43.

Moore, D.M., and Reynolds, R.C., 1997, X-ray Diffraction and the Identification and Analysis of Clay Minerals: Oxford, Oxford University Press, 378 p.

Munsell, 2009, Munsell® Soil Color Book: Revised Edition.

Murphy, K., 1987, Eolian Origin of Upper Paleozoic Red Siltstones at Mexican Hat and Dark Canyon, Southeastern Utah, M.S. Thesis, The University of Nebraska, 128 p.

Myrow, P.M., 1995, *Thalassinoides* and the Enigma of Early Paleozoic Open-Framework Burrow Systems: PALAIOS, vol. 10, no. 1, p. 58–74.

Nuccio, V.F. and Condon, S.M., 1996, Burial and Thermal History of the Paradox Basin, Utah and Colorado, and Petroleum Potential of the Middle Pennsylvanian Paradox Formation in Huffman Jr., A.C., Lund, W.R., and Goodwin, L.H., eds., Geology and Resources of the Paradoc Basin: Utah Geological Association Guidebook 25, p. 57–76.

Ohlen, H.R. and McIntyre, L.B., 1965, Stratigraphy and Tectonic Features of Paradox Basin, Four Corners area: Bulletin of the American Association of Petroleum Geologists, vol. 49, no.11, p.2020–2040.

O'Sullivan, R.B., 1965, Geology of the Cedar Mesa-Boundary Butte area, San Juan County, Utah: United States Geological Survey Bulletin, vol. 1186, p. 1–128.

Peterson, J.A. and Hite, R.J., 1969, Pennsylvanian Evaporate-Carbonate Cycles and Their Relation to Petroleum Occurrence, Southern Rocky Mountains: American Association of Petroleum Geologists Bulletin, vol. 53, no. 4, p.884–908.

Peterson, J.A. and Ohlen, H.R., 1963, Pennsylvanian Shelf Carbonates, Paradox Basin in Shelf Carbonates of the Paradox Basin, Fourth Field Conference: Four Corners Geological Society, p. 65–79.

Plink-Björklund, P., 2015, Morphodynamics of Rivers Strongly Affected by Monsoon Precipitation: Review of Depositional Style and Forcing Factors: Sedimentary Geology, vol. 323, p. 110–147.

Plink-Björklund, P., Birgenheier, L.P., and Golab, J.A., 2012. Signature of Climate Control in Early Eocene Fluvial Channel Systems. Abstracts Volume, American Association of Petroleum Geologists Annual Meeting, April 22-25, 2012, Long Beach, CA.

Rasmussen, D.L., 2002, Sequence Stratigraphy of the Late Pennsylvanian to Early Permian Honaker Trail and Elephant Canyon Strata, Paradox Basin, Utah and Colorado: Geological Society of America Rocky Mountain Section Meeting Technical Program, Cedar City, UT.

Rasmussen, D.L., 2014, Namakiers in Triassic and Permian Formations in the Paradox Basin (USA) with Comparisons to Modern Examples in the Zagros Fold Belt, Iran, in MacLean, J.S., Biek, R.F., and Huntoon, J.C., eds., Geology of Utah's Far South: Utah Geological Association Publication 43, p. 689–756.

Retallack, G.J., 2001, Soils of the Past: An Introduction to Paleopedology, Second Edition: Oxford, U.K., Blackwell Science, 404 p.

Sanderson, G.A., and Verville, G.J., 1990, Fusilinid Zonation of the General Petroleum No. 45-5-G core, Emery County, Utah: Mountain Geologist, vol. 27, no. 4, p. 131–136.

Schwertmann, U., 1993, Relations Between Iron Oxides, Soil Color, and Soil Formation, in Bigham, J.M. and Ciolkosz E.J., eds., Soil Color: Soil Science Society of America Special Publication 31, p. 51–69.

Scott, K.M., 2005, Cohesion, Water Vapor, and Floral Topography: Significance for the Interpretation of the Depositional Mechanisms of the Late Paleozoic Halgaito Formation, Cutler Group, Southeastern Utah in Lucas, S.G. and Zeigler, K.E., eds., The Nonmarine Permian: New Mexico Museum of Natural History and Science Bulletin No. 30, p. 296–301.

Scott, K.M., 2013, Carboniferous-Permian boundary in the Halgaito Formation, Cutler Group, Valley of the Gods and surrounding area, southeastern Utah: New Mexico Museum of Natural History and Science Bulletin, vol. 60, p. 398–409.

Sheehan, P.M. and Schiefelbein, D.R.J., 1984, The Trace Fossil *Thalassinoides* from the Upper Ordovician of the Eastern Great Basin: Deep Burrowing in the Early Paleozoic: Journal of Paleontology, vol. 58, no. 2, p. 440–447.

Stevenson, G.M. and Baars, D.L., 1987, The Paradox: A Pull-Apart Basin of Pennsylvanian Age in Geology of Cataract Canyon and Vicinity, Tenth Field Conference: Four Corners Geological Society, p. 31–50.

Smith, J.J., Hasiotis, S.T., Kraus, M.J., and Woody, D.T., 2008a, Relationship of Floodplain Ichnocoenoces to Paleopedology, Paleohydrology, and Paleoclimate in the Willword Formation, Wyoming, During the Paleocene–Eocene Thermal Maximum: Palaios, vol 23, p. 683–699.

Smith, J.J., Hasiotis, S.T., Woody, D.T., and Kraus, M.J. 2008b. Paleoclimatic Implications of Crayfish-Mediated Prismatic Structures in Paleosols of the Paleogene Willwood Formation, Bighorn Basin, Wyoming, U.S.A.: Journal of Sedimentary Research, vol 78, p.323–334.

Soil Survey Staff, 1999, Soil Taxonomy: A Basic System of Soil Classification for Making and Interpreting Soil Surveys: United States Department of Agriculture, Agriculture Handbook, no. 436.

Taylor, A.M. and Goldring, R., 1993, Description and Analysis of Bioturbation and Ichnofabric: Journal of the Geological Society, London, vol 150, p. 141–148.

Vepraskas, M.J., Wilding, L.P., and Drees, L.R., 1992, Aquic Conditions for Soil Taxonomy: Concepts, Soil Morphology and Micromorphology, in Ringrose-Voase, A.J. and Humphreys, G.S., eds., Soil Micromorphology: Studies in Management and Genesis, p. 117–131.

Wengerd, S.A, 1955, Geology of the Mexican Hat oil field, San Juan County, Utah: Four Corners Geological Society Guidebook, Field Conference on parts of Paradox, Black Mesa, and San Juan basins, p. 150–163.

Wengerd, S.A., Pennsylvanian Sedimentation in Paradox Basin, Four Corners Region in AAPG Special Publication 23: Pennsylvanian System in the United States, 264–240.

Wengerd, S.A. and Matheny, M.L., 1958, Pennsylvanian System of the Four Corners Region: American Association of Petroleum Geologists Bulletin vol. 42, p. 2048–2106.

Wentworth, C.K., 1922, A Scale of Grade and Class Terms for Clastic Sediments: Journal of Geology, vol. 31, p. 377–392.

Whidden, K.J., Lillis, P.G., Anna, L.O., Pearson, K.M., and Dubiel, R.F., 2014, Geology and Total Petroleum Systems of the Paradox Basin, Utah, Colorado, New Mexico, and Arizona: The Mountain Geologist, vol. 51, no. 2, p.119–138.

Winter, A.G. and Hosoi, A.E., 2011, Identification and Evaluation of the Atlantic Razor Clam (*Ensis directus*) for Biologically Inspired Subsea Burrowing Systems: Integrative and Comparative Biology, vol. 51, no 1, p. 151–157.

Zonneveld, J.P. and Gingras, M.K., 2013, The Ichnotaxonomy of Vertically Oriented, Bivalve-Generated Equilibrichnia: Journal of Paleontology, vol. 87, no. 2, p. 243–253.

Appendix I

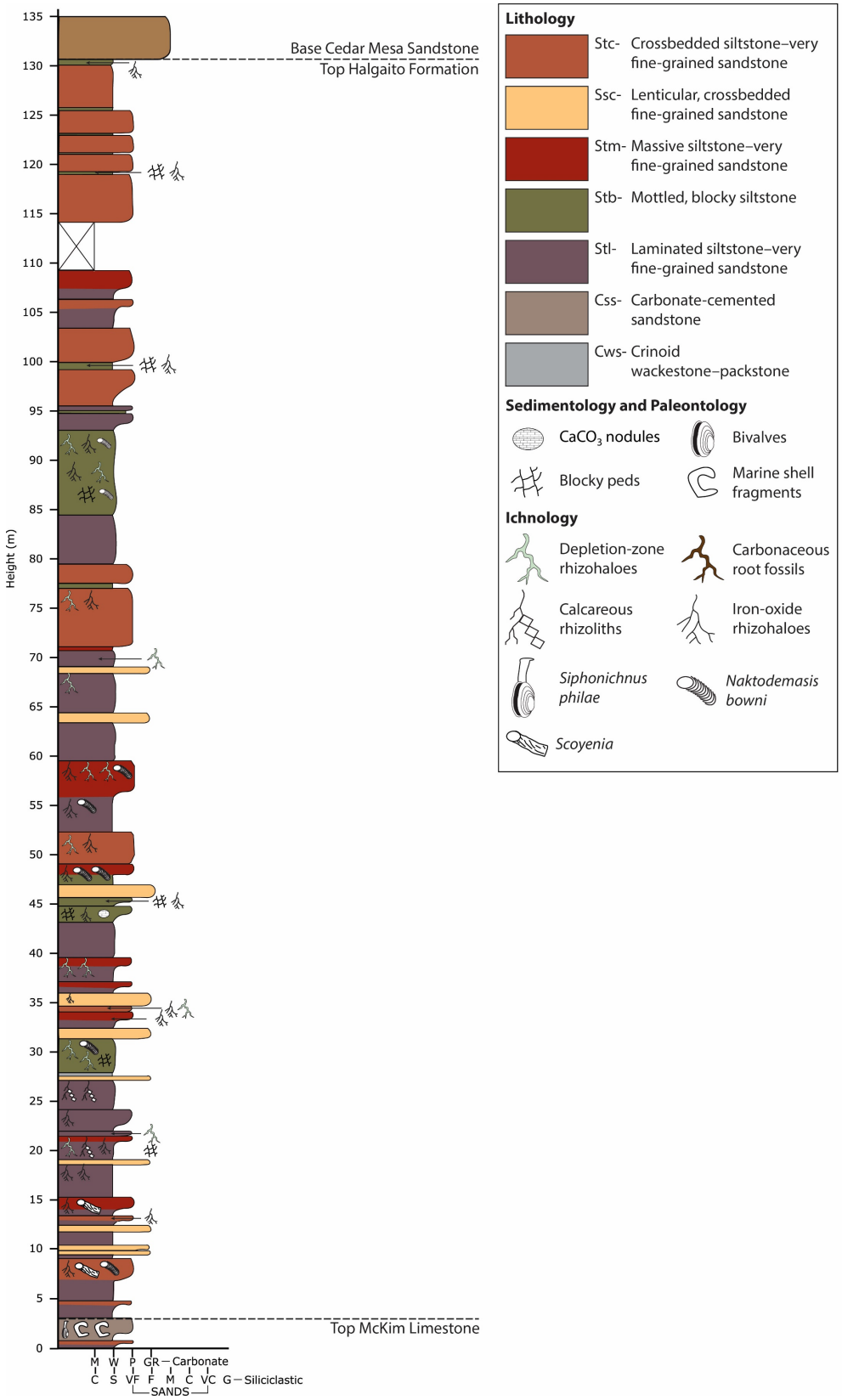
Base Cedar Mesa Sandstone
Top Halgaito Formation
Top McKim Limestone
Height (m)
135
130
125
120
115
110
105
100
95
90
85
80
75
70
65
60
55
50
45
40
35
30
25
20
15
10
5
0
M C
W S
P VF
GR F
M
C
VC
G
Carbonate
Siliciclastic
SANDS
Lithology
Stc- Crossbedded siltstone–very fine-grained sandstone
Ssc- Lenticular, crossbedded fine-grained sandstone
Stm- Massive siltstone–very fine-grained sandstone
Stb- Mottled, blocky siltstone
Stl- Laminated siltstone–very fine-grained sandstone
Css- Carbonate-cemented sandstone
Cws- Crinoid wackestone–packstone
Sedimentology and Paleontology
CaCO3 nodules
Bivalves
Blocky peds
Marine shell fragments
Ichnology
Depletion-zone rhizohaloes
Carbonaceous root fossils
Calcareous rhizoliths
Iron-oxide rhizohaloes
Siphonichnus philae
Naktodemasis bowni
Scoyenia

Supplemental Figure 1. Stratigraphic column GH-1 showing lithology, sedimentological structures, paleontology, and ichnological features. Section was measured along the Moki Dugway and contains the continental portion of the Halgaito Formation from the top of the McKim Limestone to the contact with the overlying Cedar Mesa Formation.

Appendix II

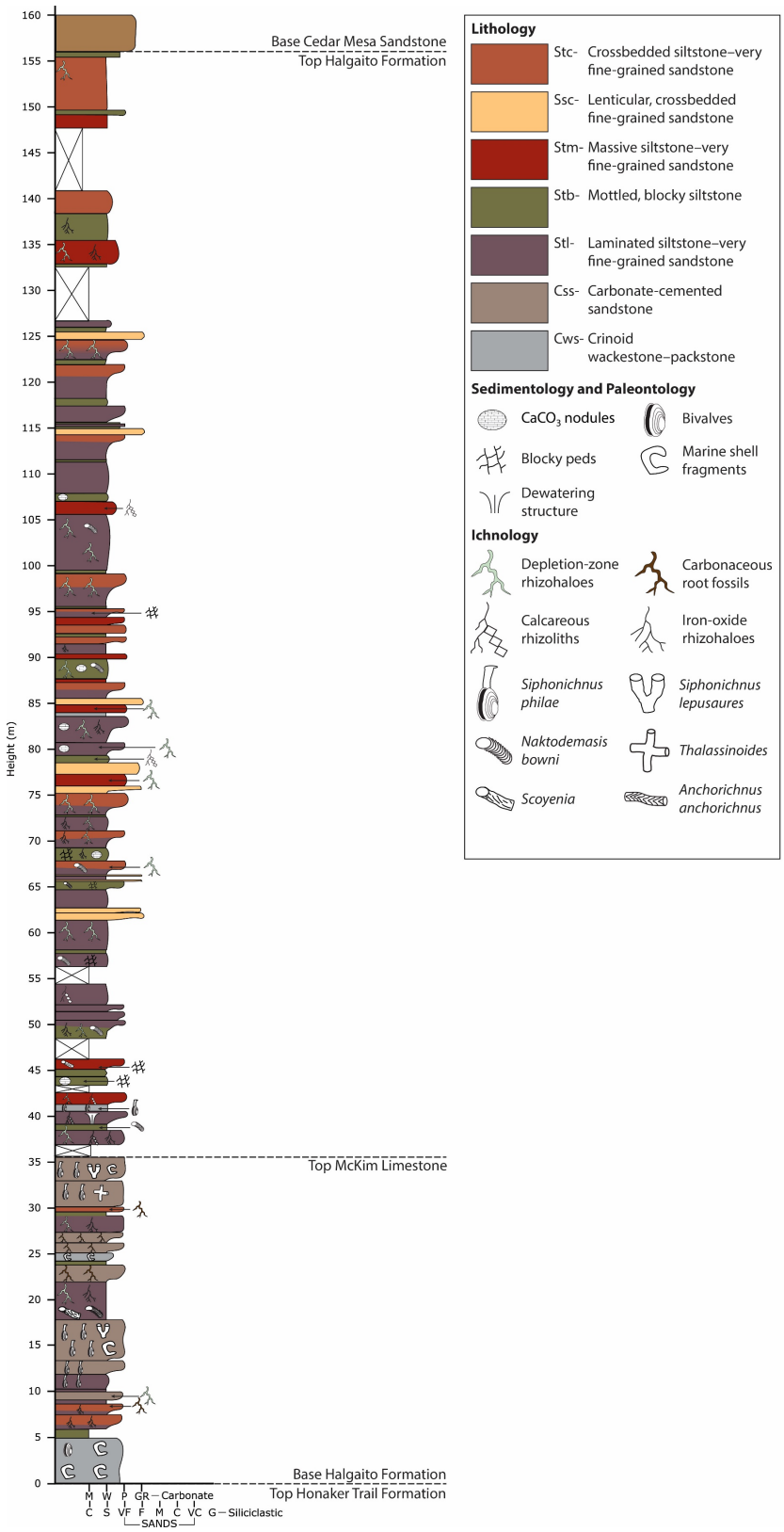
Base Cedar Mesa Sandstone
Top Halgaito Formation
Top McKim Limestone
Base Halgaito Formation
Top Honaker Trail Formation
Height (m)
M W P GR – Carbonate
C S VF F M C VC G – Siliciclastic
SANDS
Lithology
Stc- Crossbedded siltstone–very fine-grained sandstone
Ssc- Lenticular, crossbedded fine-grained sandstone
Stm- Massive siltstone–very fine-grained sandstone
Stb- Mottled, blocky siltstone
Stl- Laminated siltstone–very fine-grained sandstone
Css- Carbonate-cemented sandstone
Cws- Crinoid wackestone–packstone
Sedimentology and Paleontology
CaCO3 nodules
Bivalves
Blocky peds
Marine shell fragments
Dewatering structure
Ichnology
Depletion-zone rhizohaloes
Carbonaceous root fossils
Calcareous rhizoliths
Iron-oxide rhizohaloes
Siphonichnus philae
Siphonichnus lepusaures
Naktodemasis bowni
Thalassinoides
Scoyenia
Anchorichnus anchorichnus

Supplemental Figure 2. Stratigraphic column GH-2 showing lithology, sedimentological structures, paleontology, and ichnological features. Section was measured on the south side of the Cedar Mesa and contains the entire Halgaito Formation.

Appendix III

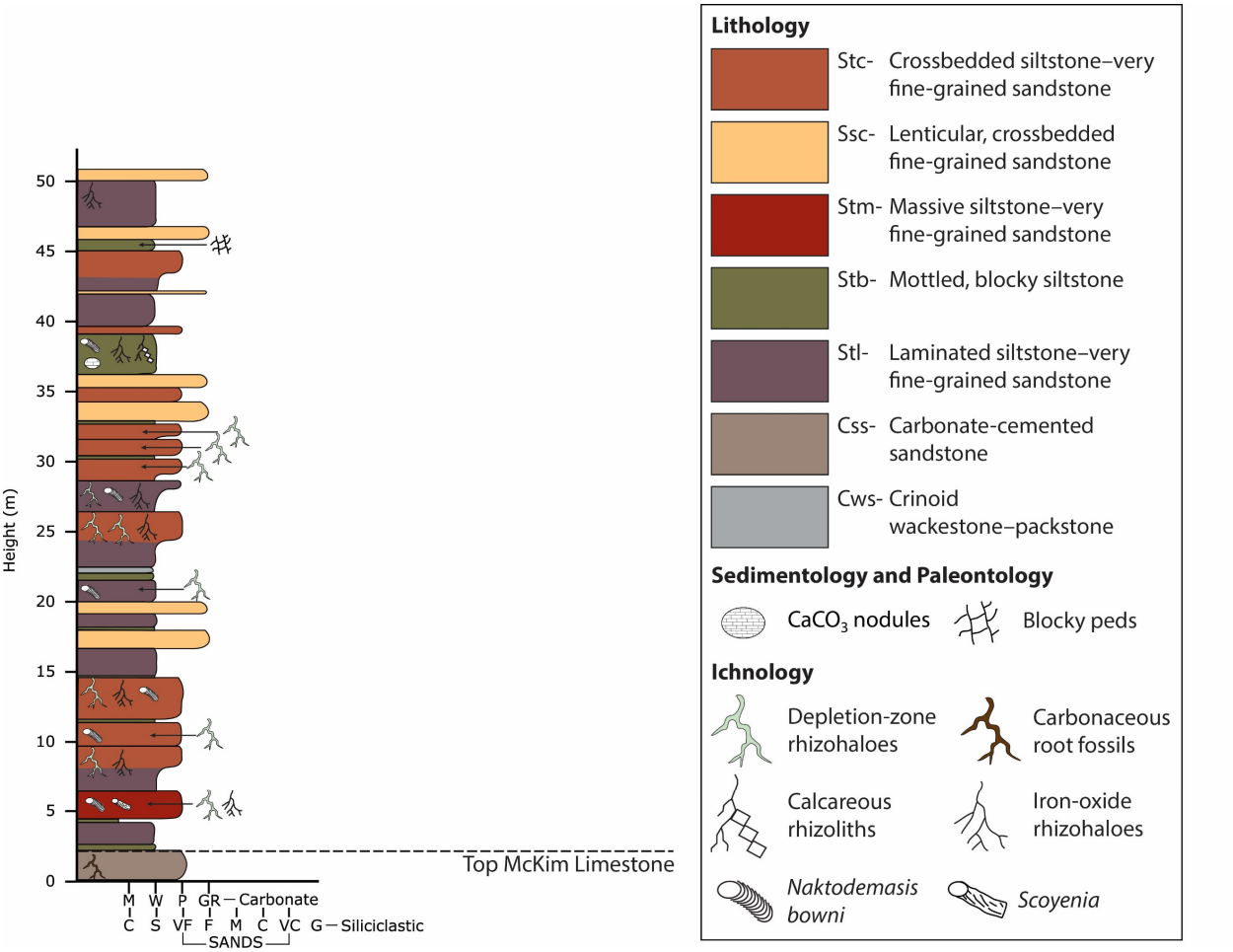

Supplemental Figure 3. Stratigraphic column GH-3 showing lithology, sedimentological structures, paleontology, and ichnological features. Section was measured ~0.5 km north of GH-1 and contains part of the continental portion of the Halgaito Formation above the McKim Limestone.

Appendix IV

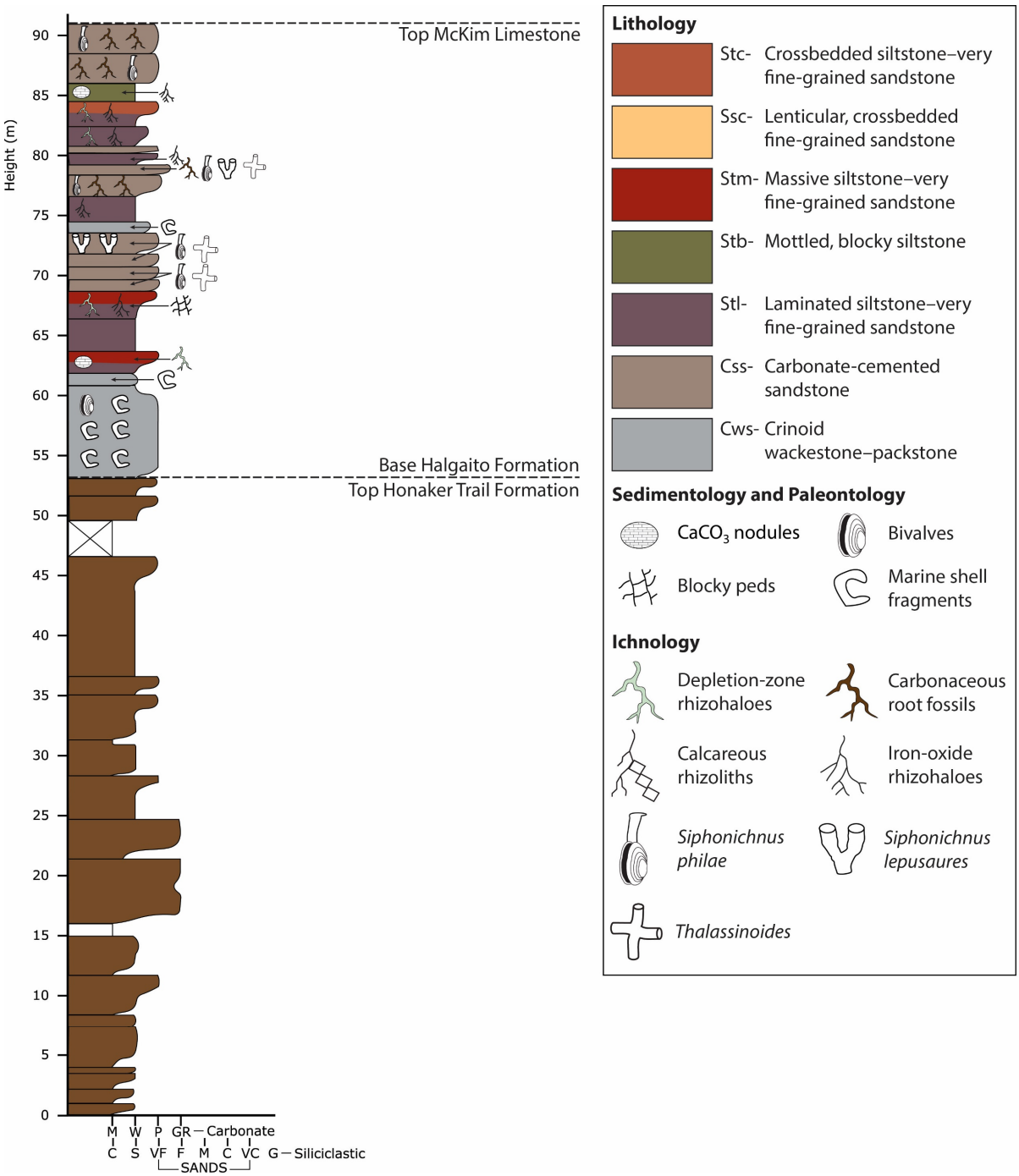
Top McKim Limestone
Base Halgaito Formation
Top Honaker Trail Formation
Height (m)
0
5
10
15
20
25
30
35
40
45
50
55
60
65
70
75
80
85
90
M W P GR — Carbonate
C S VF F M C VC G — Siliciclastic
SANDS
Lithology
Stc- Crossbedded siltstone–very fine-grained sandstone
Ssc- Lenticular, crossbedded fine-grained sandstone
Stm- Massive siltstone–very fine-grained sandstone
Stb- Mottled, blocky siltstone
Stl- Laminated siltstone–very fine-grained sandstone
Css- Carbonate-cemented sandstone
Cws- Crinoid wackestone–packstone
Sedimentology and Paleontology
CaCO3 nodules
Bivalves
Blocky peds
Marine shell fragments
Ichnology
Depletion-zone rhizohaloes
Carbonaceous root fossils
Calcareous rhizoliths
Iron-oxide rhizohaloes
Siphonichnus philae
Siphonichnus lepusaures
Thalassinoides

Supplemental Figure 4. Stratigraphic column GH-4 showing lithology, sedimentological structures, paleontology, and ichnological features. Section was measured ~2 km south of the Cedar Mesa near the top of the Honaker Trail. Section contains the marine portion of the Halgaito formation up to the McKim Limestone. Part of the Honaker Trail Formation was measured with only general lithology shown on the column.

Appendix V

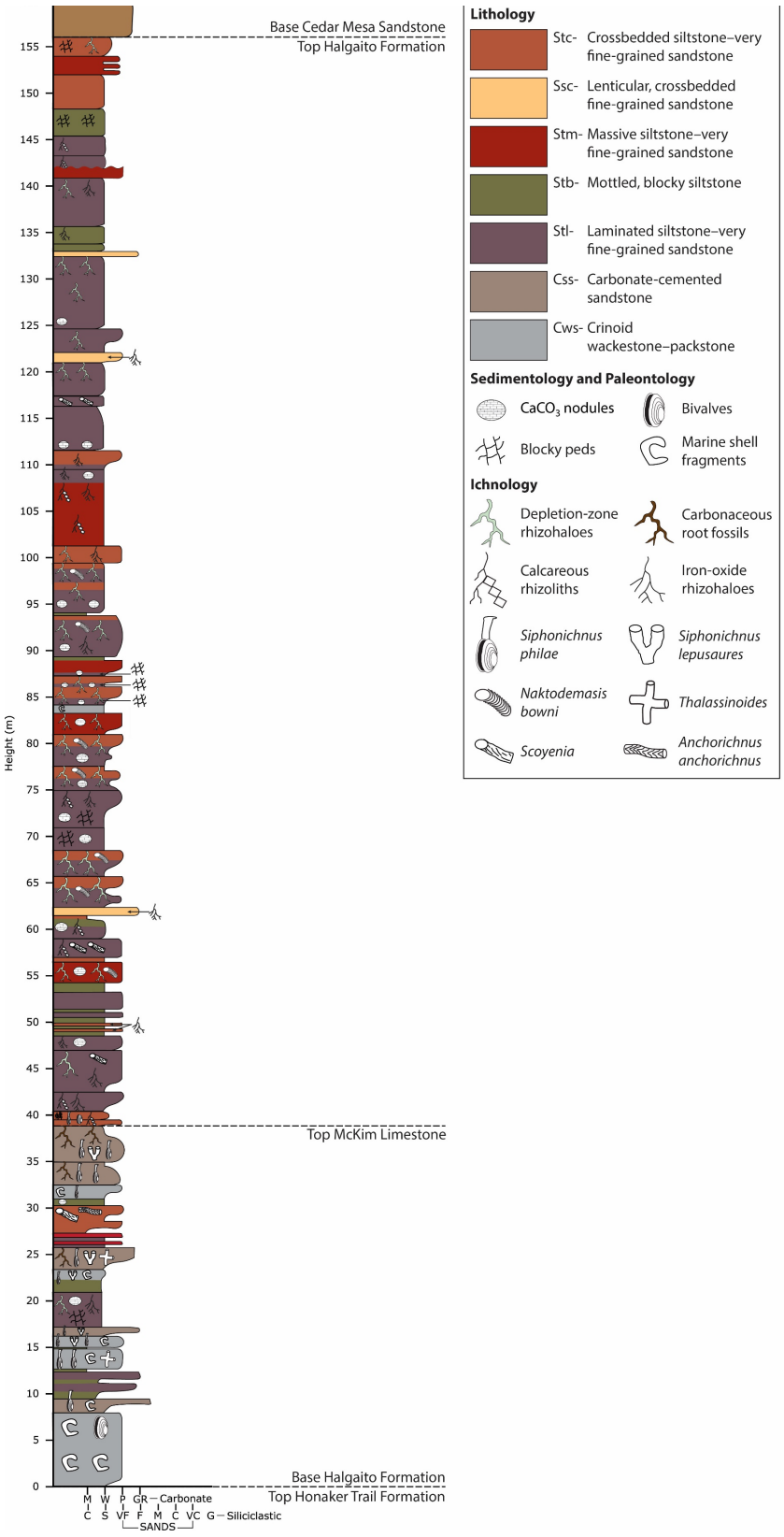
Base Cedar Mesa Sandstone
Top Halgaito Formation
Top McKim Limestone
Base Halgaito Formation
Top Honaker Trail Formation
Height (m)
M C
W S
P VF
GR F
M
C
VC
G
Carbonate
Siliciclastic
SANDS
Lithology
Stc- Crossbedded siltstone–very fine-grained sandstone
Ssc- Lenticular, crossbedded fine-grained sandstone
Stm- Massive siltstone–very fine-grained sandstone
Stb- Mottled, blocky siltstone
Stl- Laminated siltstone–very fine-grained sandstone
Css- Carbonate-cemented sandstone
Cws- Crinoid wackestone–packstone
Sedimentology and Paleontology
CaCO3 nodules
Bivalves
Blocky peds
Marine shell fragments
Ichnology
Depletion-zone rhizohaloes
Carbonaceous root fossils
Calcareous rhizoliths
Iron-oxide rhizohaloes
Siphonichnus philae
Siphonichnus lepusaures
Naktodemasis bowni
Thalassinoides
Scoyenia
Anchorichnus anchorichnus

Supplemental Figure 5. Stratigraphic column GH-5 showing lithology, sedimentological structures, paleontology, and ichnological features. Section was measured on the southwest portion of the Cedar Mesa near Muley Point and contains the entire Halgaito Formation.

CHAPTER 5. CONCLUSIONS

This dissertation shows that ichnological analysis is an important part of both hydrogeology and petroleum geology, due to its significance in aquifer and reservoir quality as well as for environmental interpretations. Ichnological assessments lead to a better understanding of the hydrological effects of bioturbation on sedimentary facies and stratigraphy and consequently on subsurface fluid pathways. Ichnofossils may directly affect physical characteristics such as porosity and permeability as well as be used to create robust, high-resolution geologic frameworks. Ichnofossils may be studied in both outcrop and core, making them easily accessible to most studies. Ichnological assessment has become increasing common in hydrocarbon reservoir analysis but is still commonly overlooked component of freshwater aquifers.

Characterizing the bioturbation-influenced fluid pathways within the karstic Glen Rose Limestone (GRL) requires the integration of lithology, structural and karstic features, and ichnology. Bioturbation commonly homogenizes sediment destroying coarse-grained horizons that direct fluid flow within aquifers that contain significant intergranular flow (Gingras et al., 2007; Tonkin et al., 2010). Many karstic systems, conversely, cannot transmit fluids through interparticle porosity rely on non-fabric selective fluid pathways such as fractures or burrow networks (Achauer, 1977; Cunningham and Sukop, 2011, 2012). The GRL is a telogenic karstic deposit and contains significant amounts of mud and marl. Meteoric water enters the GRL is through the Balcones Fault zone, a series of near-vertical fractures and is moved laterally through beds via large-scale *Thalassinoides*-dominated pore networks.

Most GRL hydrostratigraphic units (HSUs) contain m-scale coarsening-upward successions with decreasing-upward ichnofabric indices (ii). Bases of these successions are muddy, nodular strata with abundant bioturbation (ii5–6). These homogenized zones lack fluid pathways and do not transmit water readily. The successions grade upward into strata with moderate bioturbation (ii3–4) consisting of *Thalassinoides* networks as well as *Ophiomorpha*, and occasional *Palaeophycus*. These traces create well-developed burrow networks that are commonly filled with coarse-grained, higher permeability material than the surrounding matrix. These moderately-bioturbated zones are more commonly observed in transmissive HSUs and are interpreted as the most prominent area of bioturbation influenced porosity and permeability. The tops of successions sometimes consist of mildly bioturbated (ii1–2) strata where fluid flow would be restricted to intergranular pore space.

The ichnological patterns that were identified in outcrop were also directly correlated to wireline log data. The GRL is fairly unusual as it can be observed in both outcrop and subsurface due to the offsets caused by the Balcones Fault Zone. Traditional resistivity and natural gamma logs were used to show that interconnected bioturbation-influenced porosity can be identified and correlated in the subsurface. The m-scale successions containing interconnected *Thalassinoides* networks identified from outcrop were identified in logs from the Camp Stanley Storage Activity and support the interpretation that these networks are a primary control on fluid pathways. Zone with high resistivity (> 300 Ω-m) correlate with *Thalassinoides* networks in core and very high resistivity (> 650 Ω-m) correlate to significant solution enhanced burrows. These high-resistivity zones were previously interpreted as karstic features (e.g., Wierman et al., 2010), but all wells within the GRL display such cyclical resistivity kicks, even when not located in proximity to major faults and associated karstic features.

The results of these studies on the GRL are important because commonly used methods to measure porosity and permeability usually only account for intergranular matrix porosity. Methods such as point-counting and helium-expansion porosity and permeability testing do not accurately reflect the subsurface hydrological characteristics of karstic strata and will almost always underestimate potential fluid flow (Cunningham et al., 2009). The overall transmissivity of HSUs within the GRL is more complex and depends on the interaction of ichnofabric index, fracture density, and karstic features. Therefore, an integrated approach using ichnology, sedimentology, and petrophysics is needed to create a complete geologic framework for the Trinity aquifer.

Ichnological assessments are not only limited to direct hydrological properties but can also be used to gain a better understanding of sedimentary facies and stratigraphy and consequently on potential reservoir architectures. Ichnologic and paleopedologic analyses from the Pennsylvanian–Permian Halgaito Formation (HF) show that such studies supplement sedimentological and stratigraphic data for interpreting depositional history and subsurface facies architecture. This study was able to interpret the paleoenvironmental history of the HF at a finer scale than previous work and demonstrated how the retreat of the Elephant Canyon Seaway out of the northern Paradox basin affected deposition in the region.

Previous paleoenvironmental and paleogeographic interpretations for the HF were commonly at odds, likely because the HF lies at the interface between a carbonate ramp system and an alluvial–eolian system. Ichnofossils and paleosol development in the lower portion of the HF indicate that the retreated of the Elephant Canyon seaway out of the Paradox basin was punctuated with at least 4 transgressions. Above these transgressive units, HF strata is primarily interpreted to be eolian siltstones. Paleosol development generally increases upsection and

ichnofossils suggest better drained conditions. The uppermost beds of the HF contain little paleosol development and few ichnofossils indicating a transition to more arid conditions prior to the deposition of the overlying Cedar Mesa Formation.

The combined results of this dissertation indicate that ichnologic assessment is invaluable to the characterization of both freshwater aquifers and hydrocarbon reservoirs that are often overlooked. Ichnofossils may directly affect the porosity and permeability characteristics of a unit or be used to refine the paleoenvironmental and paleogeographic history of a unit. Combining ichnological assessment with sedimentological and structural studies will contribute towards better aquifer characterization as well as better predictions of vertical and lateral changes in subsurface architectures.

References

Achauer, C.A., 1977, Contrasts in Cementation, Dissolution, and Porosity Development Between Two Lower Cretaceous Reefs of Texas, in Bebout, D.G., and Loucks, R.G., eds., Cretaceous carbonates of Texas and Mexico—Applications to subsurface exploration: Austin, University of Texas, Bureau of Economic Geology Report of Investigation 89, p. 127–137.

Cunningham, K.J. and Sukop, M.C., 2011, Multiple Technologies Applied to Characterization of the Porosity and Permeability of the Biscayne Aquifer, Florida: U.S. Geological Survey Open-File Report 2011-1037, 8 p.

Cunningham, K.J. and Sukop, M.C., 2012, Megaporosity and Permeability of *Thalassinoides*-Dominated Ichnofabrics in the Creataceous Karst-Carbonate Edwards-Trinity Aquifer System, Texas: U.S. Geological Survey Open-File Report 2012-1021, 4 p.

Cunningham, K.J., Sukop, M.C., Huang, H., Alvarez, P.F., Curran, H.A., Renken, R.A., and Dixon, J.F., 2009, Prominence of Ichnologically Influenced Macroporosity in the Karst Biscayne aquifer: Stratiform "super-K" zones, Geological Society of America Bulletin, vol. 121, no. 1/2; p. 164–180.

Gingras, M.K., Baniak, G., Gordon, J., Hovikoski, J., Konhauser, K.O., La Croix, A.D., Lemiski, R., Mendoza, C., Pemberton, S.G., Polo, C., and Zonneveld, J., 2012, Porosity and Permeability in Bioturbated Sediments: Developments in Sedimentology, vol. 64, p. 837–868.

Tonkin, N.S., McIlroy, D., Meyer, R., and Moore-Turpin, A., 2010, Bioturbation influence on reservoir quality: A case study from the Cretaceous Ben Nevis Formation, Jeanne d'Arc Basin, offshore Newfoundland, Canada: AAPG Bulletin, v. 94, p. 1059–1078.

Wierman, D.A., Broun, A.S., and Hunt, B.B., 2010, Hydrogeologic atlas of the hill country Trinity aquifer: Blanco, Hays, and Travis counties, central Texas: Prepared by the Hays-Trinity, Barton Springs/Edwards Aquifer, and Blanco -Perdenales Groundwater Conservation Districts, 17 p.